

CMB  
Anisotropy  
Measurements

# A MEASUREMENT OF EXCESS ANTENNA TEMPERATURE AT 4080 Mc/s

Measurements of the effective zenith noise temperature of the 20-foot horn-reflector antenna (Crawford, Hogg, and Hunt 1961) at the Crawford Hill Laboratory, Holmdel, New Jersey, at 4080 Mc/s have yielded a value about  $3.5^{\circ}$  K higher than expected. This excess temperature is, within the limits of our observations, isotropic, unpolarized, and free from seasonal variations (July, 1964–April, 1965). A possible explanation for the observed excess noise temperature is the one given by Dicke, Peebles, Roll, and Wilkinson (1965) in a companion letter in this issue.

.....

event, the spectrum would have to be very much steeper.

A. A. PENZIAS  
R. W. WILSON

May 13, 1965

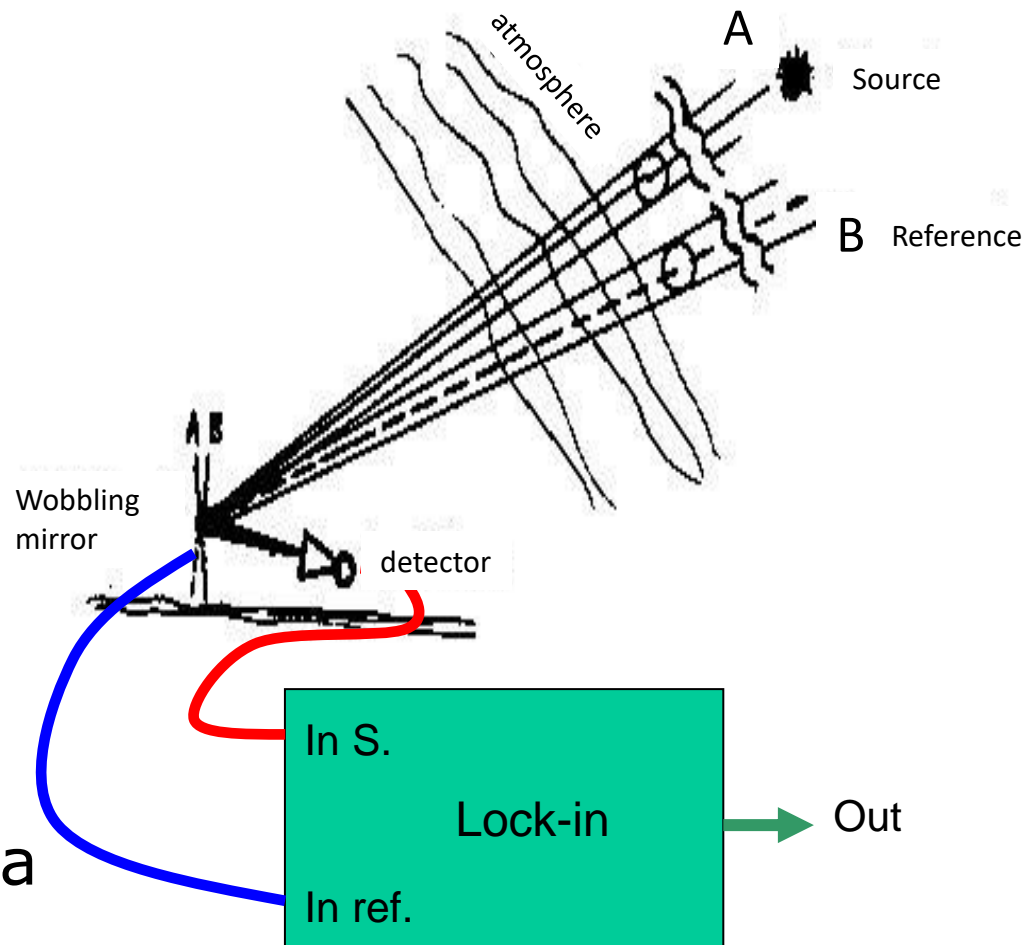
BELL TELEPHONE LABORATORIES, INC  
CRAWFORD HILL, HOLMDEL, NEW JERSEY

## REFERENCES

- Crawford, A. B., Hogg, D. C., and Hunt, L. E. 1961, *Bell System Tech. J.*, **40**, 1095.  
DeGrasse, R. W., Hogg, D. C., Ohm, E. A., and Scovil, H. E. D. 1959, "Ultra-low Noise Receiving System for Satellite or Space Communication," *Proceedings of the National Electronics Conference*, **15**, 370.  
Dicke, R. H., Peebles, P. J. E., Roll, P. G., and Wilkinson, D. T. 1965, *Ap J.*, **142**, 414.  
Hogg, D. C. 1959, *J Appl Phys*, **30**, 1417  
Ohm, E. A. 1961, *Bell System Tech. J.*, **40**, 1065  
Pauliny-Toth, I. I. K., and Shakeshaft, J. R. 1962, *M.N.*, **124**, 61.  
Penzias, A. A. 1965, *Rev Sci. Instr.*, **36**, 68.  
Penzias, A. A., and Wilson, R. W. 1965, *Ap J* (in press).

# Anisotropy Measurements

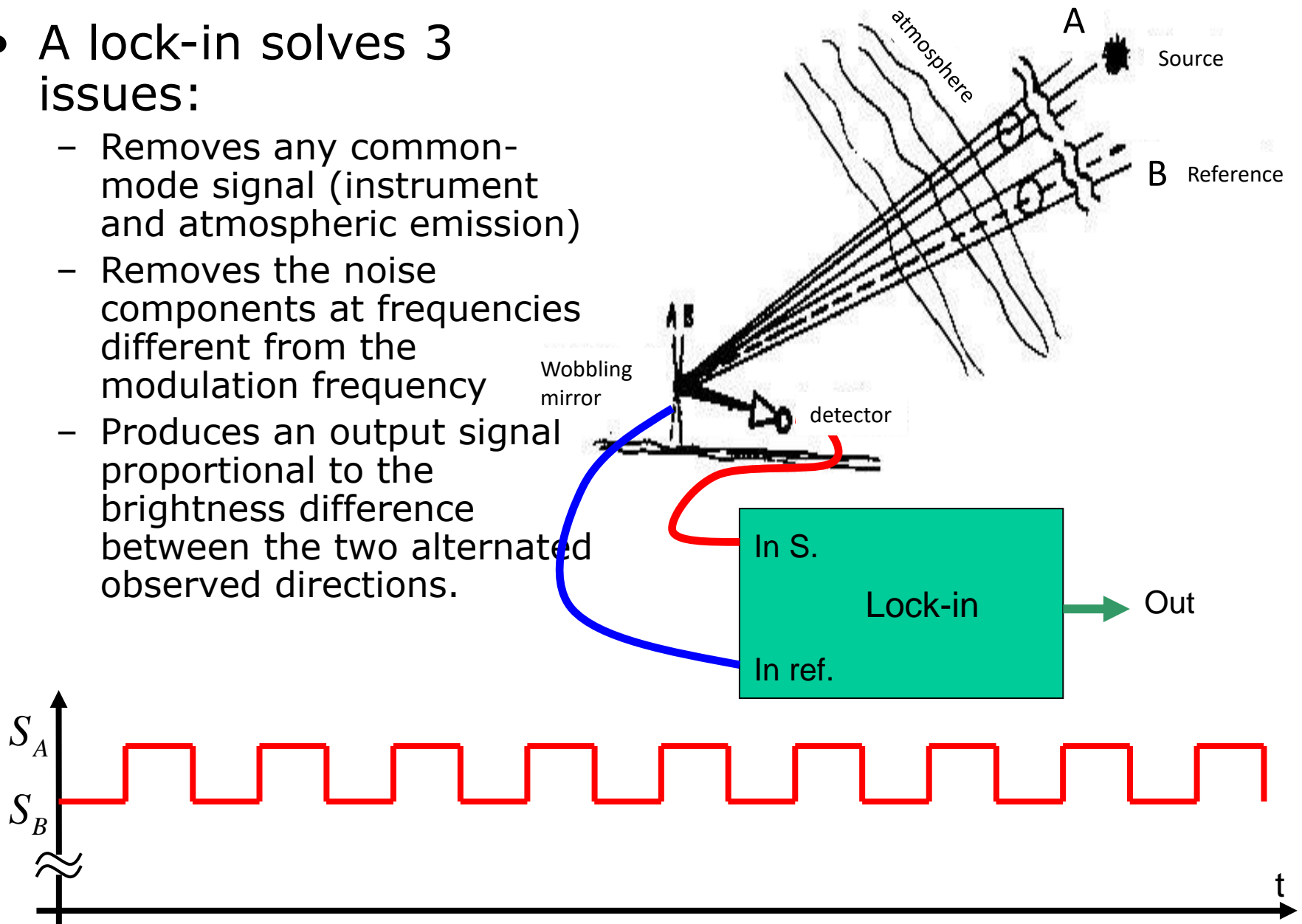
- Anisotropy: sky brightness variation with direction.
- Early anisotropy measurements were statistical samplings of the sky, towards a limited number of selected regions.
- The brightness from different directions was compared using a modulation / demodulation technique.



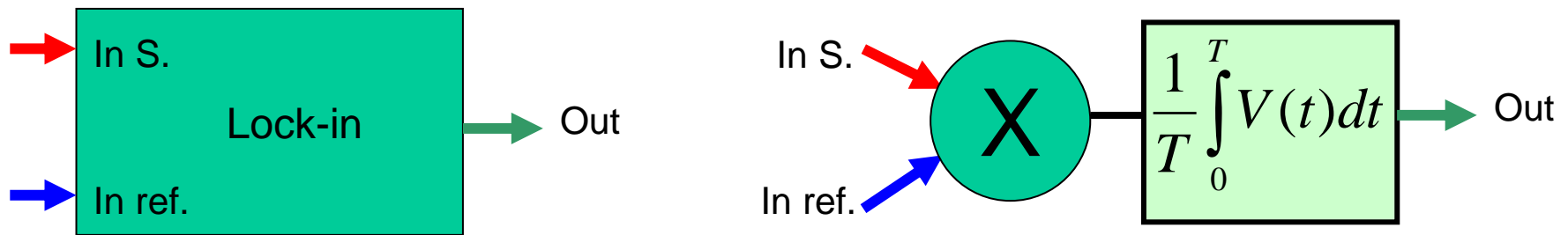
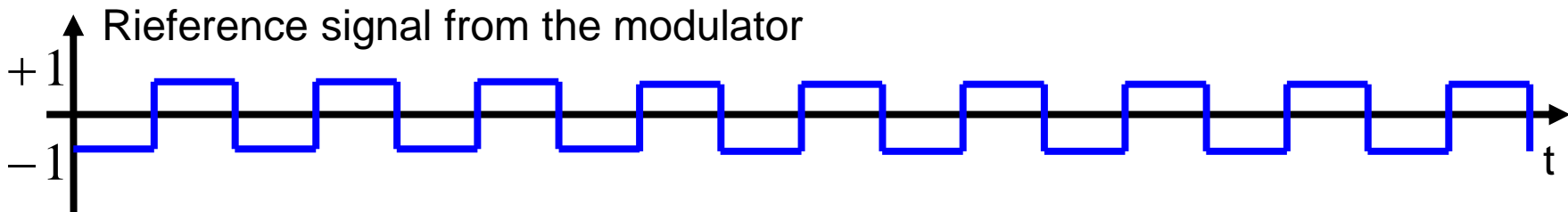
$$\Delta P = A\Omega ERT_{atm} \{B_c(A) - B_c(B)\}$$

# Anisotropy Measurements

- A lock-in solves 3 issues:
  - Removes any common-mode signal (instrument and atmospheric emission)
  - Removes the noise components at frequencies different from the modulation frequency
  - Produces an output signal proportional to the brightness difference between the two alternated observed directions.

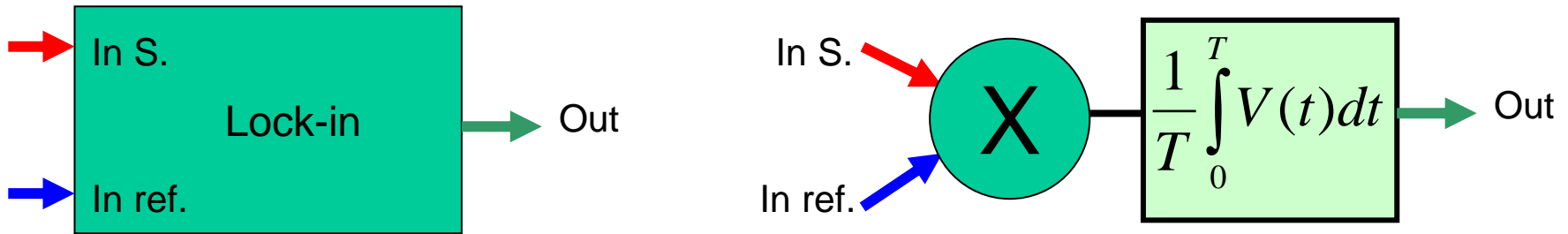


# Lock-in



$$S_{out} = \langle S(t)R(t) \rangle = \frac{1}{2} \langle S_A \times 1 \rangle + \frac{1}{2} \langle S_B \times -1 \rangle = \frac{1}{2} [S_A - S_B]$$

# Lock-in



In presence of noise :

$$\begin{aligned} S_{out} &= \langle [S(t) + n(t)]R(t) \rangle = \\ &= \frac{1}{2} \langle S_A \times 1 \rangle + \frac{1}{2} \langle S_B \times -1 \rangle + \frac{1}{2} \langle n(t) \times 1 \rangle + \frac{1}{2} \langle n(t) \times -1 \rangle = \\ &= \frac{1}{2} [S_A - S_B] + n' \end{aligned}$$

$n'$  is a null-average noise. Due to the absence of correlation between the noise  $n(t)$  and the reference signal,  $n'$  tends to 0 if averaged over long periods (many modulation cycles).

Cominciamo a vedere la risposta del lock-in nel caso semplice in cui sia il segnale che il riferimento siano sinusoidali, e manteniamo per ora differenti le due frequenze. Avremo

$$s(t) = \sqrt{2}V_s \cos(\omega_s t + \phi_s) \quad ; \quad r(t) = \sqrt{2}V_R \cos(\omega_R t + \phi_R) \quad (3.20)$$

e quindi

$$v_p(t) = V_s V_R \cos[(\omega_s + \omega_R)t + \phi_s + \phi_R] + V_s V_R \cos[(\omega_s - \omega_R)t + \phi_s - \phi_R] \quad (3.21).$$

Il segnale all' uscita del moltiplicatore e' quindi costituito da un termine alla frequenza somma ed un termine alla frequenza differenza. Si passa ora questo segnale attraverso un filtro passa basso con risposta in frequenza  $H_L(j\omega)$ , con taglio a frequenze ben inferiori alla frequenza di riferimento, in modo da rimuovere il termine a frequenza somma. Si ottiene una componente di *battimento* con ampiezza

$$|V_{out}| = V_s V_R |H_L(|\omega_s - \omega_R|)| \quad (3.22)$$

Siccome il filtro e' passa basso, attenuera' tutte le frequenze lontane dalla frequenza di riferimento: si vede quindi che la combinazione del moltiplicatore piu' il filtro passa basso opera come un filtro passa banda intorno alla frequenza di modulazione  $\omega_R$ . Tale filtro e' tanto piu' stretto quanto piu' bassa e' la frequenza di taglio del passa basso: la larghezza di banda del passa banda equivalente e' il doppio della larghezza di banda del filtro passa basso (fig.3.9). Useremo questa proprieta' per calcolare il rumore sul segnale in uscita.

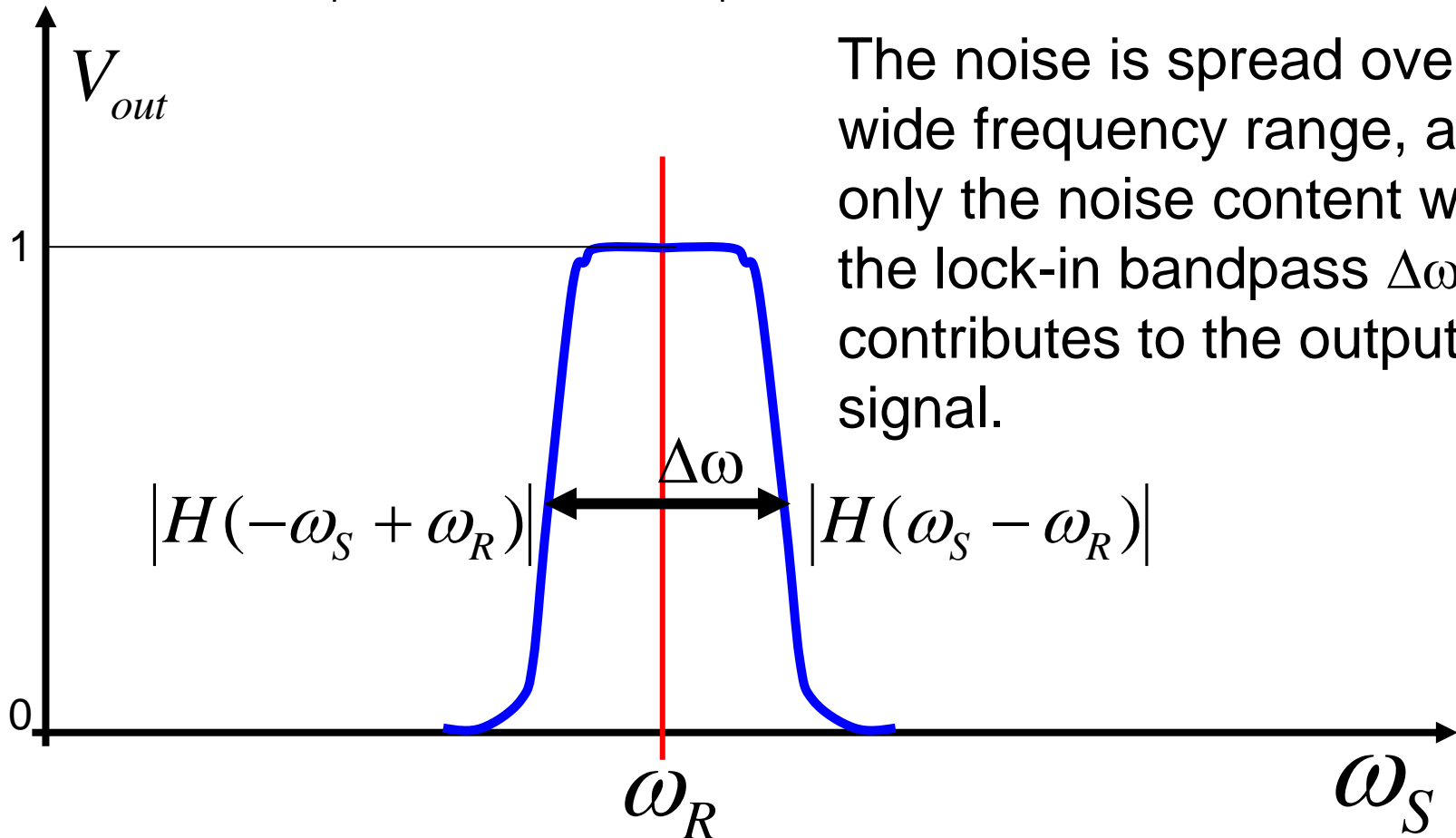
$$s(t) = \sqrt{2}V_S \cos(\omega_S t + \varphi_S)$$

$$r(t) = \sqrt{2}V_R \cos(\omega_R t + \varphi_R)$$

$$V_{out} = \langle s(t)r(t) \rangle$$

$\langle \rangle = \text{Low Pass Filter } H(\omega)$

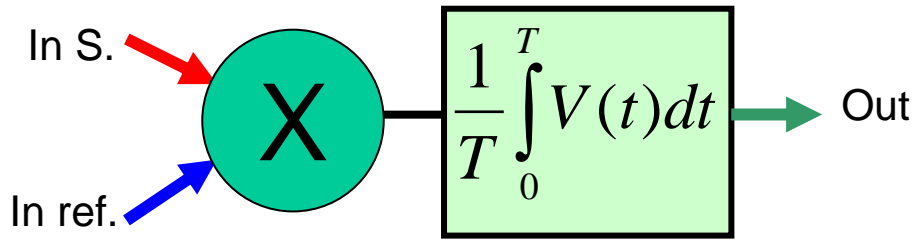
$$V_{out} = V_S V_R |H(|\omega_S - \omega_R|)|$$



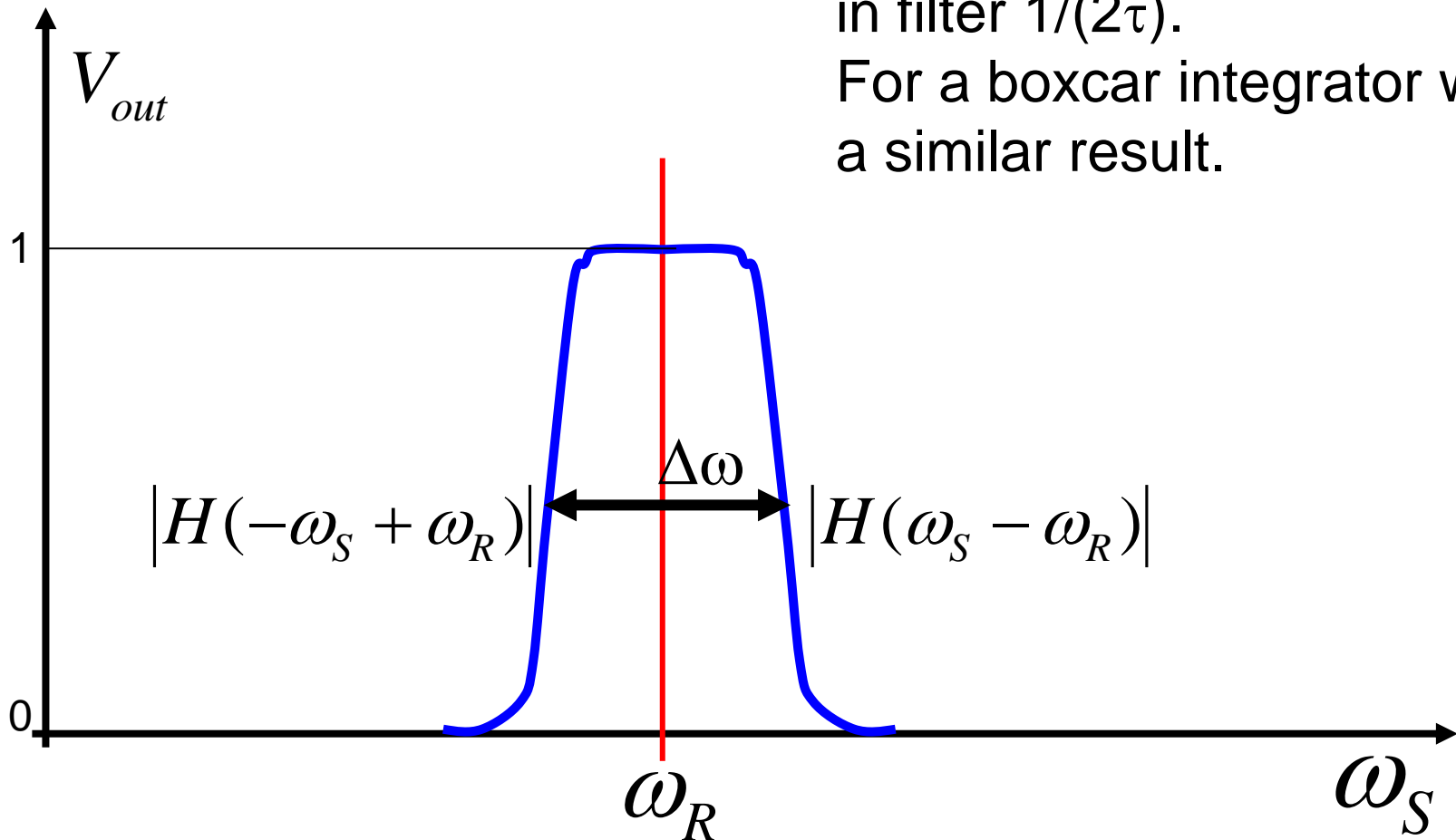
The signal to be detected is usually at the same frequency as the reference signal, so it contributes additively to the output signal.

The noise is spread over a wide frequency range, and only the noise content within the lock-in bandpass  $\Delta\omega$  contributes to the output signal.





Example: for a low-pass RC circuit the noise equivalent bandwidth is  $1/(4\tau)$ , so if the lock-in uses such a low-pass filter, the bandpass of the lock-in filter  $1/(2\tau)$ . For a boxcar integrator we get a similar result.



- The use of a lock-in amplifier improves the signal to noise ratio (S/N) proportionally to the square root of the time constant of the low pass filter (or the square root of the integration time if filtering is obtained by averaging over a period longer than the time constant).

$$N_{in} = \sqrt{w_V f_{\max}} \quad ; \quad N_{out} = \sqrt{\frac{w_V}{2\tau}}$$

$$\frac{S / N_{out}}{S / N_{in}} = \sqrt{2\tau f_{\max}}$$

- If the noise in the input signal is wide-band, the S/N improvement is very significant.

## Example:

- CMB anisotropy:

$$\frac{\Delta T}{T} \approx 10^{-5} \quad \rightarrow \quad \Delta T \approx 3 \times 10^{-5} K = 30 \mu K$$

- For a good bolometer @0.3K  $NEP \approx 10^{-17} W / \sqrt{Hz}$

$$\frac{\Delta B}{B} = \frac{x e^x}{e^x - 1} \frac{\Delta T}{T} \quad \rightarrow \quad \frac{NEP}{BA\Omega} = \frac{x e^x}{e^x - 1} \frac{NET}{T} \quad \rightarrow$$

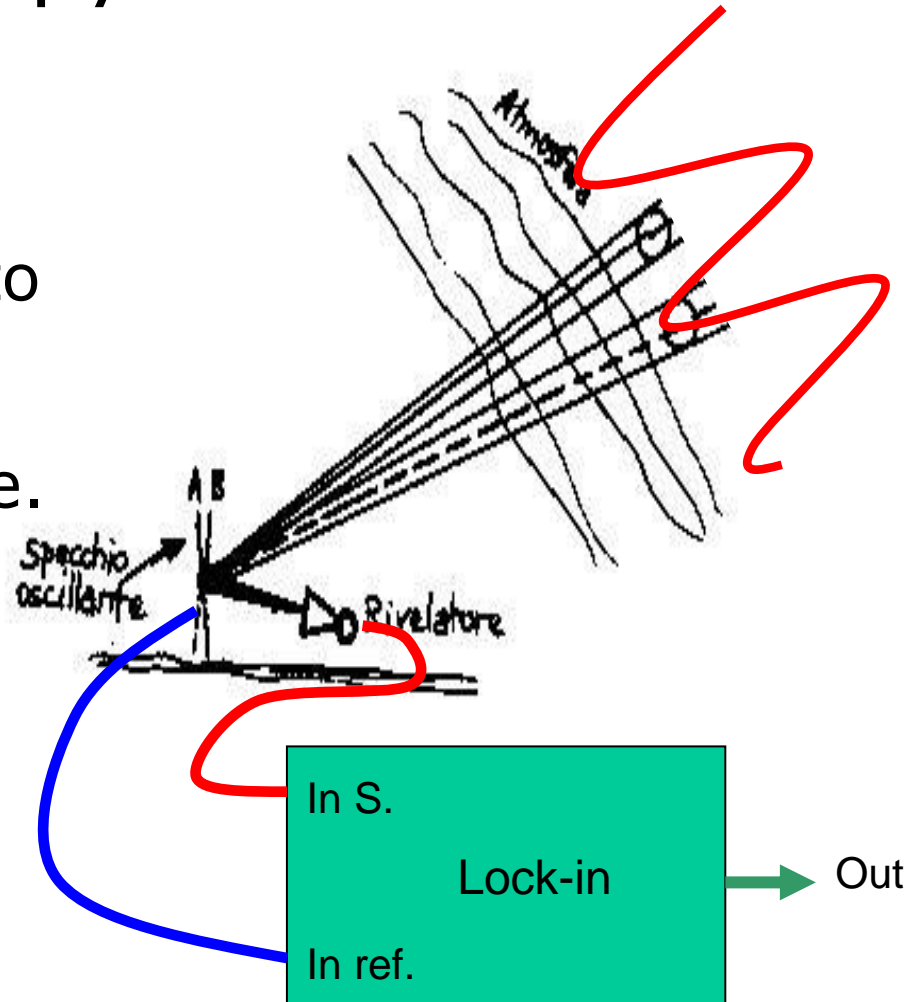
$$\rightarrow \quad NET \approx 150 \mu K / \sqrt{Hz} \quad @ 150 GHz, \quad A\Omega = \lambda^2$$

- So that  $\frac{S}{N} \approx \frac{\Delta T}{\sqrt{NET / 2t}} = 0.23 \times \sqrt{t(s)}$

- The integration time required to get S/N=3 is 200s !

# Anisotropy measurements

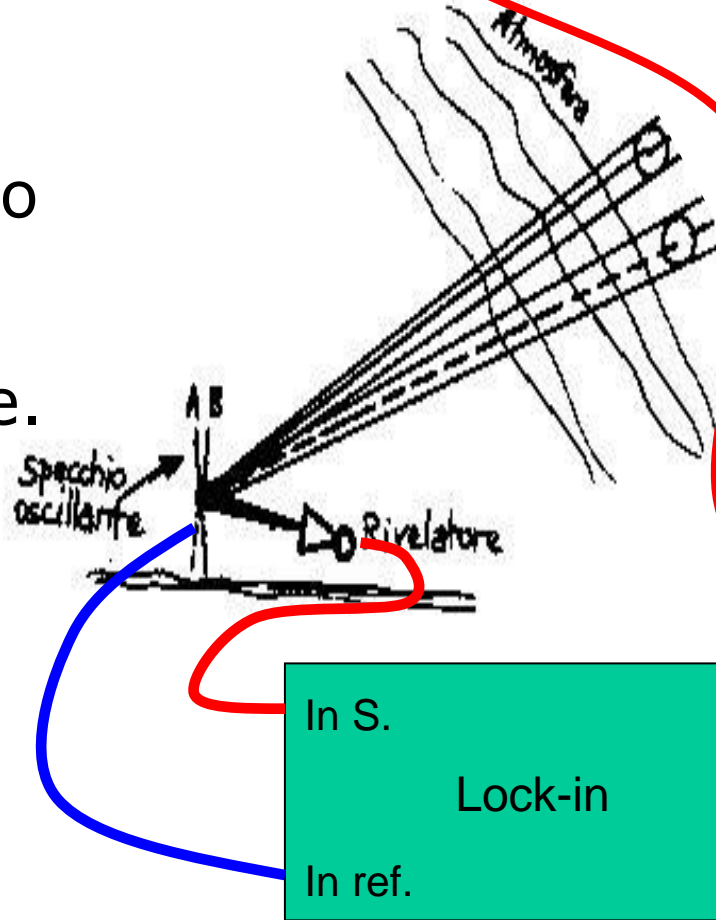
- A modulation experiment is maximally sensitive to structures (angular scales) similar to the modulation amplitude.
- However, we are interested to all angular scales (we aim at measuring a power spectrum)



$$\Delta P = A\Omega ERT_{atm} \{B_c(A) - B_c(B)\}$$

# Anisotropy measurements

- A modulation experiment is maximally sensitive to structures (angular scales) similar to the modulation amplitude.
- However, we are interested to all angular scales (we aim at measuring a power spectrum)

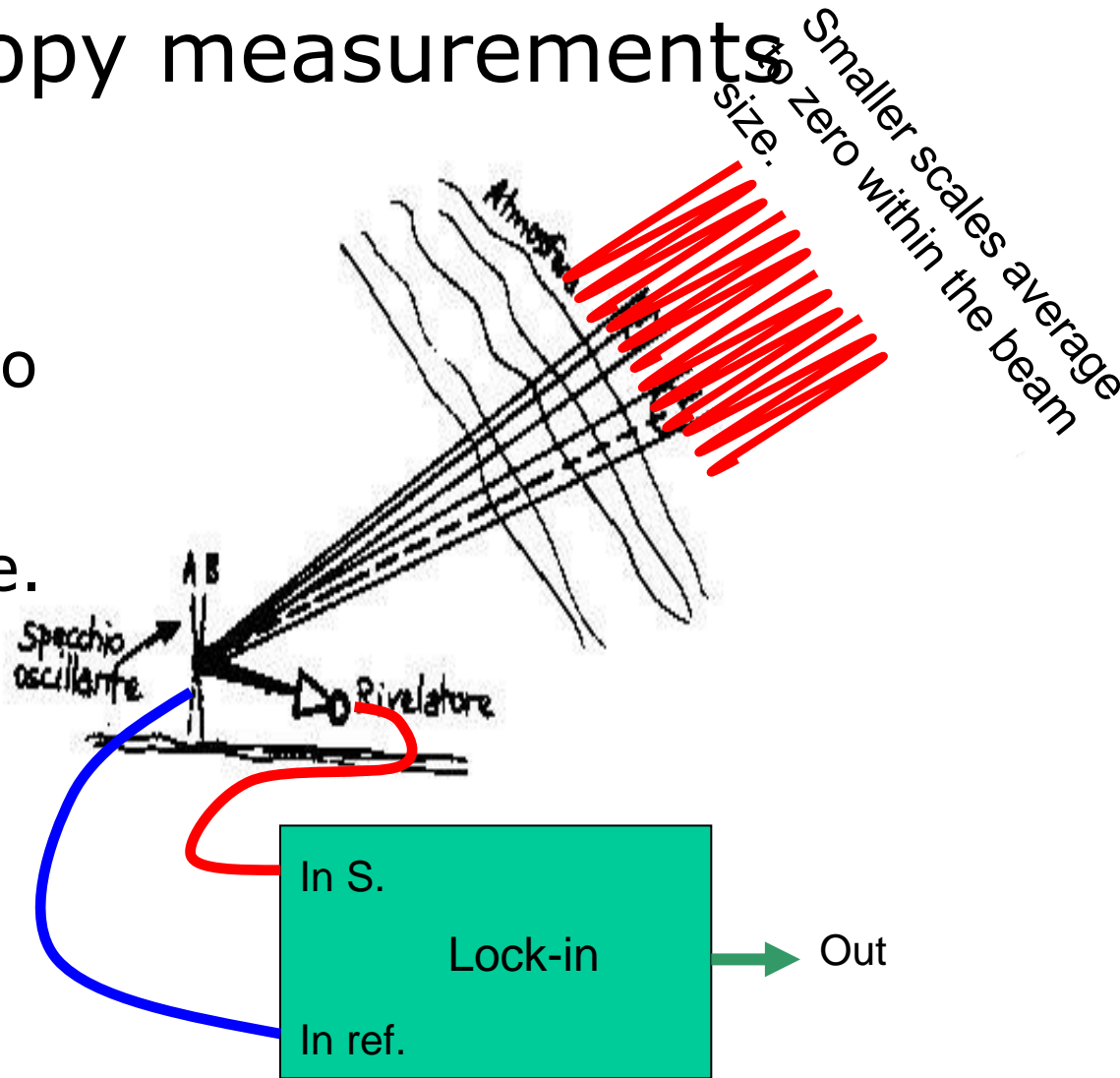


Larger scales produce the same signal in the two beams being compared

$$\Delta P = A\Omega ERT_{atm} \{B_c(A) - B_c(B)\}$$

# Anisotropy measurements

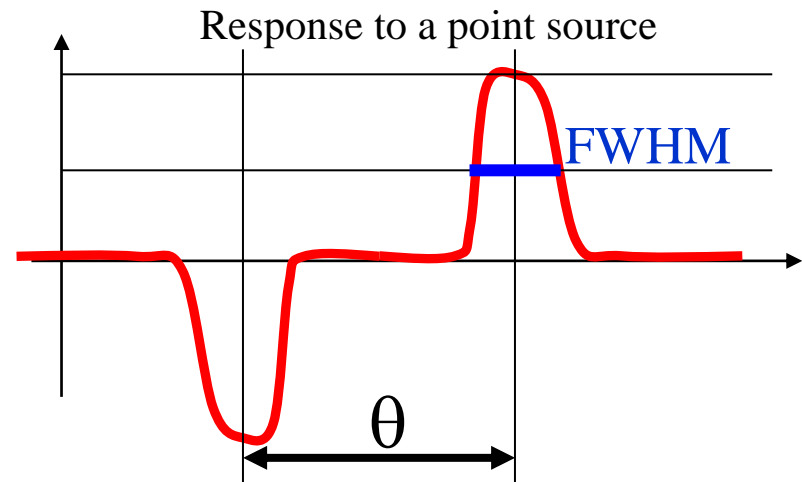
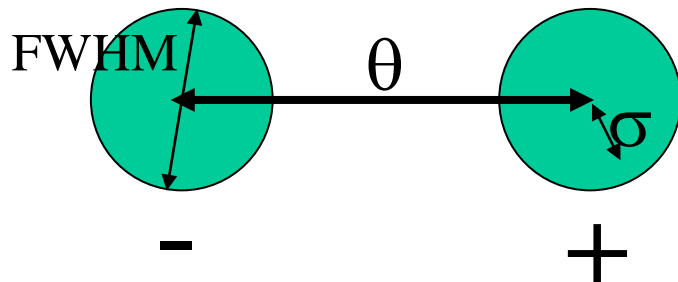
- A modulation experiment is maximally sensitive to structures (angular scales) similar to the modulation amplitude.
- However, we are interested to all angular scales (we aim at measuring a power spectrum)



$$\Delta P = A\Omega ERT_{atm} \{B_c(A) - B_c(B)\}$$

# Early anisotropy experiments

- Were statistical samples of the sky.
- $\Delta T_i$  measurements for  $n$  different sky directions, where for each direction a brightness difference between contiguous positions is measured.
- beam-switching and lock-in demodulation.
- Important parameters :
  - beamsize : width of the angular response. Approximately a Gaussian profile with standard deviation  $\sigma$ .
  - Beamthrough : angular distance  $\theta$  between the centers of the two regions being compared by the beam-switching – amplitude of the angular modulation.



1980

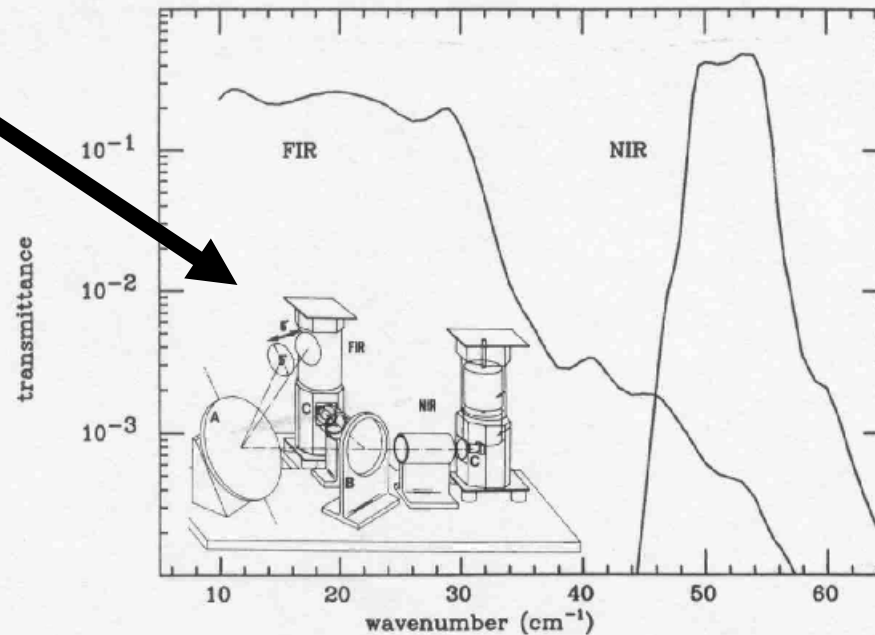


FIG. 1.—Spectral response of the two photometric channels. In the panel is sketched the instrumental setup. The two photometers FIR and NIR, the detectors C, the mesh beam-splitter B, and the wobbling mirror A are indicated.

modynamic temperature fluctuations of a 2.735 K blackbody. The instrumental offset stability turned out to be less than  $200 \mu\text{K hr}^{-1}$ .

## 2. OBSERVATIONS, CALIBRATION, AND EXPERIMENTAL RESULTS

The observations were carried out during a trans-Mediterranean balloon flight from Sicily to Spain, at an altitude of 41 km. The temperature of the bolometers was monitored during the flight and was found to be very stable. The noise level, after removal of cosmic-ray glitches, was consistent with that observed in the laboratory. The beam-switch direction was adjusted mechanically during the flight to be

the three scans were consistent within the noise level and were averaged together. As a result, we measured a set of 25 independent CMB anisotropy data, roughly equally spaced along the observed sky strip. These data are plotted in Figures 2b and 2c for both the channels. In order to evaluate the diffuse dust emission, we have simulated the ULISSE experiment on the  $100 \mu\text{m}$  IRAS all-sky maps, taking into account the finite resolution of our antenna beam and the sinusoidal modulation. The corresponding differential signals are also plotted in Figure 2a. The rms is of the order of  $1 \text{ MJy sr}^{-1}$ . Using the COBE FIRAS spectrum (Wright et al. 1991) for the extrapolation at longer wavelengths of this dust emission fluctuation, we estimate that significant dust signals should be present in both the photometric channels; in fact the comparison



1980

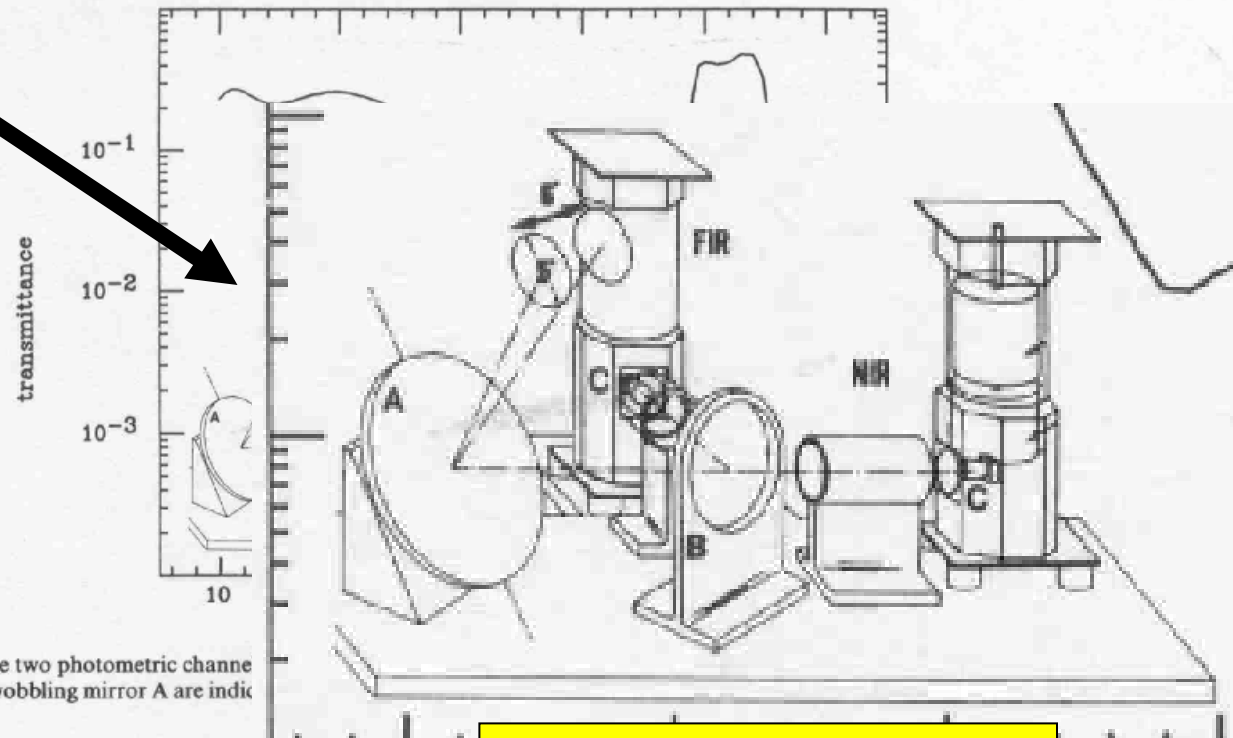


FIG. 1.—Spectral response of the two photometric channels. The mesh beam-splitter B, and the wobbling mirror A are indicated.

moderately dynamic temperature fluctuations of a 2.735 K blackbody. The instrumental offset stability turned out to be less than  $200 \mu\text{K hr}^{-1}$ .

## 2. OBSERVATIONS, CALIBRATION, AND EXPERIMENTAL RESULTS

The observations were carried out during a trans-Mediterranean balloon flight from Sicily to Spain, at an altitude of 41 km. The temperature of the bolometers was monitored during the flight and was found to be very stable. The noise level, after removal of cosmic-ray glitches, was consistent with that observed in the laboratory. The beam-switch direction was adjusted mechanically during the flight to be

$$\theta = 6^\circ$$

$$\text{FWHM} = 5^\circ$$

level and were set of 25 independently spaced along Figures 2b and the diffuse dust experiment on the count the finite social modulation also plotted in  $\text{sr}^{-1}$ . Using the for the extrapolation fluctuation, d be present in

both the photometric channels; in fact the comparison

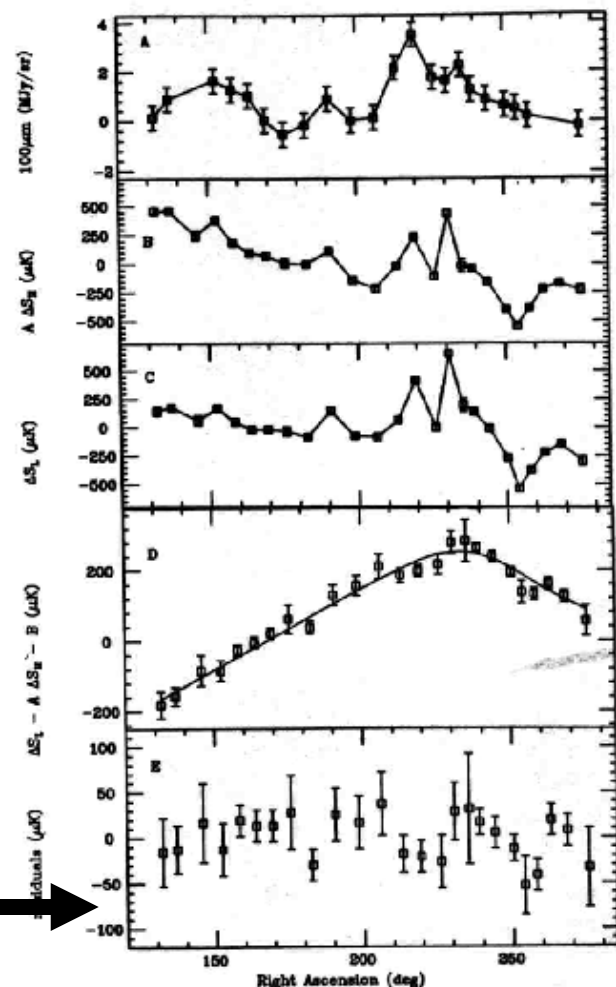


FIG. 2.—Top to bottom: (a) IRAS 100  $\mu\text{m}$  data in the same sky regions observed in the ULISSE experiment; (b) data from the high-frequency channel of the ULISSE experiment, renormalized to best fit the low-frequency channel data; (c) data in the low-frequency channel of ULISSE; (d) difference between low-frequency data and high-frequency data (see text for details) (the continuous line is the expected dipole anisotropy in the observed fields, taking into account the modulation); (e) residuals from the observed signals, after subtraction for the best-fit dipole anisotropy. Note that in (b) and (c) the error bars are hidden inside the squares indicating the points.

expansion,  $a_l^m$ , assumed to be stochastic variables, Gaussian distributed around a vanishing mean. The function  $W_l(\sigma_B) = \exp\{-[(l+0.5)\sigma_B]^2\}$  describes the effect of the finite antenna resolution on the large-scale CMB pattern (Scaramella & Vittorio 1988), while the  $P_l(x)$  are Legendre polynomials. In the scale-invariant cold dark matter (CDM) scenario, there is a simple scaling (Peebles 1982):

$$a_l^2 = (A/4\pi)(H_0^4/c^4)/[l(l+1)].$$

For an open, pure baryonic (BDM) model, with a substantial reheating of the intergalactic medium, it is possible to write (Scaramella & Vittorio 1991)

$$a_l^2 = \int k^2 P_{\text{rad}}(k) j_l^2(kr_{\text{LS}}) dk / (8\pi).$$

Here  $r_{\text{LS}}$  is the distance of the last scattering surface,  $P_{\text{rad}}$  is the radiation power spectrum, and  $j_l$  is a Bessel function. We use for the radiation power spectrum the following approximate expression (cf. Gorski & Silk 1989):

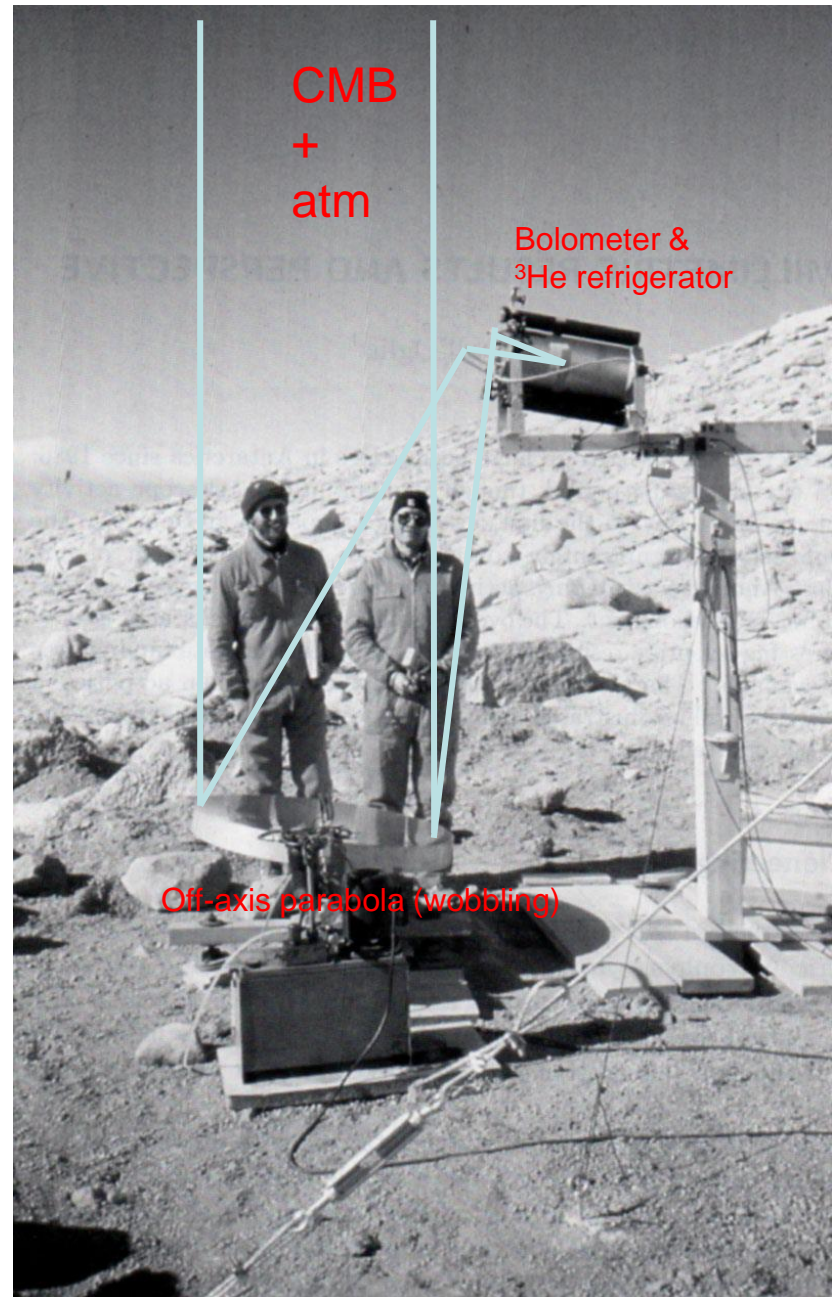
$$P_{\text{rad}} \sim (8/5)^2 A k^n \exp(-1.5k^2/k_J^2),$$

where  $k_J$  is the comoving wavenumber associated with the matter-radiation Jeans length at decoupling, and  $n$  is the primordial spectral index. We restrict the discussion here to BDM models with a residual ionization fraction  $x_e = 0.1$ .

Knowing the correlation properties of the temperature field, we can evaluate the variance of the differential (single-subtracted) temperature anisotropy at the angular scale of interest for the ULISSE experiment:  $\Delta_{\text{rms}}^2(6^\circ, 2^\circ:2) = 2[C(0, 2^\circ:2) - C(6^\circ, 2^\circ:2)]$ . The previous expressions for  $a_l^2$  depend upon the normalization constant  $A$ : for CDM it is evaluated by requiring the rms mass fluctuation in a sphere of  $8 h^{-1}$  Mpc to be  $b^{-1}$ ,  $b$  being the biasing factor; for BDM we use the same normalization, but with  $b = 1$ . In the normalization procedure, we have used the CDM and BDM density fluctuation power spectra given by Davis et al. (1985) and Peebles (1987), respec-

The first CMB  
telescope in  
Antarctica  
(Nov. 1986)

P. de Bernardis (left)  
G. Dall' Oglia (right)



## ARGO: a balloon-borne telescope for measurements of the millimeter diffuse sky emission

P. de Bernardis<sup>1</sup>, E. Aquilini<sup>2</sup>, A. Boscaleri<sup>3</sup>, M. De Petris<sup>1</sup>, M. Gervasi<sup>1</sup>, L. Martinis<sup>2</sup>, S. Masi<sup>1</sup>, V. Natale<sup>4</sup>, P. Palumbo<sup>2</sup>, F. Scaramuzzi<sup>2</sup>, and L. Valenziano<sup>1</sup>

<sup>1</sup> Dipartimento di Fisica, Universita' La Sapienza, Roma;

<sup>2</sup> ENEA-TECRI, Frascati

<sup>3</sup> IROE-CNR, Firenze

<sup>4</sup> CAISMI-CNR, Firenze

Received November 6, accepted December 1, 1992

Early '90s:  
Quest for angular resolution  
A true CMB telescope:  
- 1.2 m Cassegrain  
- Wobbling secondary mirror

P. de Bernardis et al.: ARGO: A balloon-borne telescope

685

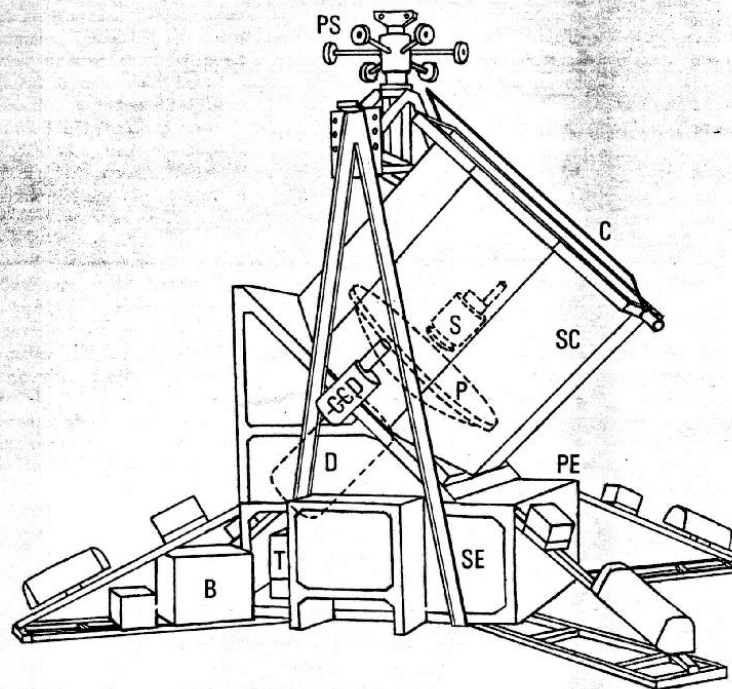
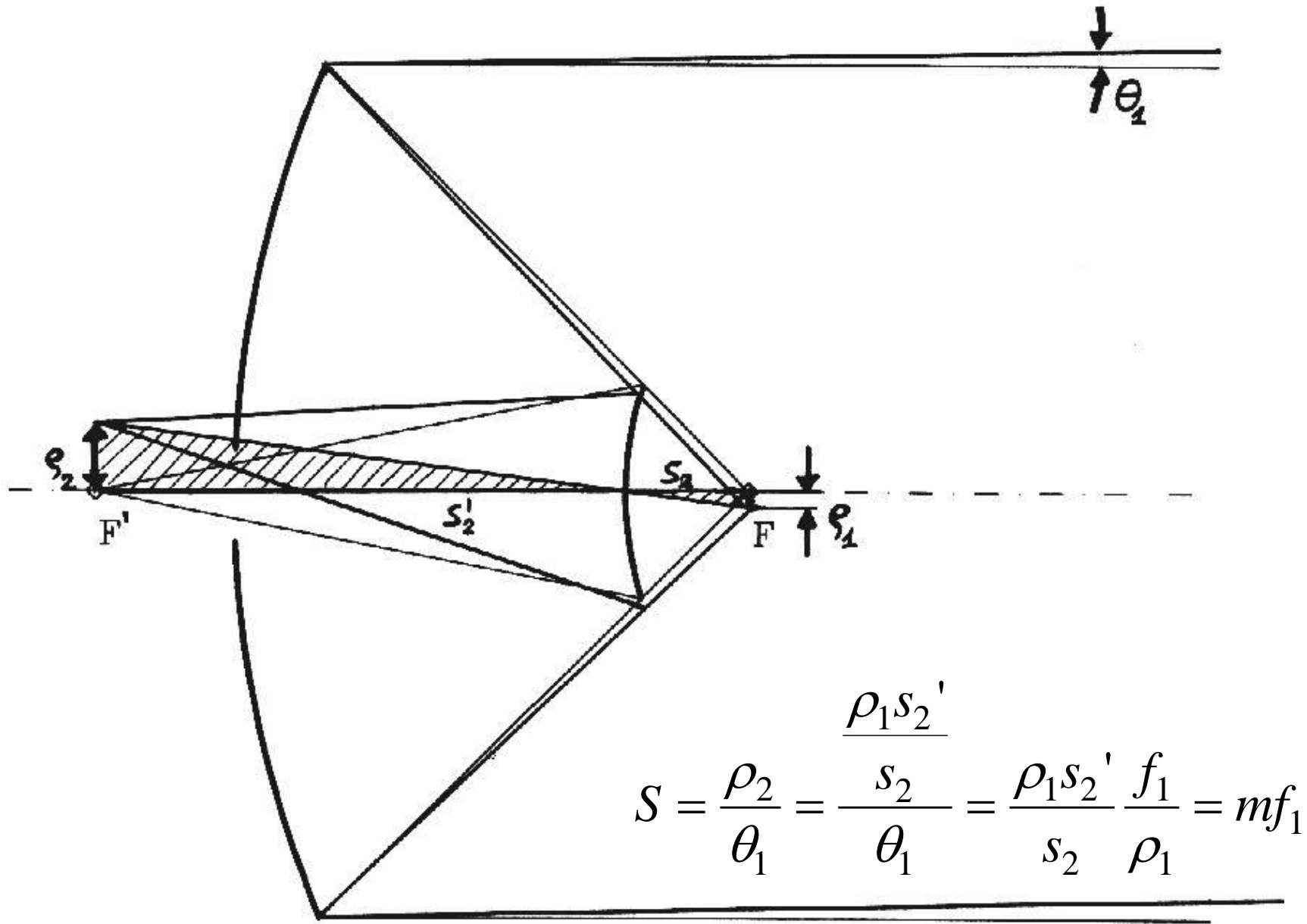
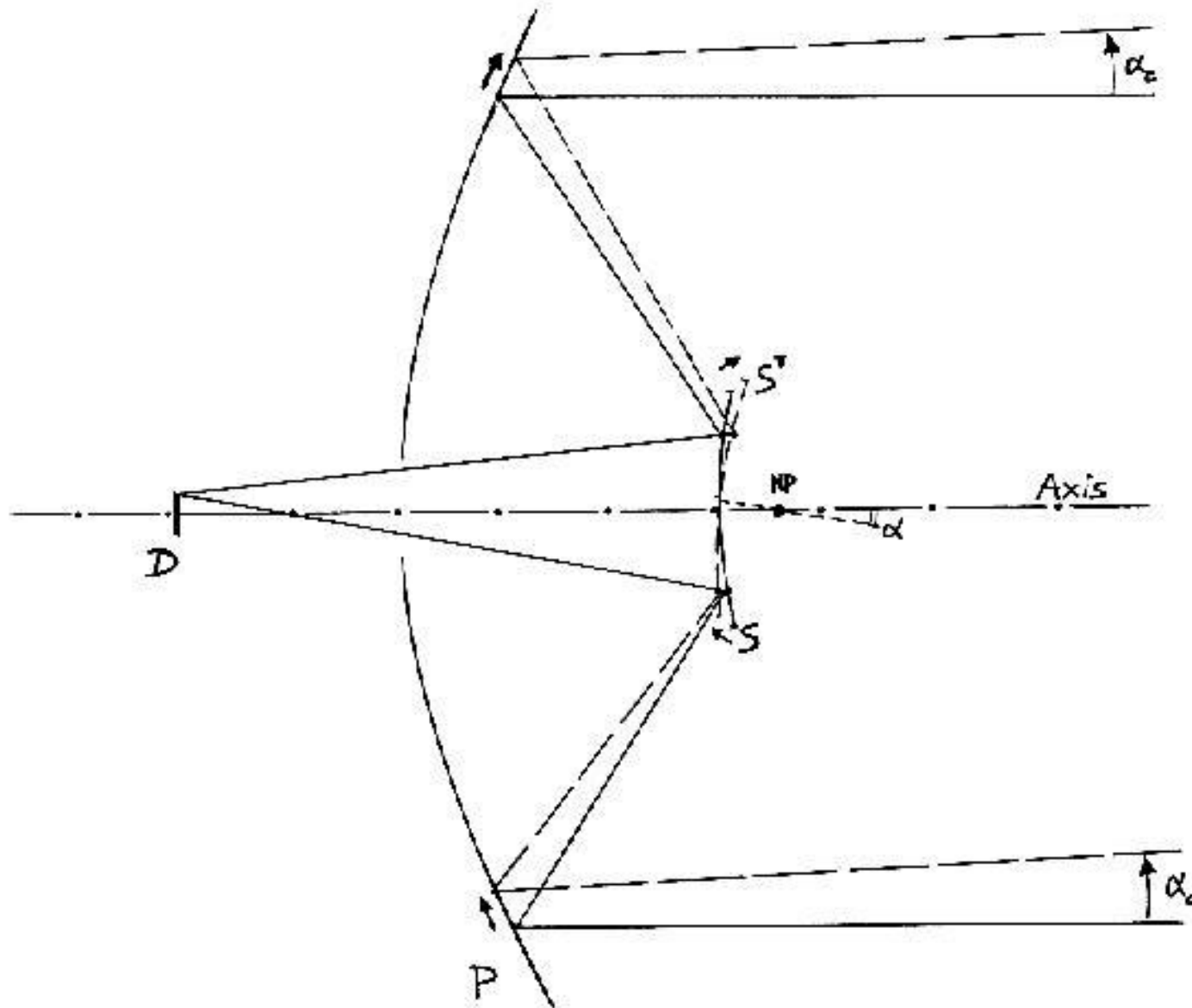


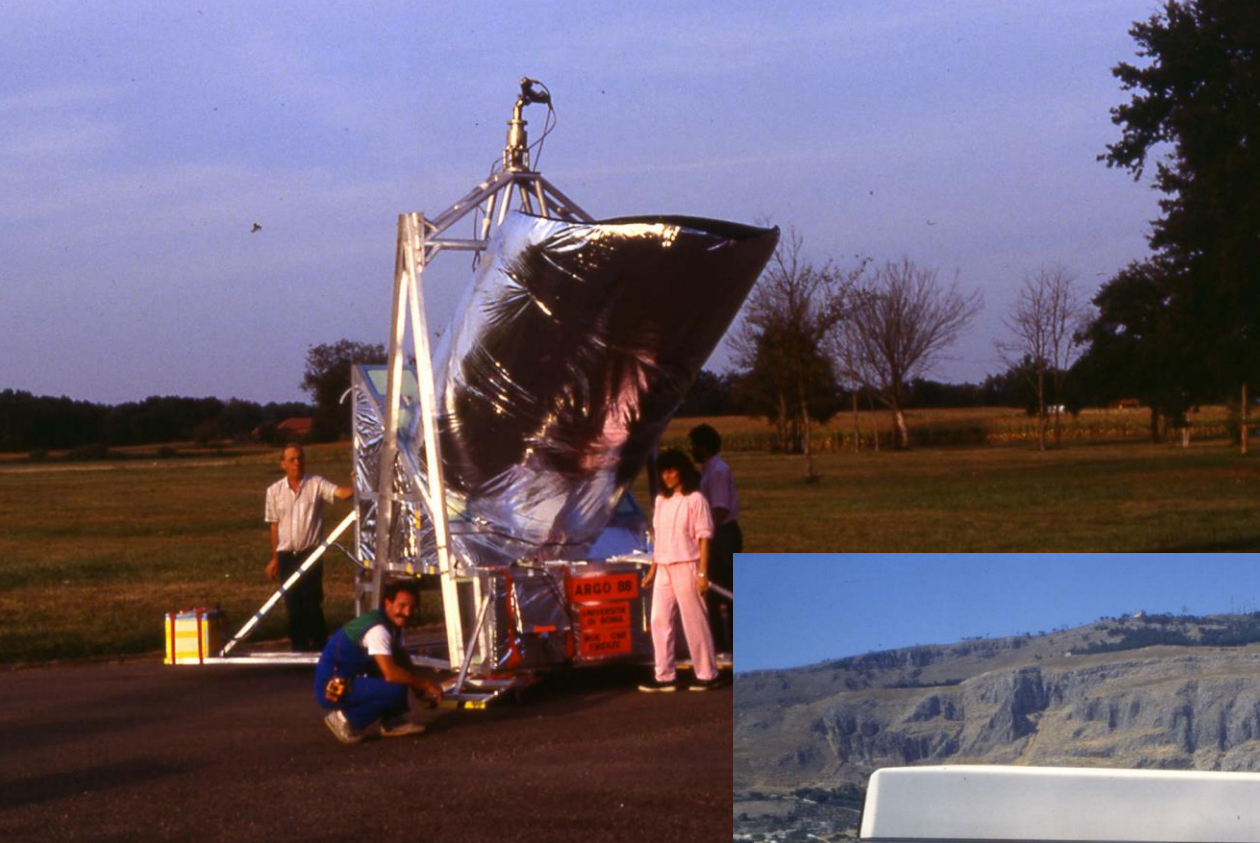
Fig. 3. The ARGO payload. The subsystems are labelled as follows: P: primary mirror; S: wobbling secondary mirror; SC: telescope screen; C: calibrator; D: detector; CCD: CCD star sensor; SE: signal electronics; T: telemetry electronics; PE: pointing system electronics; PS: pointing system; B: batteries



La dimensione del rivelatore e la focale totale determinano la FWHM.  
 Per ARGO era 0.8 gradi a 2 mm di lunghezza d' onda



1988 Aire sur l' Adour  
(France)  
The first m-sized CMB  
telescope



## 1992 Trapani

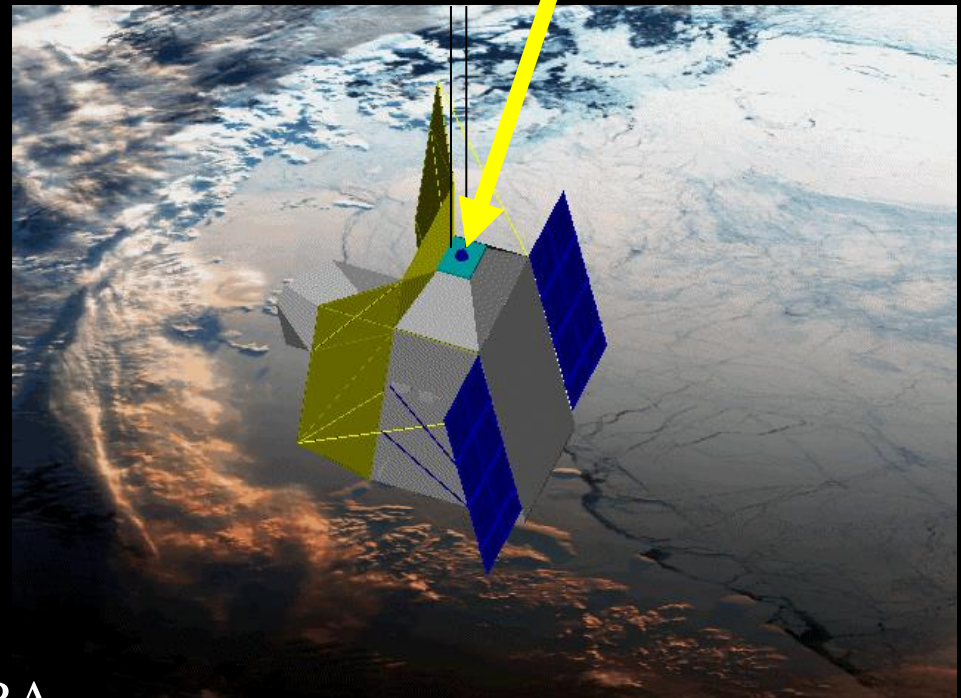
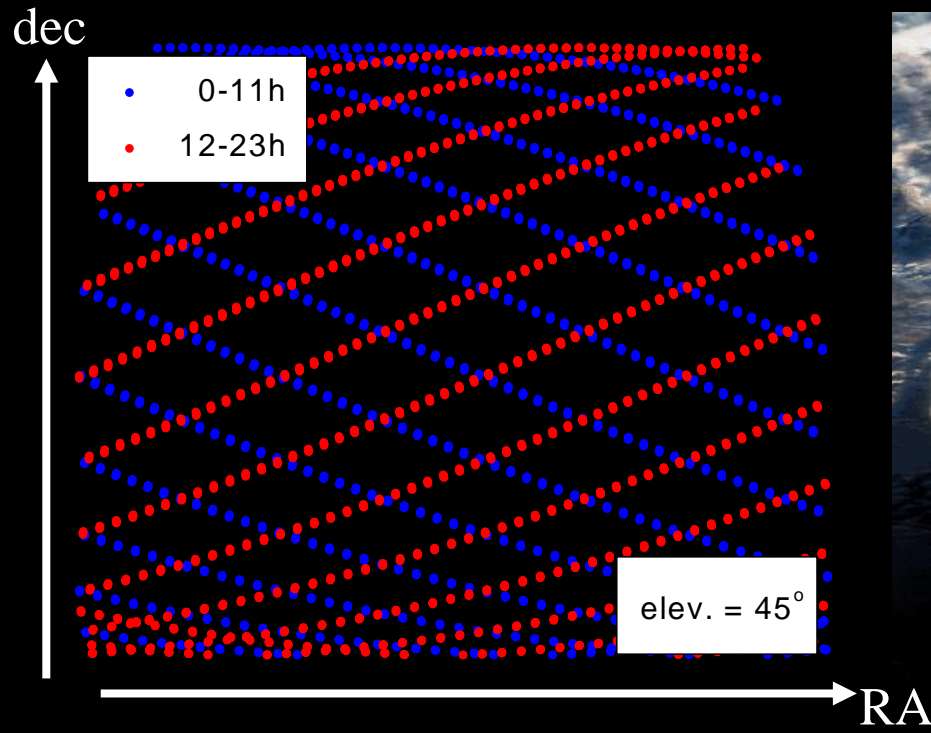
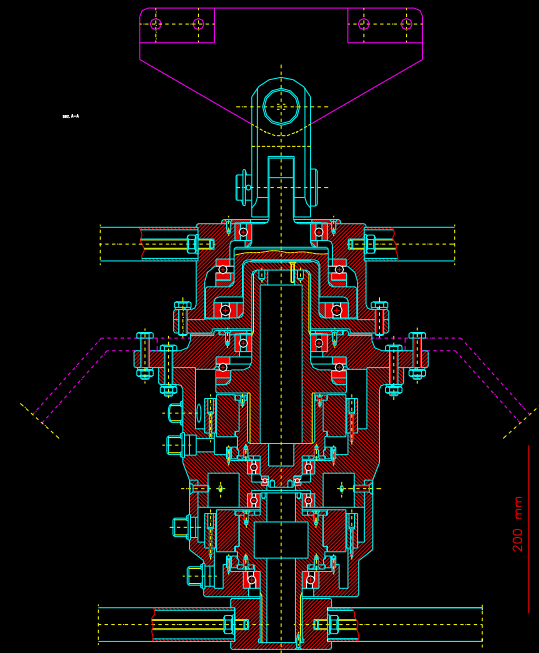
Left to right:  
Silvia Masi, Antonella De Luca,  
Michele Epifani, Luca Amicone,  
Marco De Petris, Paolo de  
Bernardis, the 1.2m telescope

Additional upper limits !



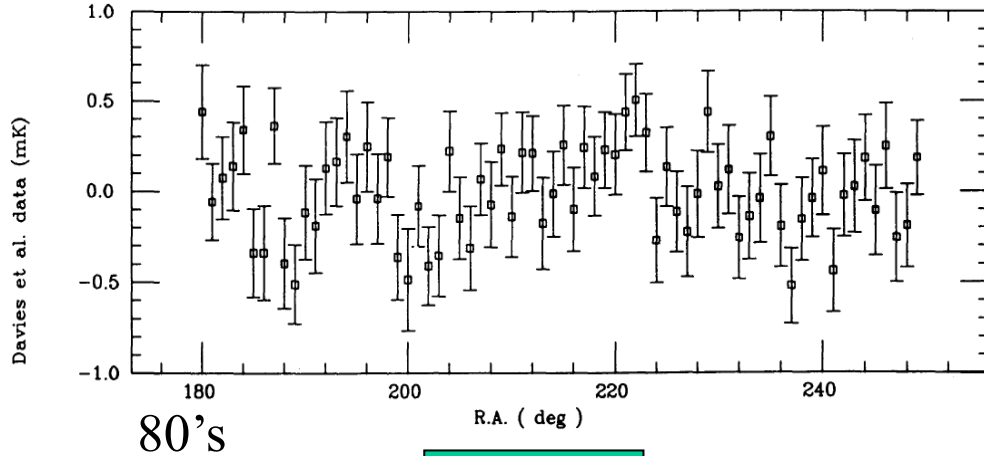
# Scanning Telescopes

- BOOMERanG
- Archeops
- WMAP
- Planck
- EBEX, SPIDER, LSPE

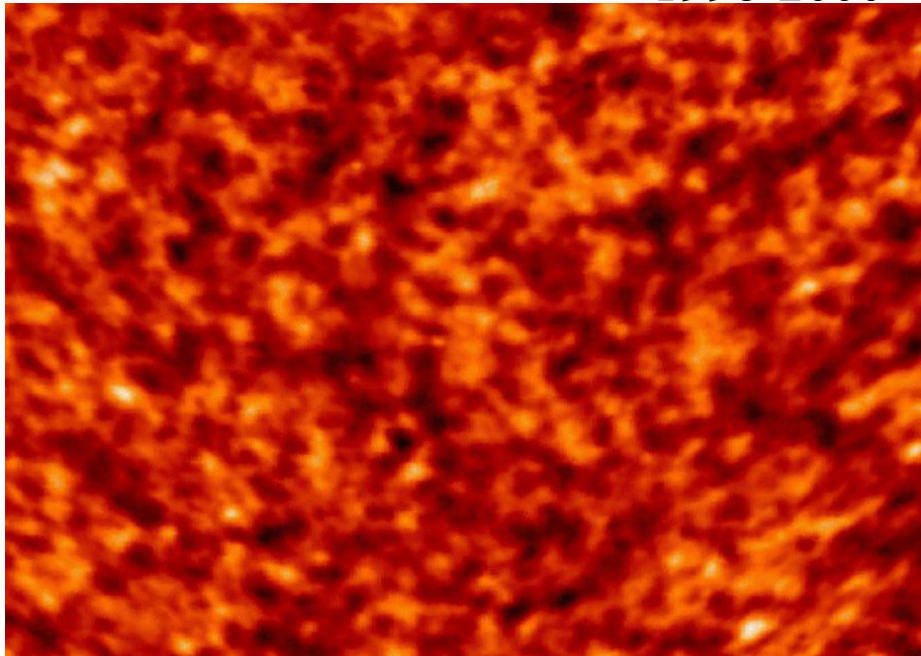




# From statistical samples of the sky to CMB maps

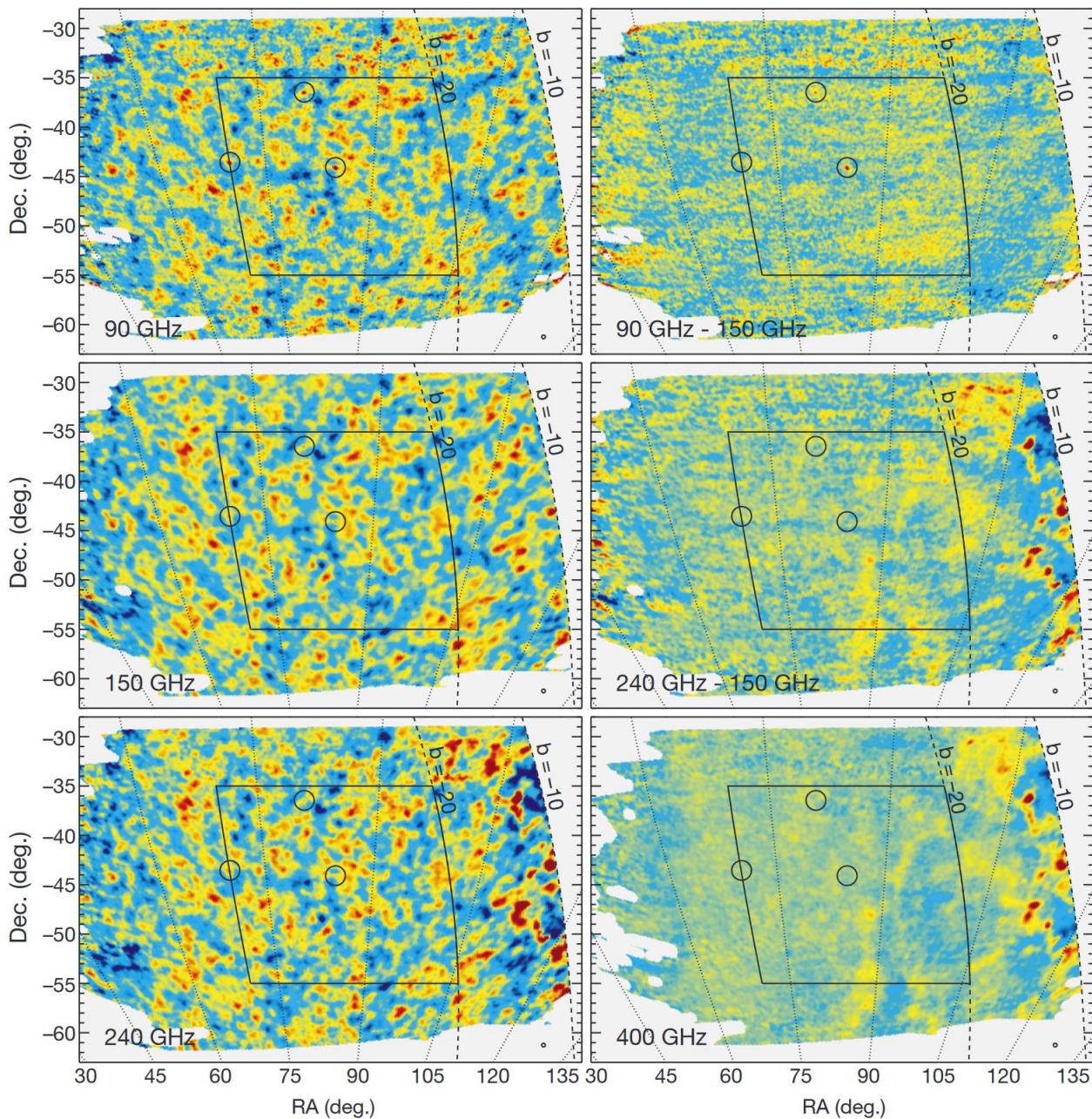


1998-2000



The transition was obtained via several breakthroughs:

- Sensitive detectors and scanning telescopes
- Efficient map-making algorithms
- Arrays of CMB detectors at different frequencies
- Redundant, diversified measurements allowing for extensive null tests



BOOMERanG  
Nature 404 955 (2000)

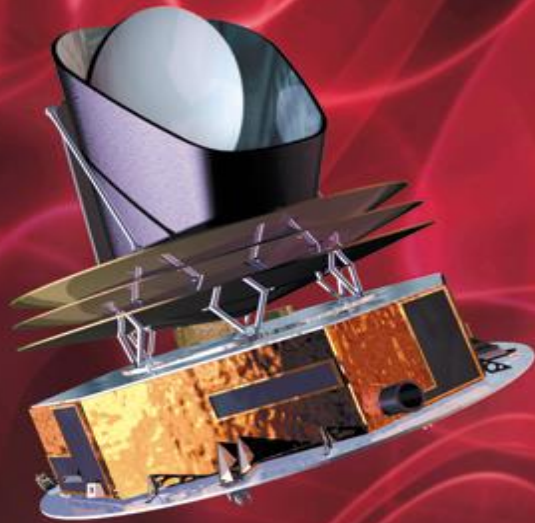
The first maps where  
degree-sized  
anisotropies due to  
causal horizons were  
resolved

Planck was a very ambitious experiment.

It carries a complex CMB experiment (the state of the art, a few years ago) all the way to L2,

improving the sensitivity wrt WMAP by at least a factor 10,

extending the frequency coverage towards high frequencies by a factor about 10



**PLANCK**

Looking back to the dawn of time  
Un regard vers l'aube du temps

<http://sci.esa.int/planck>



Almost 20 years of hard work of a very large team, coordinated by:

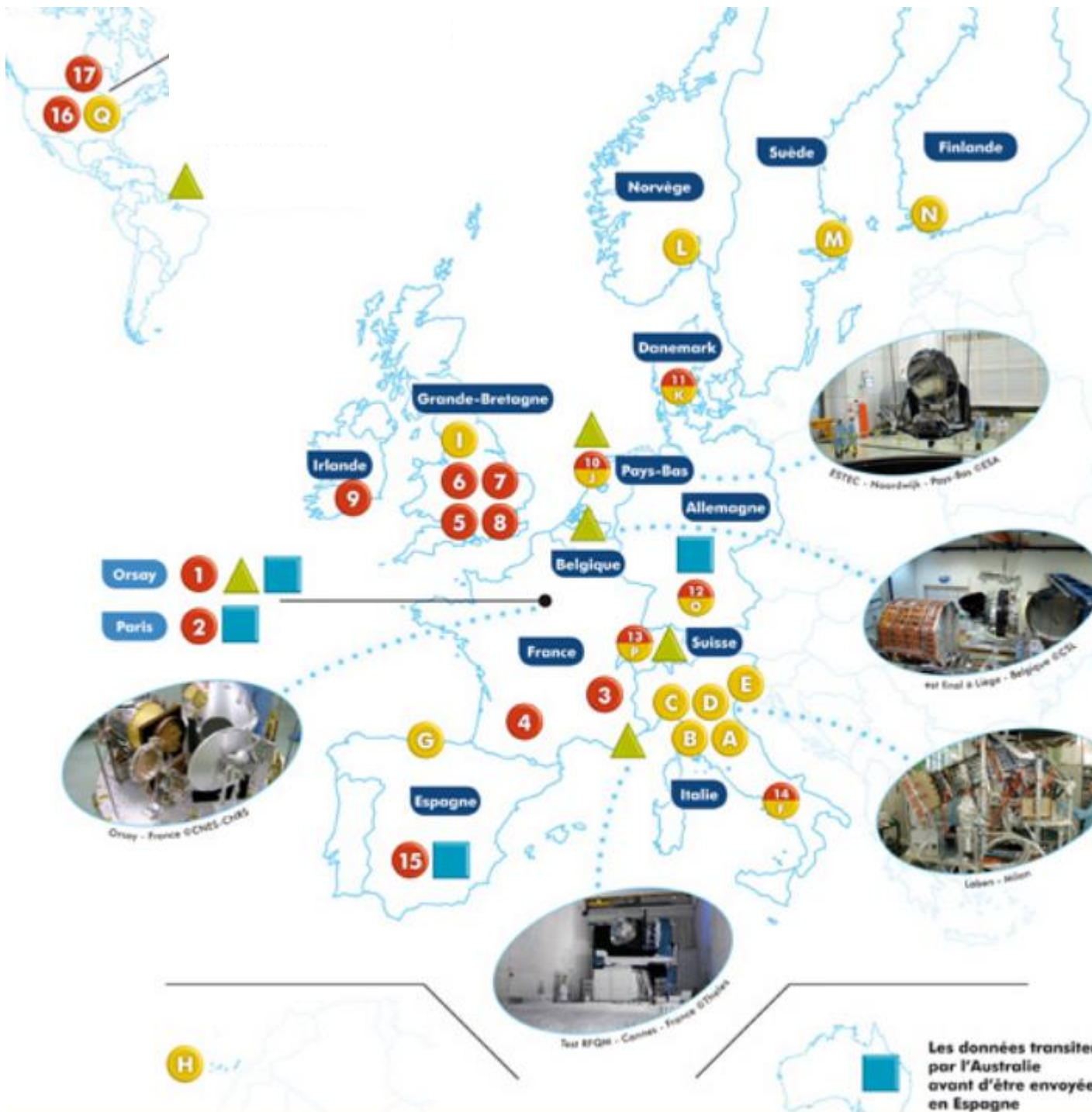
ESA : Jan Tauber

HFI PI : Jean Loup Puget (Paris)

HFI IS : Jean Michel Lamarre (Paris)

LFI PI : Reno Mandolesi (Bologna)

LFI IS : Marco Bersanelli (Milano)



### National Agencies



### Scientific Laboratories

● HFI PI Puget

● LFI PI Mandolesi

### Satellite

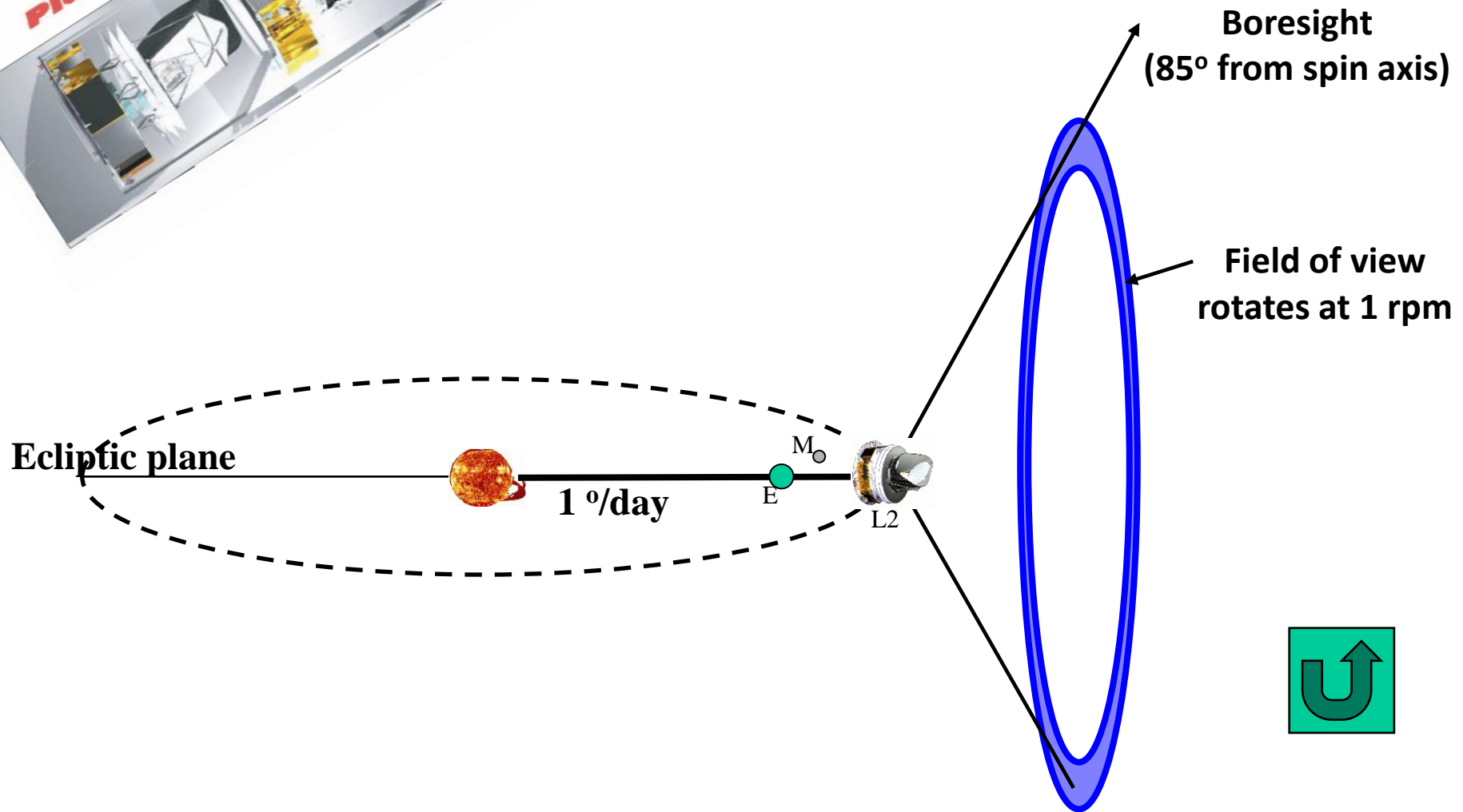


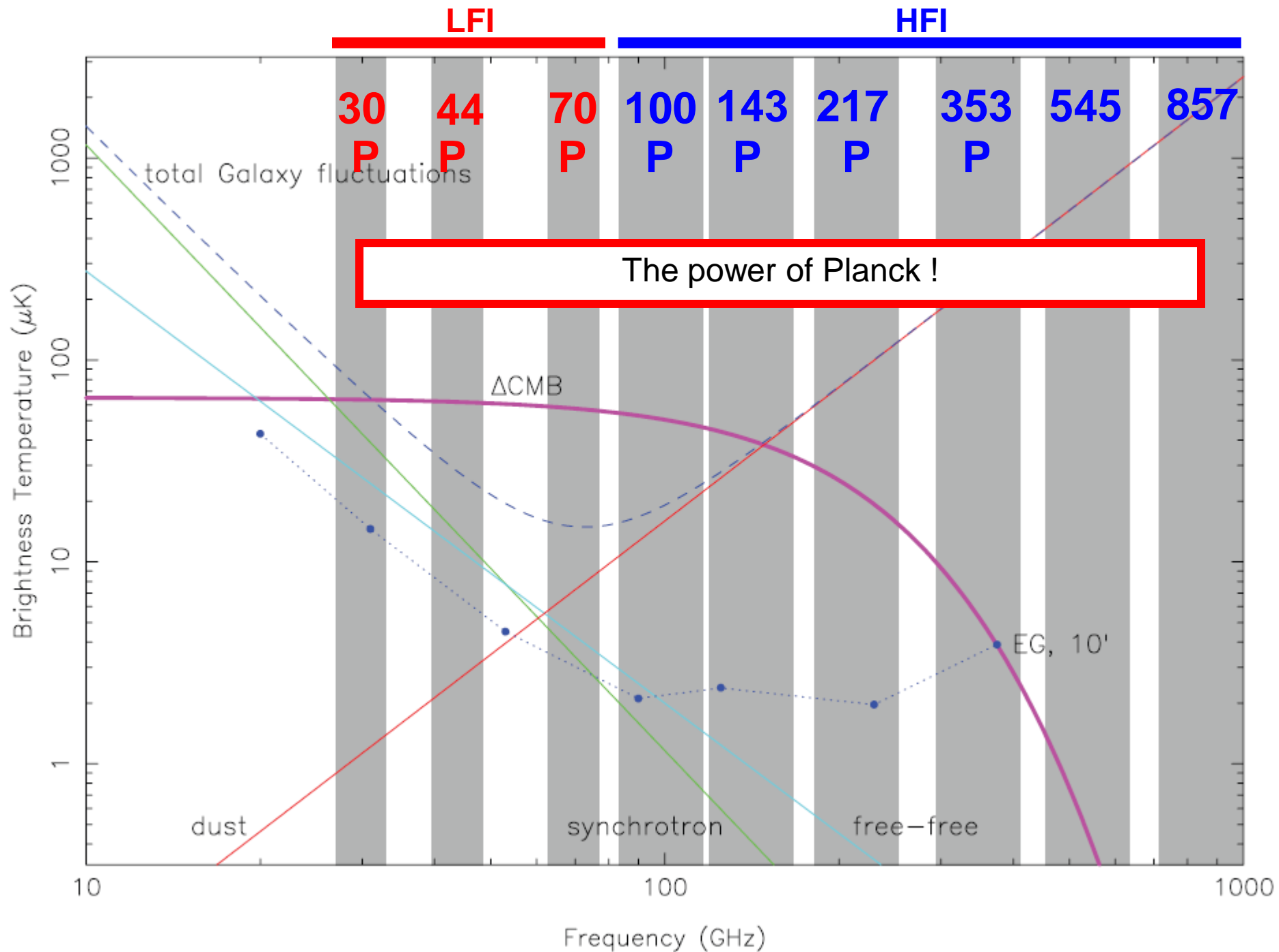
+ subcontractors

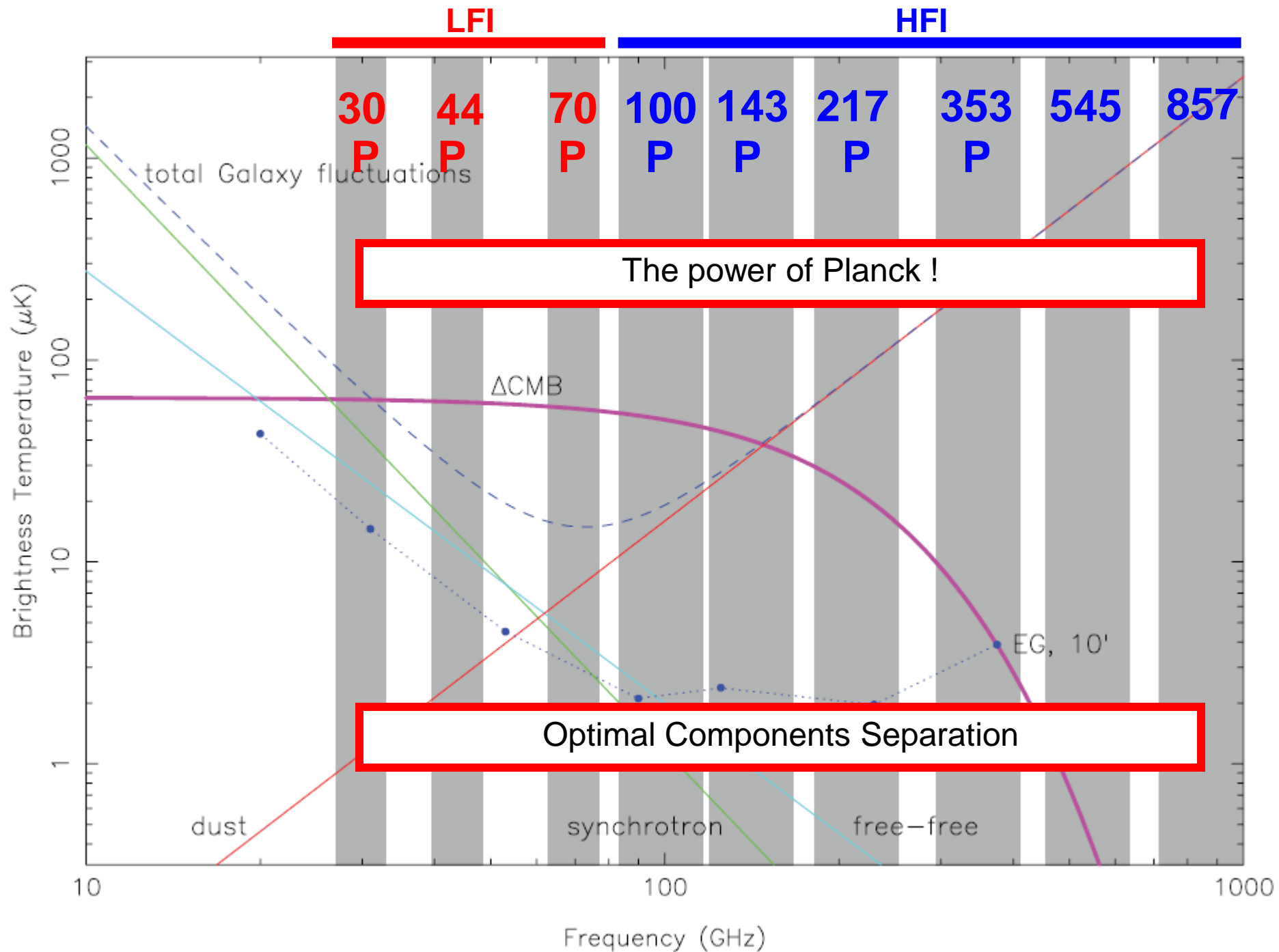
Les données transitent par l'Australie avant d'être envoyées en Espagne

# Observing strategy

The payload works in L2, to avoid the emission of the Earth, of the Moon, of the Sun





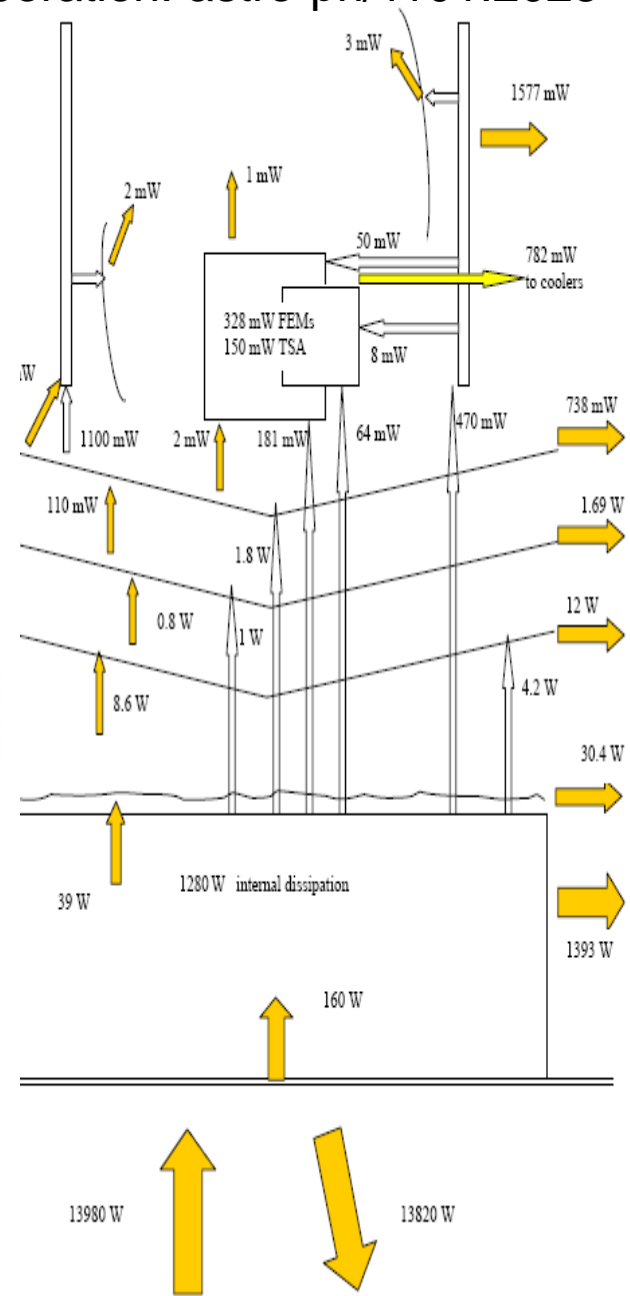
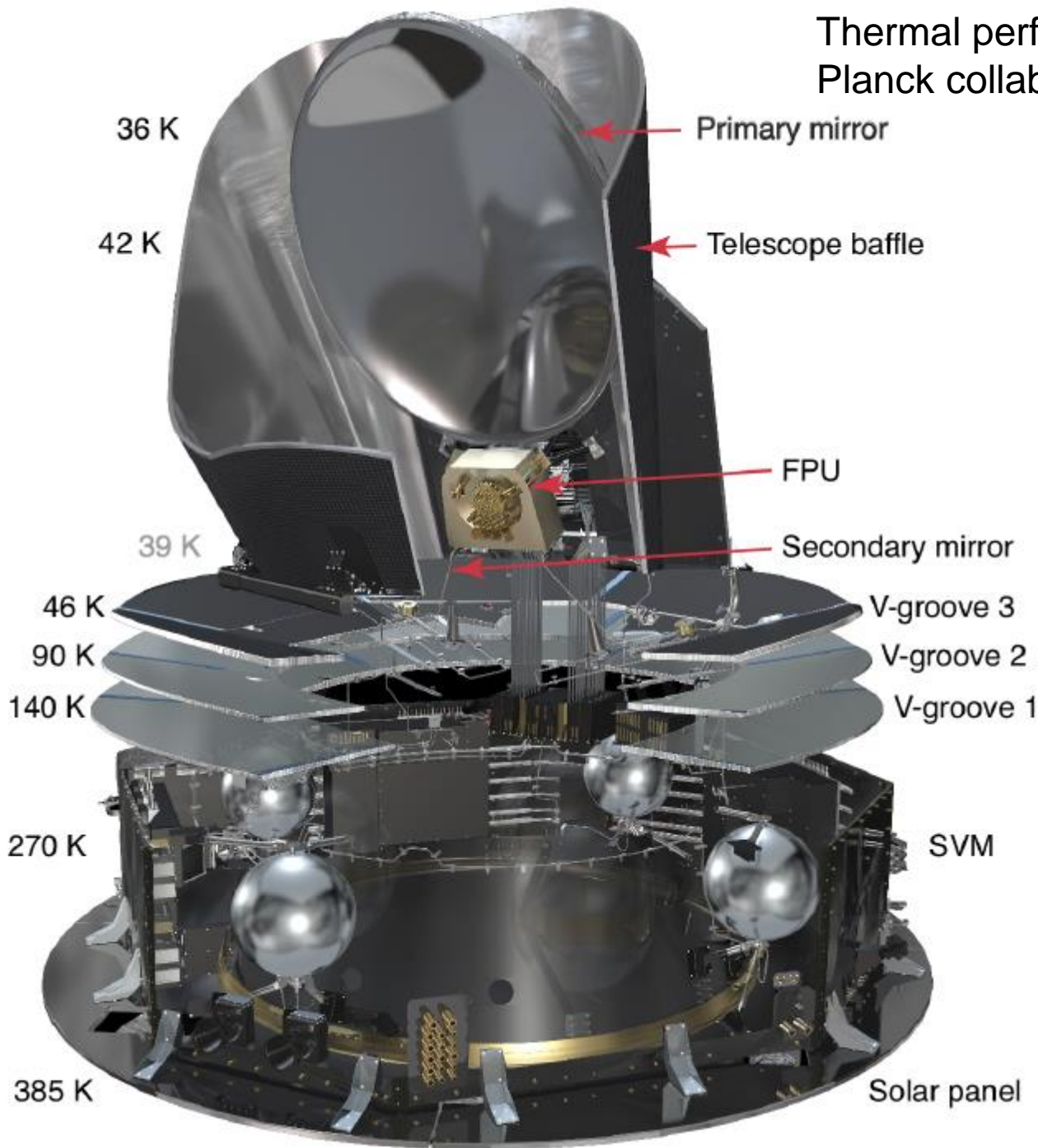




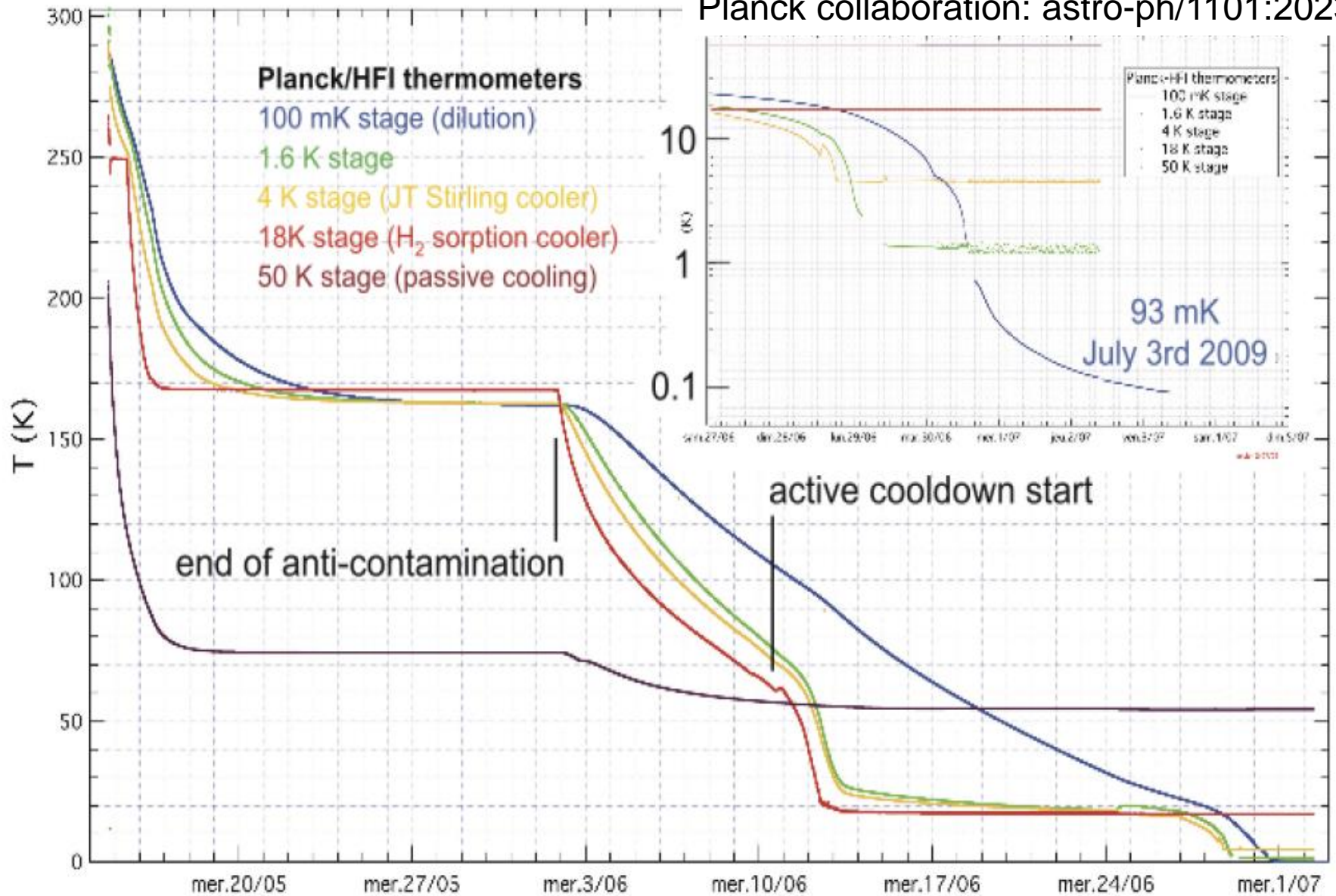


14 / May / 2009

Thermal performance :  
 Planck collaboration: astro-ph/1101:2023



Thermal performance :  
Planck collaboration: astro-ph/1101:2023



Mission :

Planck collaboration: astro-ph/1101:2022

**Table 1.** *Planck* coverage statistics.

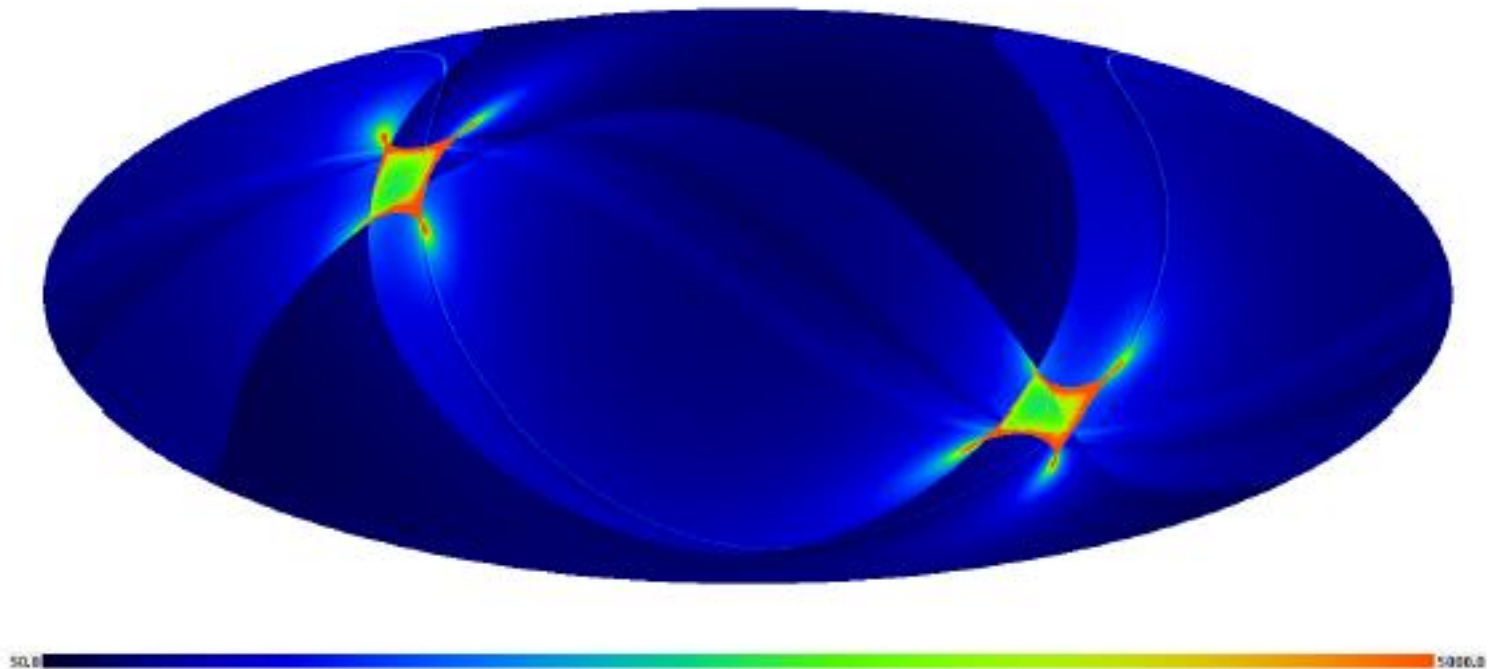
	30 GHz	100 GHz	545 GHz	
Mean <sup>a</sup>	2293	4575	2278	sec deg <sup>2</sup>
Minimum	440	801	375	sec deg <sup>2</sup>
< half Mean <sup>b</sup>	14.4	14.6	15.2	%
> 4× Mean <sup>c</sup>	1.6	1.5	1.2	%
> 9× Mean <sup>d</sup>	0.41	0.42	0.41	%

<sup>a</sup> Mean over the whole sky of the integration time cumulated for all detectors (definition as in Table 3) in a given frequency channel.

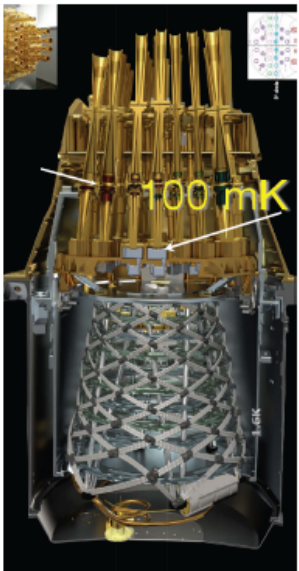
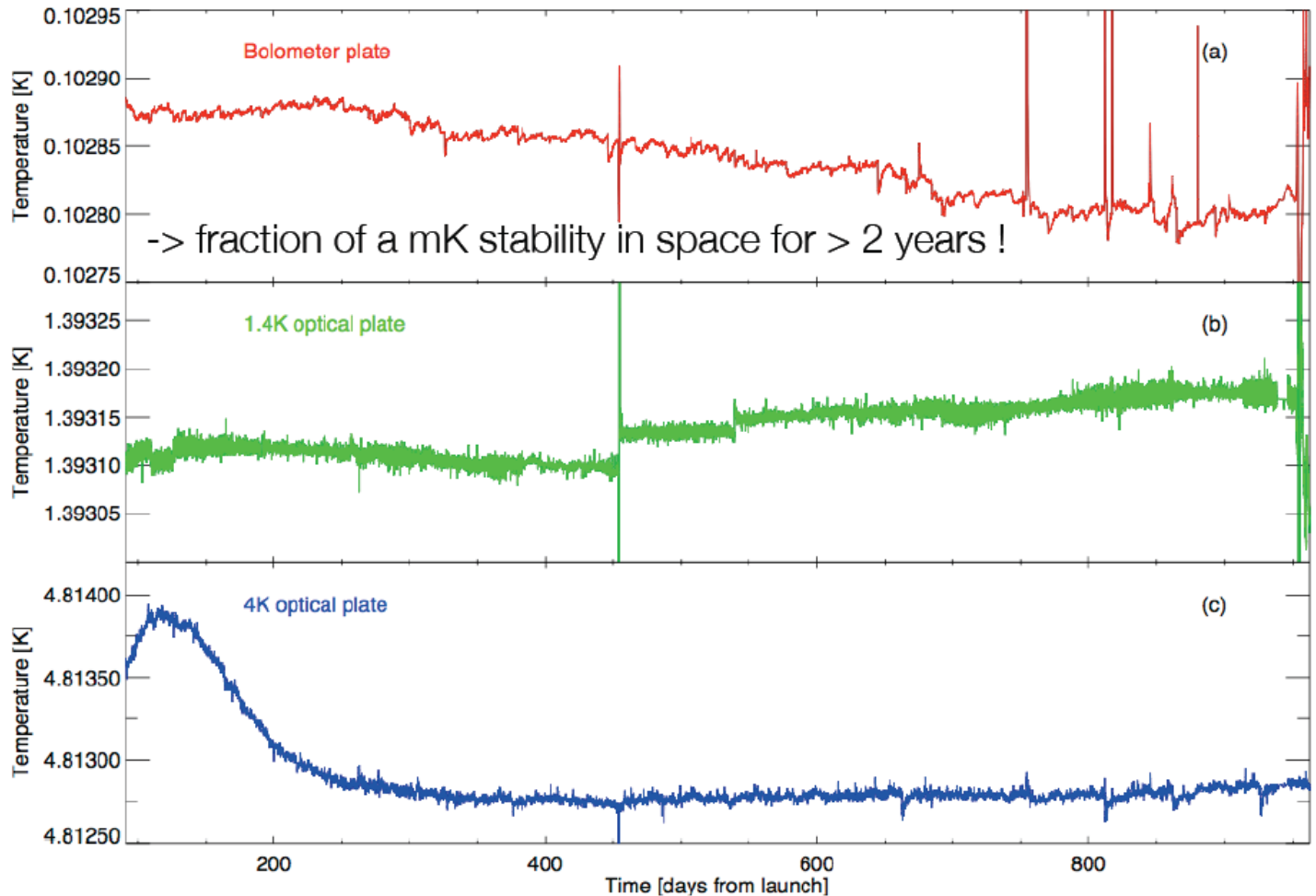
<sup>b</sup> Fraction of the sky whose coverage is less than half the Mean.

<sup>c</sup> Fraction of the sky whose coverage is larger than four times the Mean.

<sup>d</sup> Fraction of the sky whose coverage is larger than nine times the Mean.



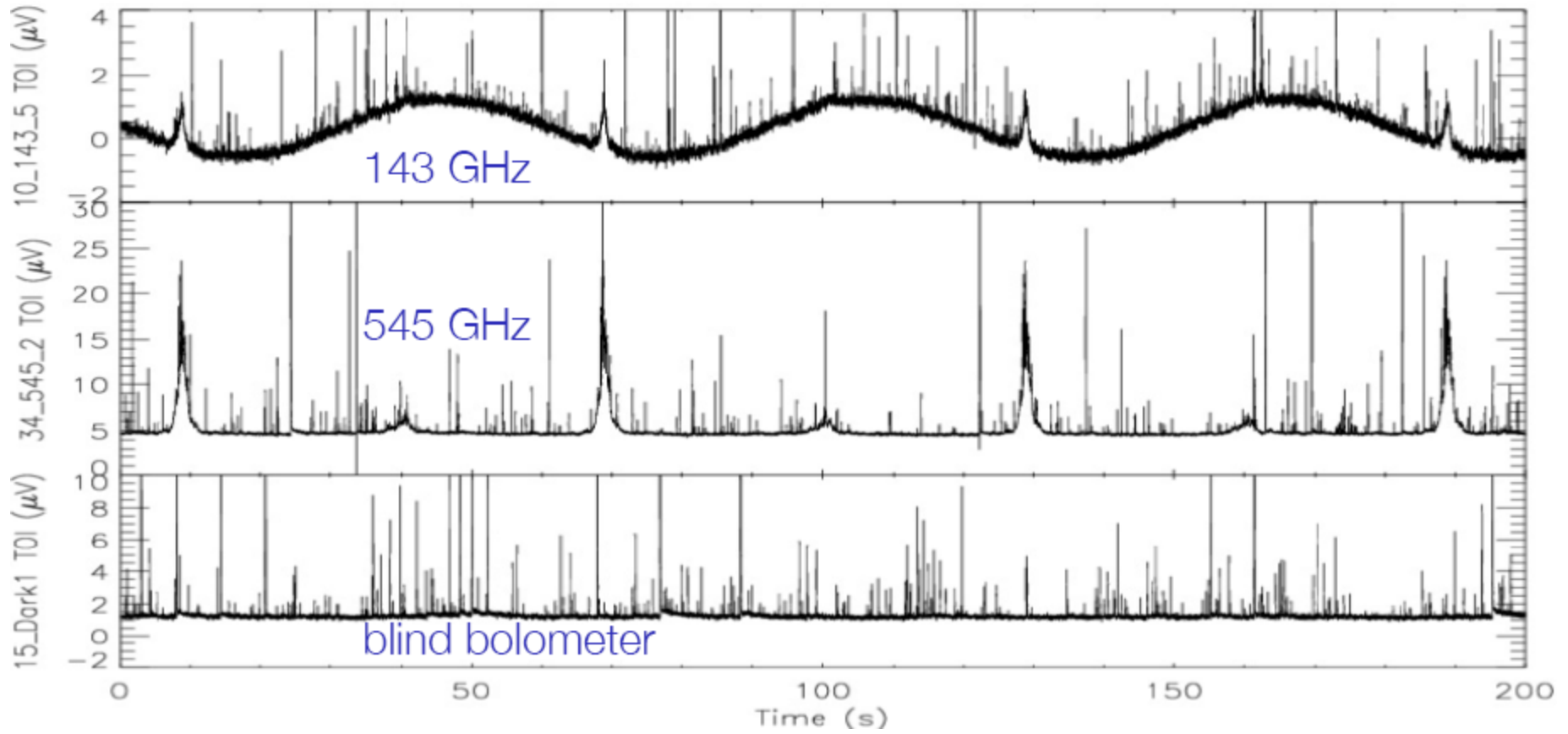
# A very stable environment



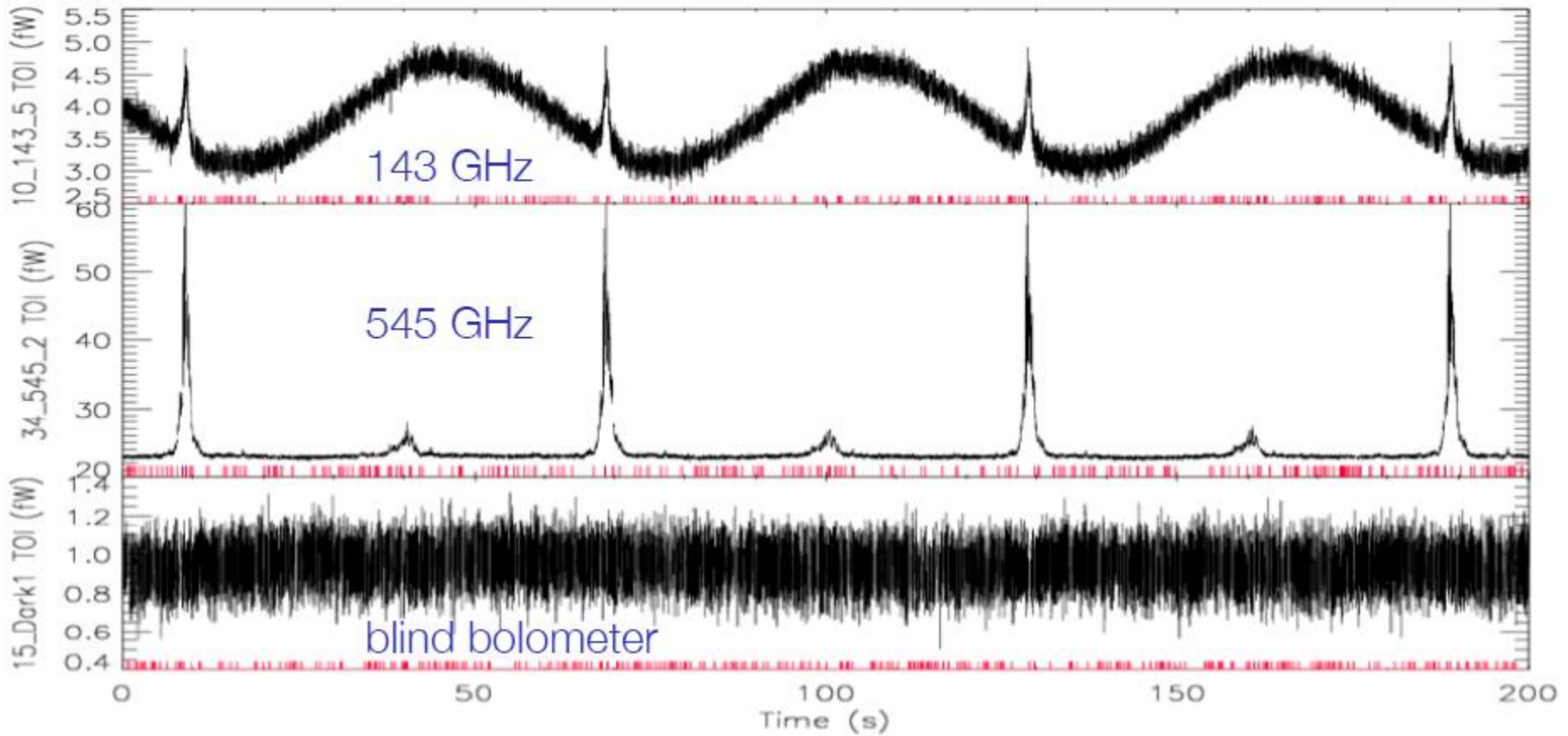
Cryostat:  
dilution He3/He4

**Fig. 7.** The impressive stability of the HFI thermal stages during operations. Shown is the temperature evolution of the bolometer stage (*top*), the 1.6 K optical filter stage (*middle*) and the 4-K cooler reference load stage (*bottom*). The horizontal axis displays days since the beginning of the nominal mission.

# Raw HFI data

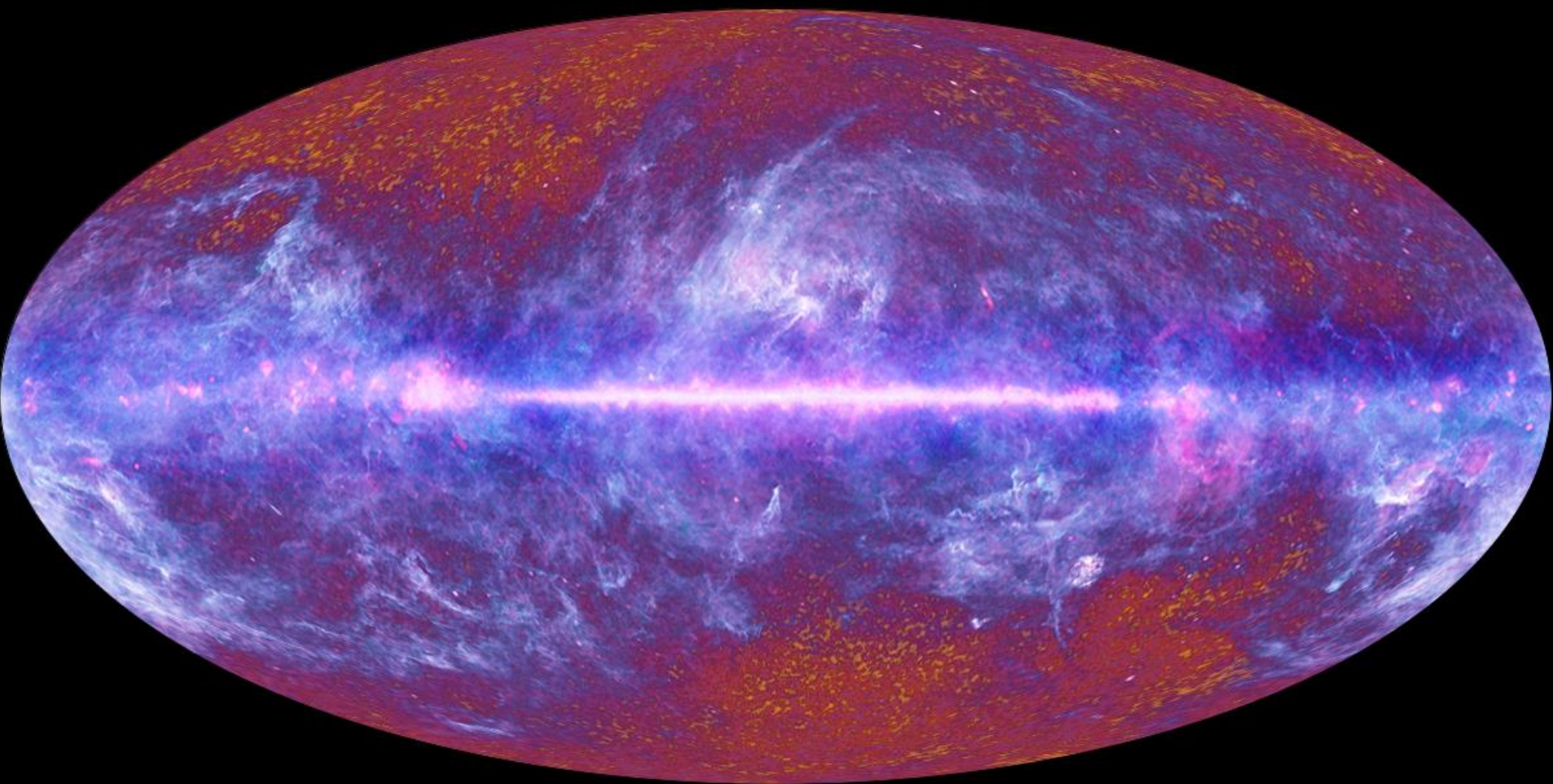


# De-spiked HFI data



<20% of data flagged

2011 data release



Planck one-year all-sky survey



(c) ESA, HFI and LFI consortia, J



# The 2013 Planck results

- Planck 2013 results. I. Overview of products and results
- Planck 2013 results. II. Low Frequency Instrument data processing
- Planck 2013 results. III. LFI systematic uncertainties
- Planck 2013 results. IV. LFI beams
- Planck 2013 results. V. LFI calibration
- Planck 2013 results. VI. High Frequency Instrument data processing
- Planck 2013 results. VII. HFI time response and beams
- Planck 2013 results. VIII. HFI calibration and mapmaking
- Planck 2013 results. IX. HFI spectral response
- Planck 2013 results. X. HFI energetic particle effects
- Planck 2013 results. XI. Consistency of the data
- Planck 2013 results. XII. Component separation
- Planck 2013 results. XIII. Galactic CO emission
- Planck 2013 results. XIV. Zodiacal emission
- Planck 2013 results. XV. CMB power spectra and likelihood
- Planck 2013 results. XVI. Cosmological parameters
- Planck 2013 results. XVII. Gravitational lensing by large-scale structure
- Planck 2013 results. XVIII. The gravitational lensing-infrared background correlation
- Planck 2013 results. XIX. The integrated Sachs-Wolfe effect
- Planck 2013 results. XX. Cosmology from Sunyaev-Zeldovich cluster counts
- Planck 2013 results. XXI. All-sky Compton-parameter map and characterization
- Planck 2013 results. XXII. Constraints on inflation
- Planck 2013 results. XXIII. Isotropy and statistics of the CMB
- Planck 2013 results. XXIV. Constraints on primordial non-Gaussianity
- Planck 2013 results. XXV. Searches for cosmic strings and other topological defects
- Planck 2013 results. XXVI. Background geometry and topology of the Universe
- Planck 2013 results. XXVII. Special relativistic effects on the CMB dipole
- Planck 2013 results. XXVIII. The Planck Catalogue of Compact Sources
- Planck 2013 results. XXIX. The Planck catalogue of Sunyaev-Zeldovich sources
- Planck 2013 results. Explanatory supplement

**29 papers (+1 to come on CIB);**

**800+ pages**

**1 Explanatory Supplement**

**all products available online**

# The 2013 Planck results

- Planck 2013 results. I. Overview of products and results
- Planck 2013 results. II. Low Frequency Instrument data processing
- Planck 2013 results. III. LFI systematic uncertainties
- Planck 2013 results. IV. LFI beams
- Planck 2013 results. V. LFI calibration
- Planck 2013 results. VI. High Frequency Instrument data processing
- Planck 2013 results. VII. HFI time response and beams
- Planck 2013 results. VIII. HFI calibration and mapmaking
- Planck 2013 results. IX. HFI spectral response
- Planck 2013 results. X. HFI energetic particle effects
- Planck 2013 results. XI. Consistency of the data

- Planck 2013 results. XII. Component separation
- Planck 2013 results. XIII. Galactic dust emission
- Planck 2013 results. XIV. Zodiacal emission

- Planck 2013 results. XV. CMB power spectra and likelihood
- Planck 2013 results. XVI. Cosmological parameters

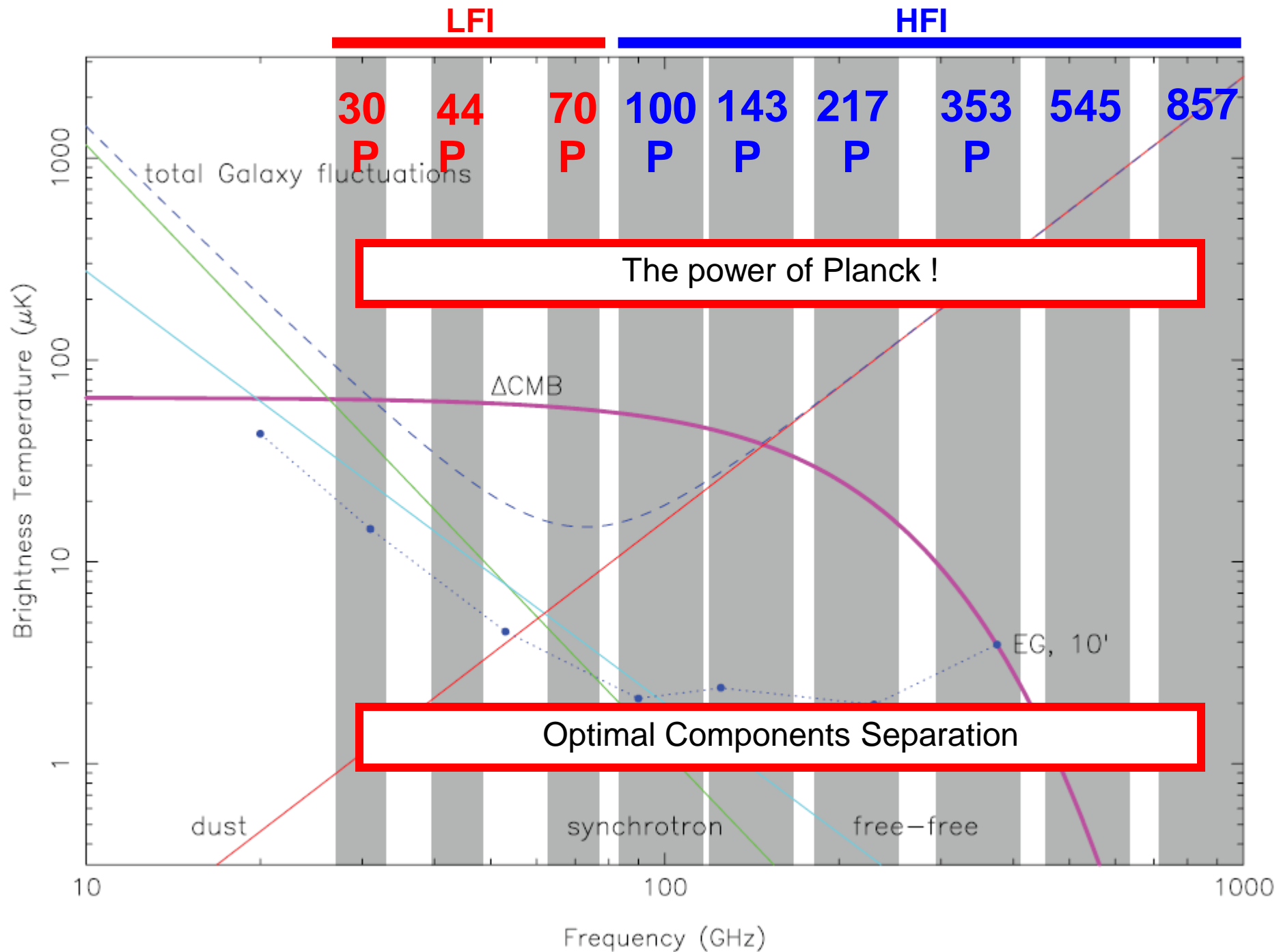
- Planck 2013 results. XVII. Gravitational lensing by large-scale structure
- Planck 2013 results. XVIII. The gravitational lensing-infrared background correlation
- Planck 2013 results. XIX. The integrated Sachs-Wolfe effect

- Planck 2013 results. XX. Cosmology from Sunyaev-Zeldovich cluster counts
- Planck 2013 results. XXI. All-sky Compton-parameter map and characterization

- Planck 2013 results. XXII. Constraints on inflation
- Planck 2013 results. XXIII. Isotropy and statistics of the CMB
- Planck 2013 results. XXIV. Constraints on primordial non-Gaussianity
- Planck 2013 results. XXV. Searches for cosmic strings and other topological defects
- Planck 2013 results. XXVI. Background geometry and topology of the Universe
- Planck 2013 results. XXVII. Special relativistic effects on the CMB dipole

- Planck 2013 results. XXVIII. The Planck Catalogue of Compact Sources
- Planck 2013 results. XXIX. The Planck catalogue of Sunyaev-Zeldovich sources
- Planck 2013 results. Explanatory supplement

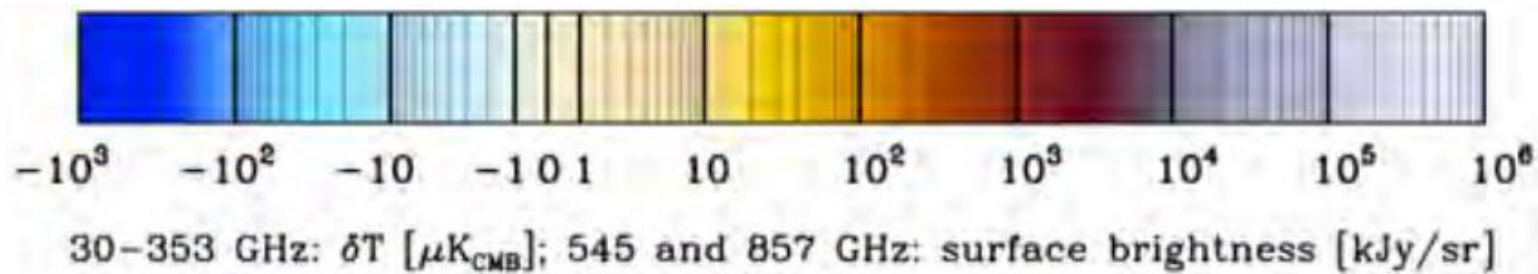
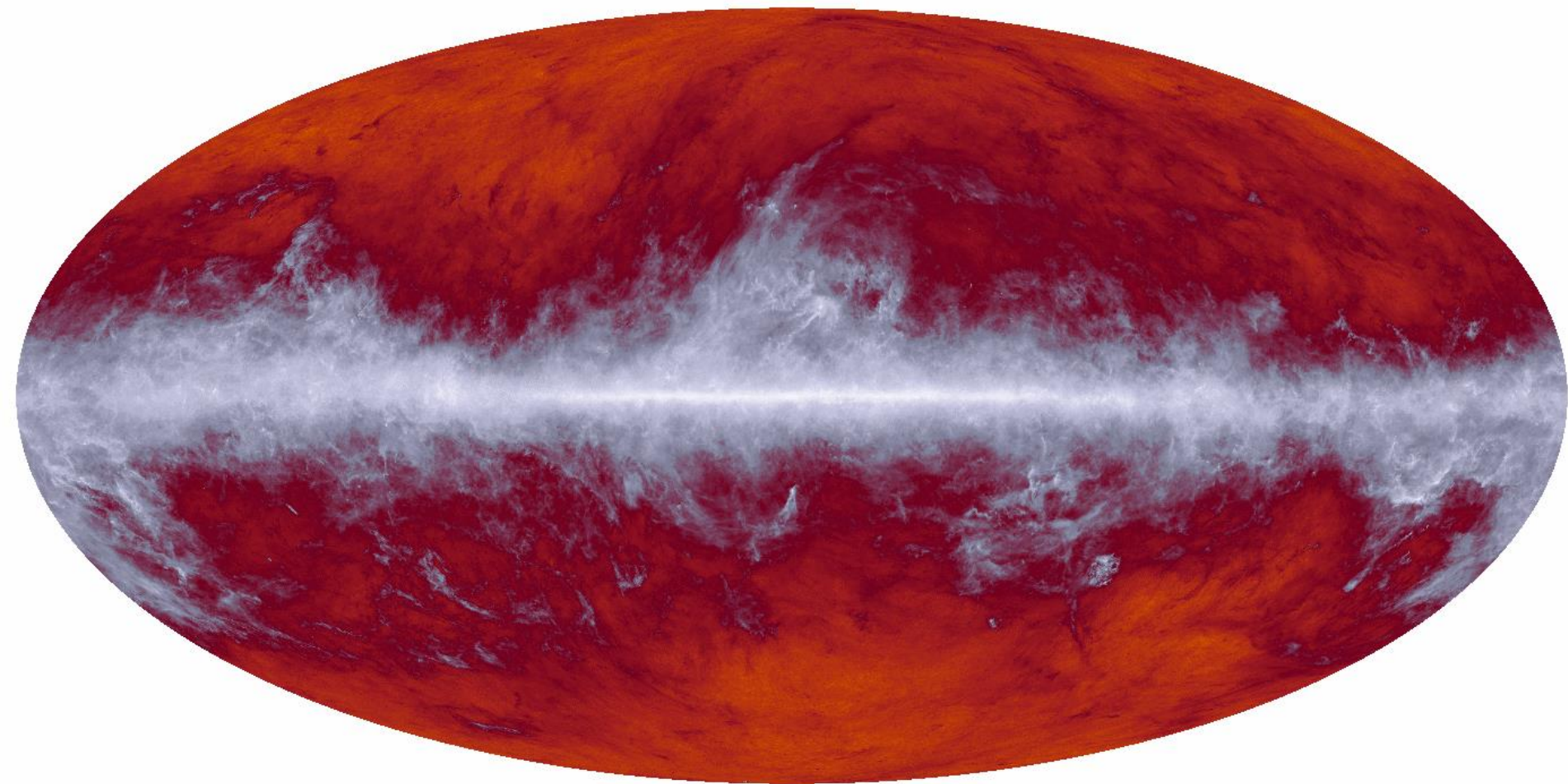
**29 papers (+1 to come on CIB);**  
**800+ pages**  
**1 Explanatory Supplement**  
**all products available online**



# Planck Legacy Maps

$6 \times 10^6$  pixels (5')

857 GHz



# How are the maps obtained ?

- In a scanning telescope each detector explores different sky pixels during the sky scan.
- The measured signal (in Volt) versus time is called TOD (time-ordered data). The TOD  $V(t)$  is the sum of the signal from the sky in the direction explored at a given time plus the noise at the same time.
- The signal can be converted into a brightness or a brightness temperature if the measurement system is calibrated, i.e. if responsivity, throughput, angular response are known:

$$V(t) = \eta \mathcal{R} A \int_0^{\infty} d\nu \int_{4\pi} d\Omega RA(\theta, \varphi) B(\theta, \varphi, \nu) e(\nu) + n(t)$$

- Given the statistical nature of this equation, where the  $n(t)$  term is stochastic and can be dominant, **our goal is to find the most likely sky map given the measured TOD.**
- To do that, one has to know the pointing information  $\theta(t)$  and  $\phi(t)$ , and the noise properties of the measured data.
- The statistical procedure to find the most likely map is called MAP-MAKING

- A suitable pixelization (e.g. Healpix) associates univocally, for the  $i$ -th sample

$$(\theta_i, \varphi_i) \leftrightarrow p_j$$

where  $j$  defines the observed pixel, while  $i$  defines the data sample

- The measurement can be rewritten in simplified form

$$V_i = kB_j + n_i$$

where  $k$  depends on the calibration and  $B_j$  is the sky brightness in pixel  $j$ , convolved with the angular response of the instrument.

- The equation  $V_i = kB_j + n_i$  can be rewritten in matrix form

$$\vec{d} = k\vec{A}\vec{m} + \vec{n}$$

- where  $\vec{A}$  is the pointing matrix, associating the observed pixel to each data sample
- In the case of a single-beam scanning telescope (like Planck) every line of  $A$  is filled with zeros, with just one 1 in the column of the observed pixel.
- If, instead, every sample is the result of a differential measurement (WMAP, OLIMPO...) there will be a 1 in the column of the pixel observed by beam A, and a -1 in the column of the pixel observed by beam B.

- $\vec{A}$  has  $nd \times np$  elements, where  $nd$  is the number of samples, and  $np$  is the number of pixels in the map.
- If you apply  $A$  to a sky map, you get a TOD.
- ${}^T \vec{A}$ , instead, applied to a data vector produces the sum of all the data which observed the same pixel.
- The product  ${}^T \vec{A} \vec{A}$  is a diagonal matrix including the number of samples per pixel.



- So, the solution of the system

$$\vec{d} = \vec{A}\vec{m} + \vec{n}$$

- is our best estimate  $\tilde{\vec{m}}$  of the sky map  $\vec{m}$
- And a trivial solution might be

$$\tilde{\vec{m}} = (\vec{A}^T \vec{A})^{-1} \vec{A}^T \vec{d}$$

- Which computes for each pixel the arithmetic average of the signals measured in that pixel, so that the noise somewhat averages out.
- This is the correct solution in case of white, uncorrelated noise.

- More in general:

$$\vec{d} = \overleftrightarrow{A}\vec{m} + \vec{n} \quad \rightarrow \quad \vec{n} = \overleftrightarrow{A}\vec{m} - \vec{d}$$

- If the noise properties are described by a multivariate Gaussian, to allow for correlations, the likelihood is :

$$L = \frac{1}{(2\pi)^{n/2} |\overleftrightarrow{N}|^{1/2}} \exp\left[-\frac{1}{2} \vec{n}^T \overleftrightarrow{N}^{-1} \vec{n}\right]$$

- where

$$\overleftrightarrow{N} = \vec{n} \cdot \vec{n}^T$$

is the autocorrelation function of the noise.

- Noting that  $\vec{n} = \vec{A}\vec{m} - \vec{d}$

$$L = \frac{1}{(2\pi)^{n/2} |N|^{1/2}} \exp\left[-\frac{1}{2} \vec{n}^T \vec{N}^{-1} \vec{n}\right] =$$

$$= \frac{1}{(2\pi)^{n/2} |N|^{1/2}} \exp\left[-\frac{1}{2} (\vec{A}\vec{m} - \vec{d})^T \vec{N}^{-1} (\vec{A}\vec{m} - \vec{d})\right]$$

- The maximum of the likelihood will be obtained from

$$\frac{\partial L}{\partial \vec{m}} = 0 \quad \rightarrow \quad \frac{\partial}{\partial \vec{m}} \left[ (\vec{A}\vec{m} - \vec{d})^T \vec{N}^{-1} (\vec{A}\vec{m} - \vec{d}) \right] = 0$$

$$\frac{\partial}{\partial \mathbf{x}} \mathbf{Ax} = \mathbf{A}$$

$$\frac{\partial}{\partial \mathbf{m}} (\mathbf{d} - \mathbf{Am})^T \mathbf{N}^{-1} (\mathbf{d} - \mathbf{Am}) = 0$$

$$-\mathbf{A}^T \mathbf{N}^{-1} (\mathbf{d} - \mathbf{Am}) - (\mathbf{d} - \mathbf{Am})^T \mathbf{N}^{-1} \mathbf{A} = 0$$

$$-\mathbf{A}^T \mathbf{N}^{-1} (\mathbf{d} - \mathbf{Am}) = 0$$

$$\mathbf{A}^T \mathbf{N}^{-1} \mathbf{d} = \mathbf{A}^T \mathbf{N}^{-1} \mathbf{Am}$$

$$\tilde{\mathbf{m}} = (\mathbf{A}^T \mathbf{N}^{-1} \mathbf{A})^{-1} \mathbf{A}^T \mathbf{N}^{-1} \mathbf{d}$$

To be compared to  $\tilde{\vec{m}} = (\overset{\leftrightarrow}{\mathbf{A}} \overset{\leftrightarrow}{\mathbf{A}})^{-1} \overset{\leftrightarrow}{\mathbf{A}} \vec{d}$

# Map making

- There is a rich literature on the best numerical implementation of the solution

$$\vec{\tilde{m}} = (\vec{A}^T \vec{N}^{-1} \vec{A})^{-1} \vec{A}^T \vec{N}^{-1} \vec{d}$$

- The most trivial way to solve it involves the inversion of the noise autocorrelation matrix  $N$ .
- This has dimensions  $n_d \times n_d$ , so it is huge (ex. for 1 year of Planck data  $n_d = 6 \times 10^9$ ).
- If  $N$  is not diagonal, the inversion can be performed only if  $N$  is sparse.
- Anyway, important computing resources are needed. See e.g. [astro-ph/0106451](#)

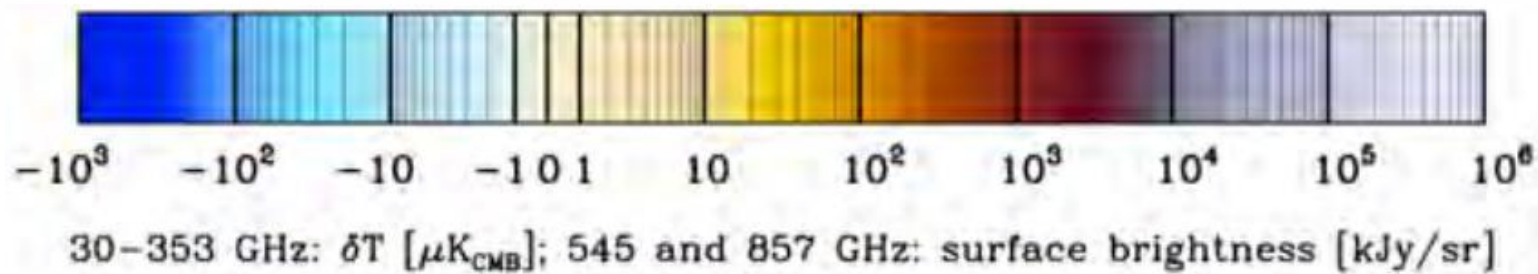
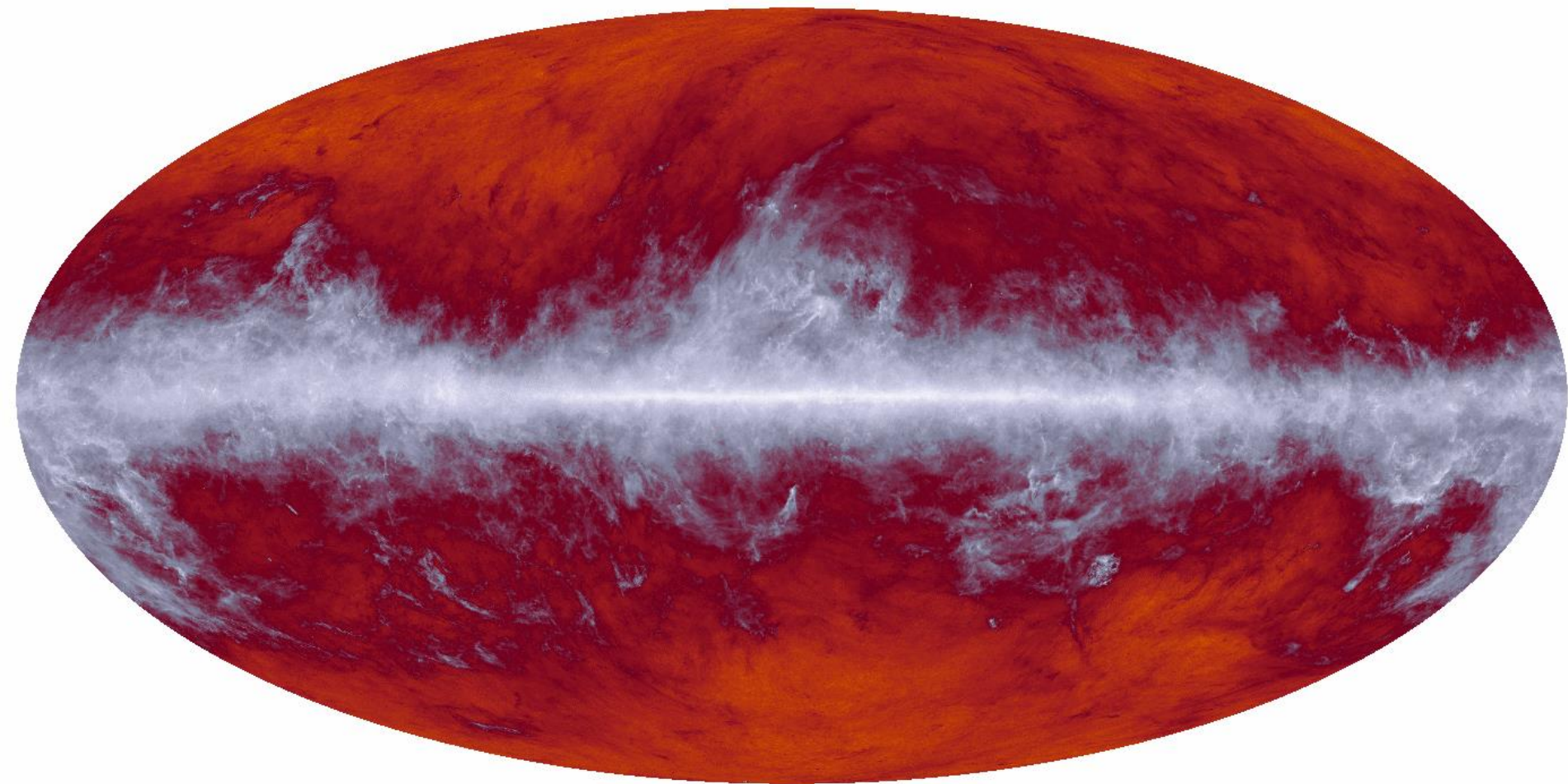
# Planck maps

- Pixelized using Healpix
  - <http://healpix.jpl.nasa.gov/>
- Formatted in FITS files (Flexible Image Transport System)
  - <http://fits.gsfc.nasa.gov/>
- Archived at the Planck Legacy Archive
  - <http://www.cosmos.esa.int/web/planck/pla>

# Planck Legacy Maps

$6 \times 10^6$  pixels (5')

857 GHz



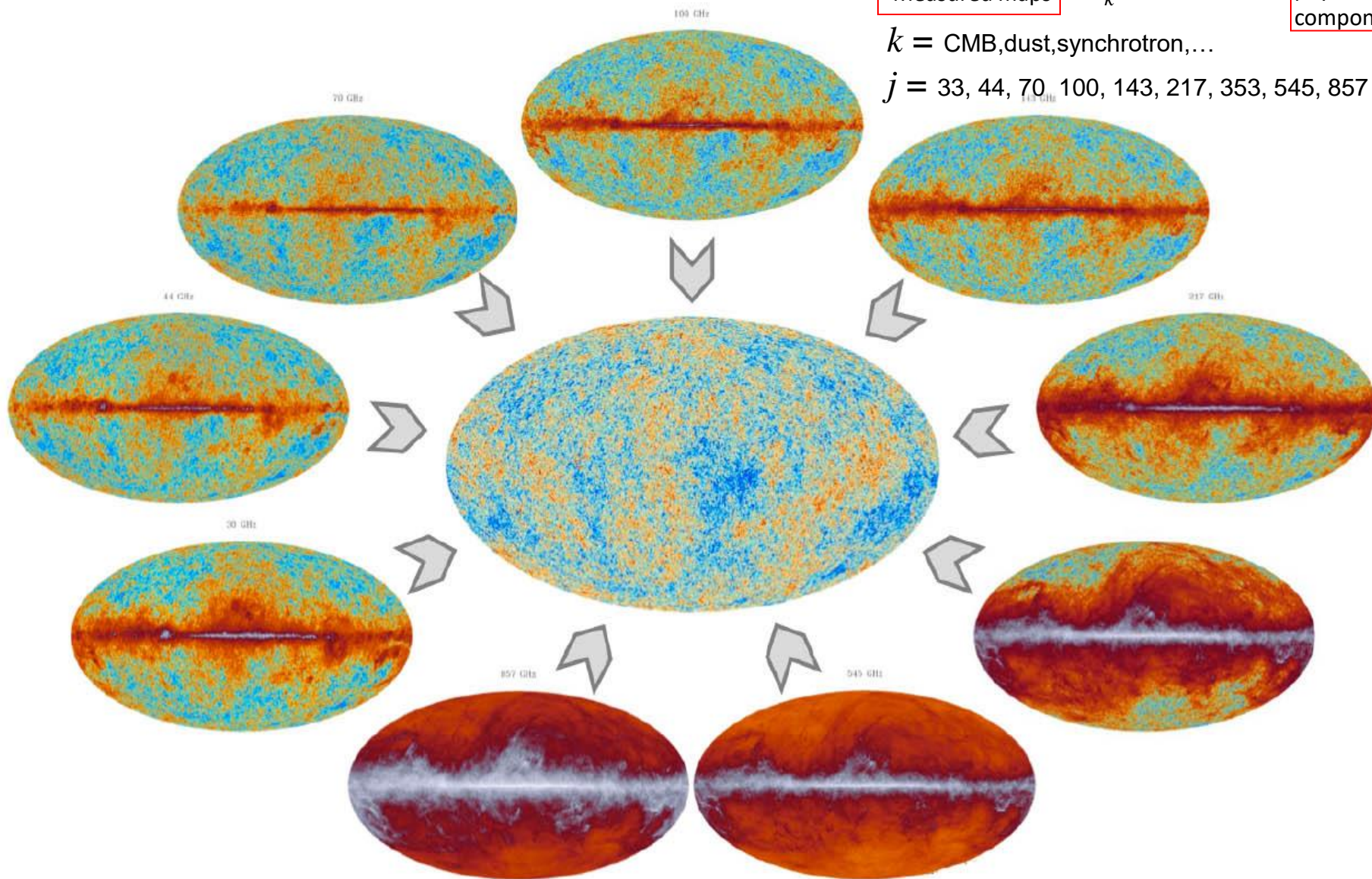
# components separation

$$\Delta T(\nu_j, \ell, b) = \sum_k a_k(\nu_j, \ell, b) C_k(\ell, b)$$

Measured maps physical components

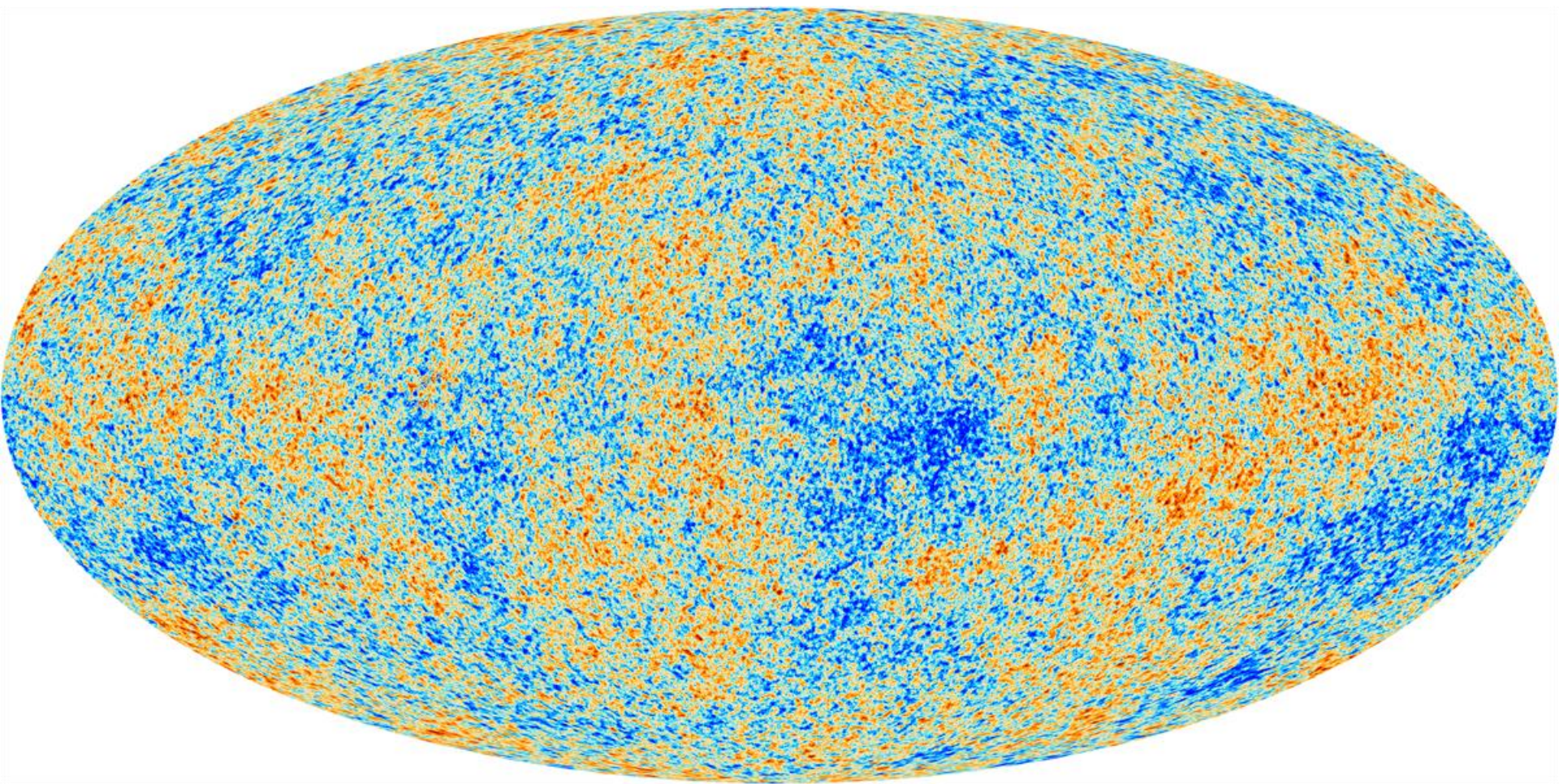
$k = \text{CMB, dust, synchrotron, ...}$

$j = 33, 44, 70, 100, 143, 217, 353, 545, 857 \text{ GHz}$



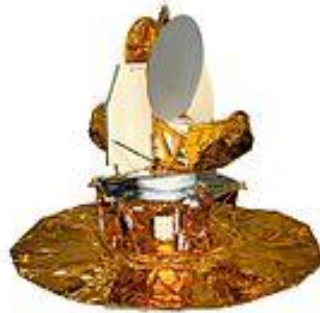


The CMB component

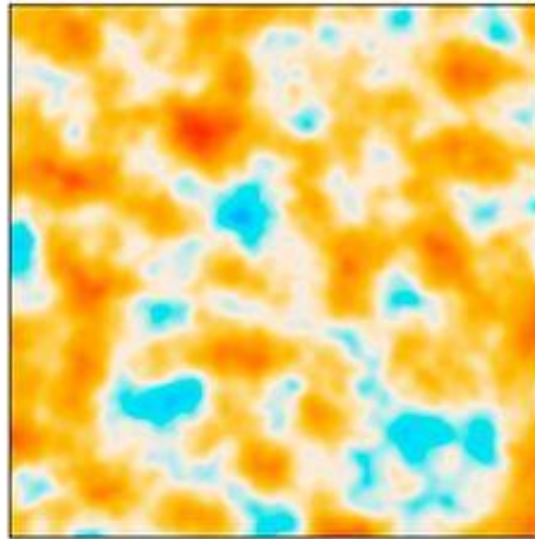




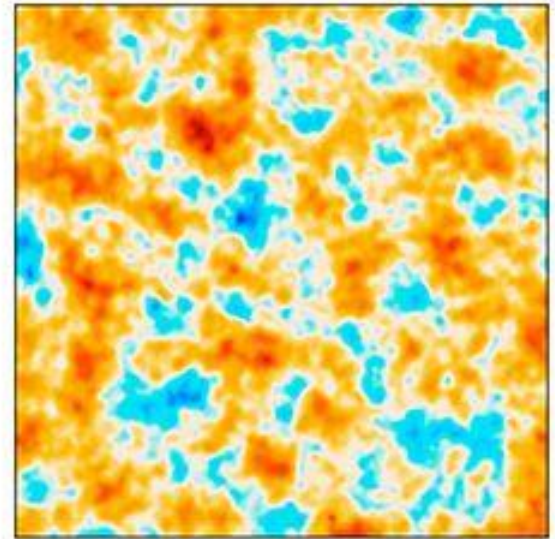
BOOMERanG  
↓



COBE



WMAP



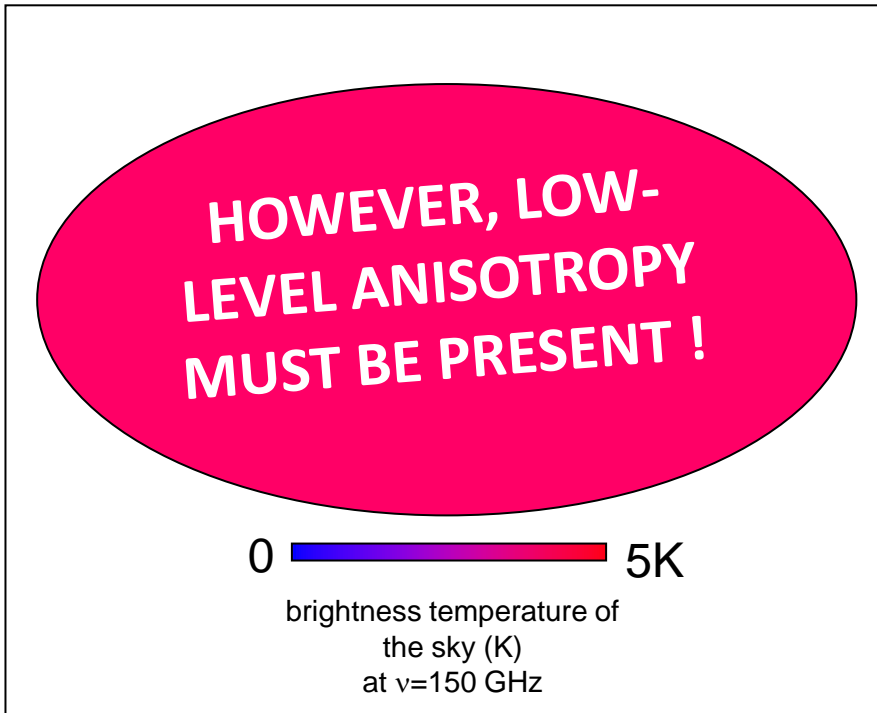
Planck

Best angular resolution  
Best control of foregrounds  
Best control of systematics

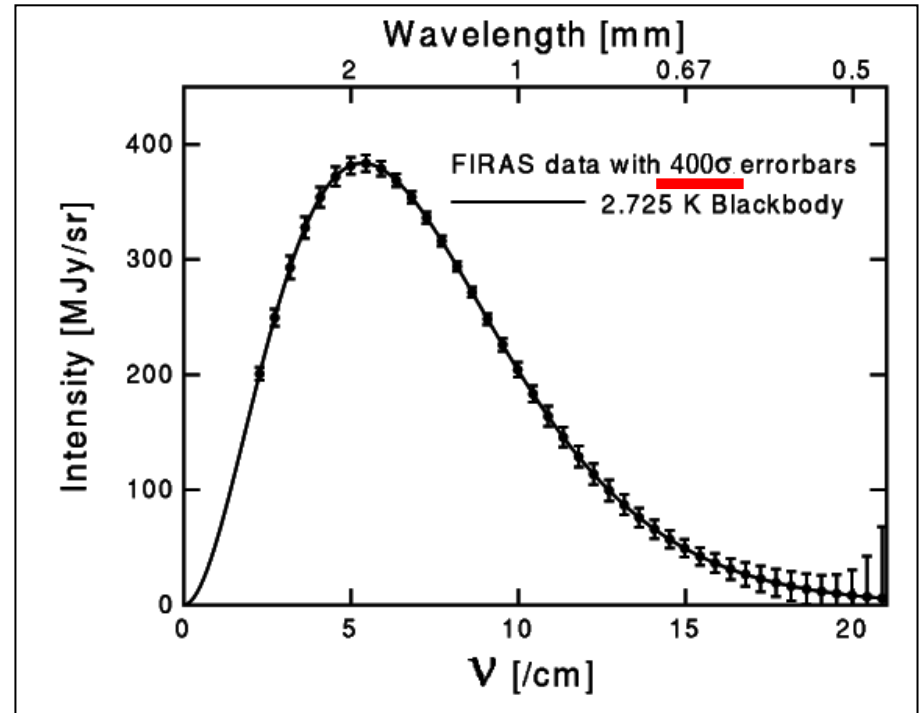
# The Cosmic Microwave Background (CMB)

- Empirically:
  - The CMB is an abundant background of photons, *remarkably isotropic* over the entire sky.
  - Its specific brightness is *remarkably close to a blackbody* with a temperature  $T_0=2.725\text{K}$

isotropy



specific brightness



# CMB anisotropy (intrinsic)

- For the first 380000 yrs the «early» universe is a plasma of baryons, dark matter, and photons.
- 380000 yrs after the big-bang the temperature drops below 3000K, and the formation of H atoms is possible. The universe becomes transparent.
- CMB photons, whose mean free path against free electrons had been very short during the early phases, now can travel without further interactions, all the way to our telescopes, 13.7 Gyrs later.
- They carry the image of the «last scattering surface», depicting how the universe was 380000 years after the big bang.
- The early universe was to first order homogenous and isotropic. However, a low-level of anisotropy in the CMB photons is expected.
- For two reasons:
  - Small inhomogeneities should be present at recombination, as seeds of the formation of cosmic structures, evident in the present universe.
  - The expansion of the universe has been so fast in the early phases that regions which are causally connected today were not causally connected at recombination, when CMB photons are released. The last scattering surface should be a patchwork of regions which are not causally connected, so cannot be exactly the same

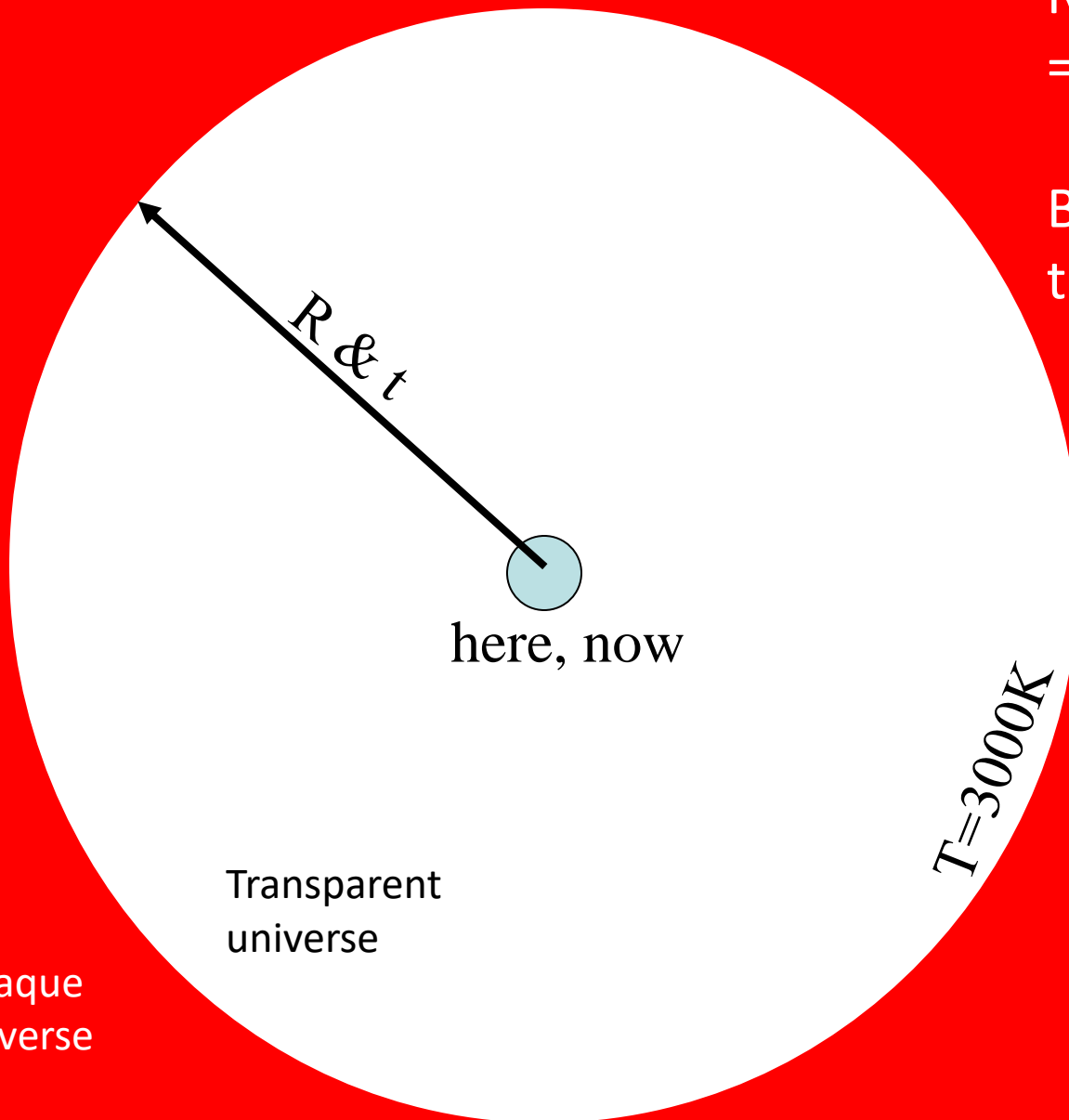
$$\frac{\Delta\rho}{\rho} \approx 10^{-5}$$



$$\frac{\Delta\rho}{\rho} \approx 10^5$$

R= distance from us  
= 8.3 Gpc = 27Gly

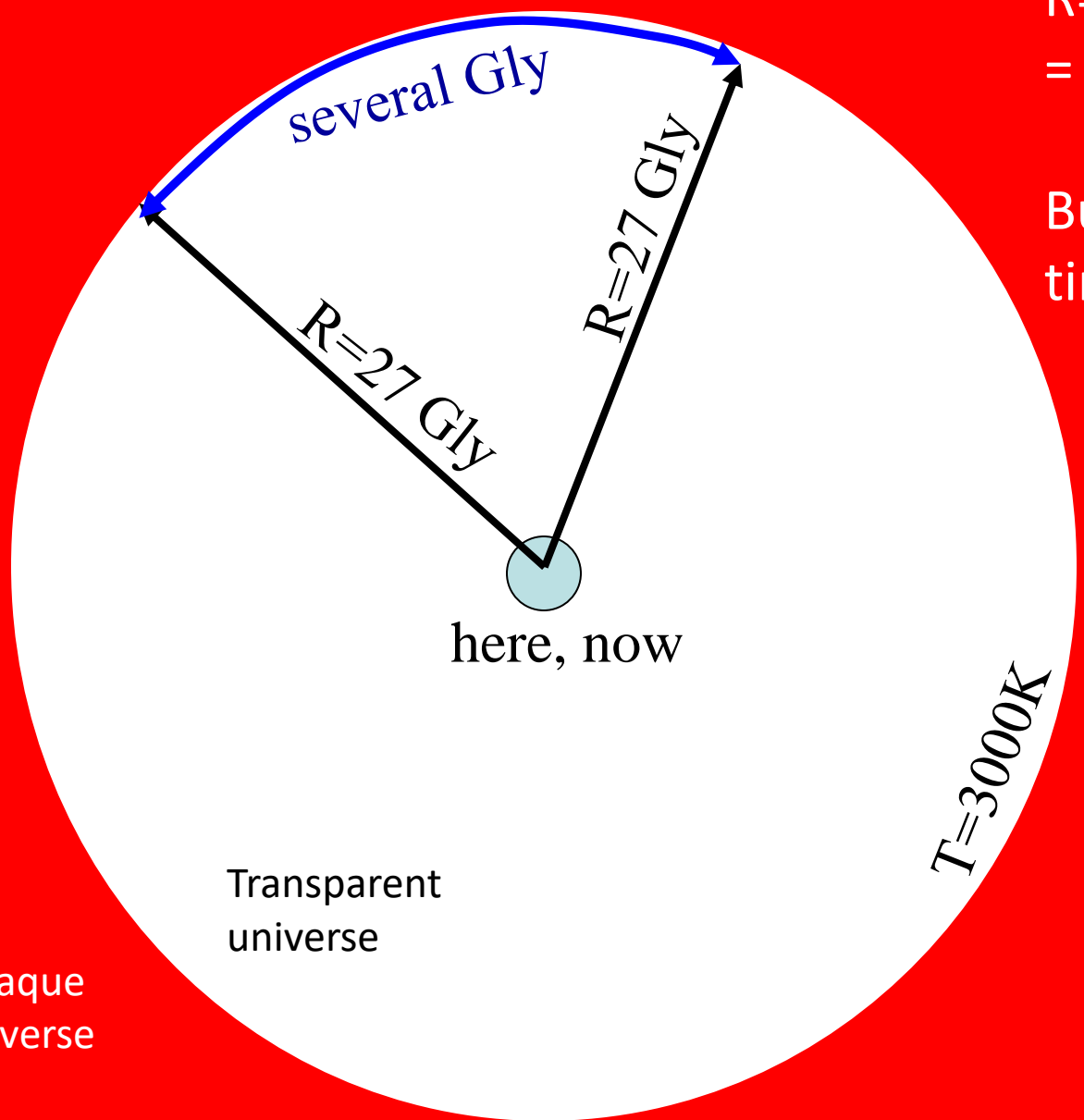
But also distance in  
time: 13.7 Gyrs ago



Opaque  
universe

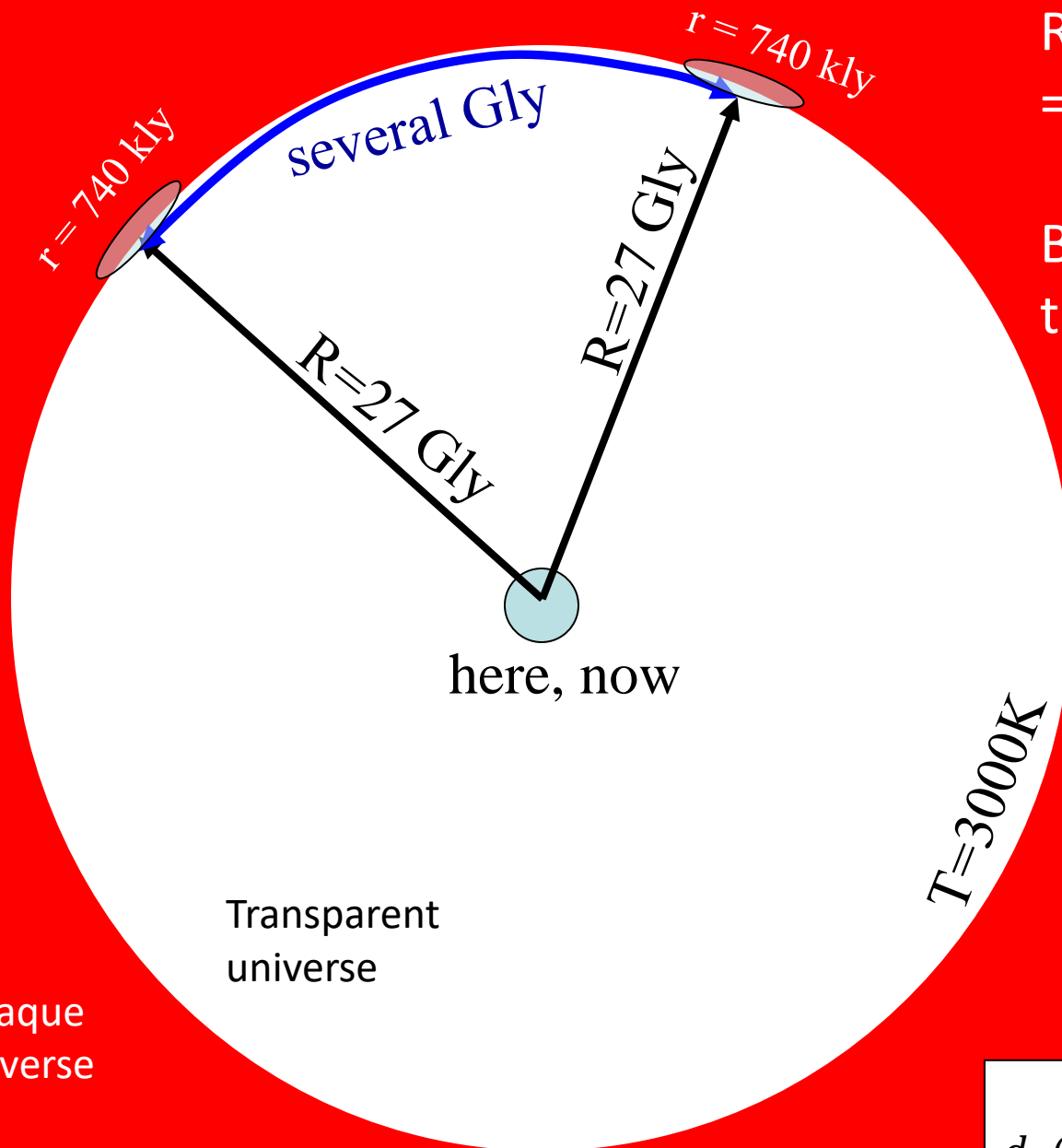
Transparent  
universe

$T=3000K$



R= distance from us  
= 8.3 Gpc = 27Gly

But also distance in  
time: 13.7 Gyrs ago



$R$  = distance from us  
 = 8.3 Gpc = 27Gly

But also distance in  
 time: 13.7 Gyrs ago

Causal horizon  
 (at a given epoch):

distance travelled by  
 light from the big-  
 bang to the epoch of  
 interest.

In a static universe  
 would be  $ct$   
 In an expanding  
 universe, can be  
 computed as:

$$d_h(t_e) = a(t_e) \int_0^{t_e} \frac{cdt}{a(t)}$$

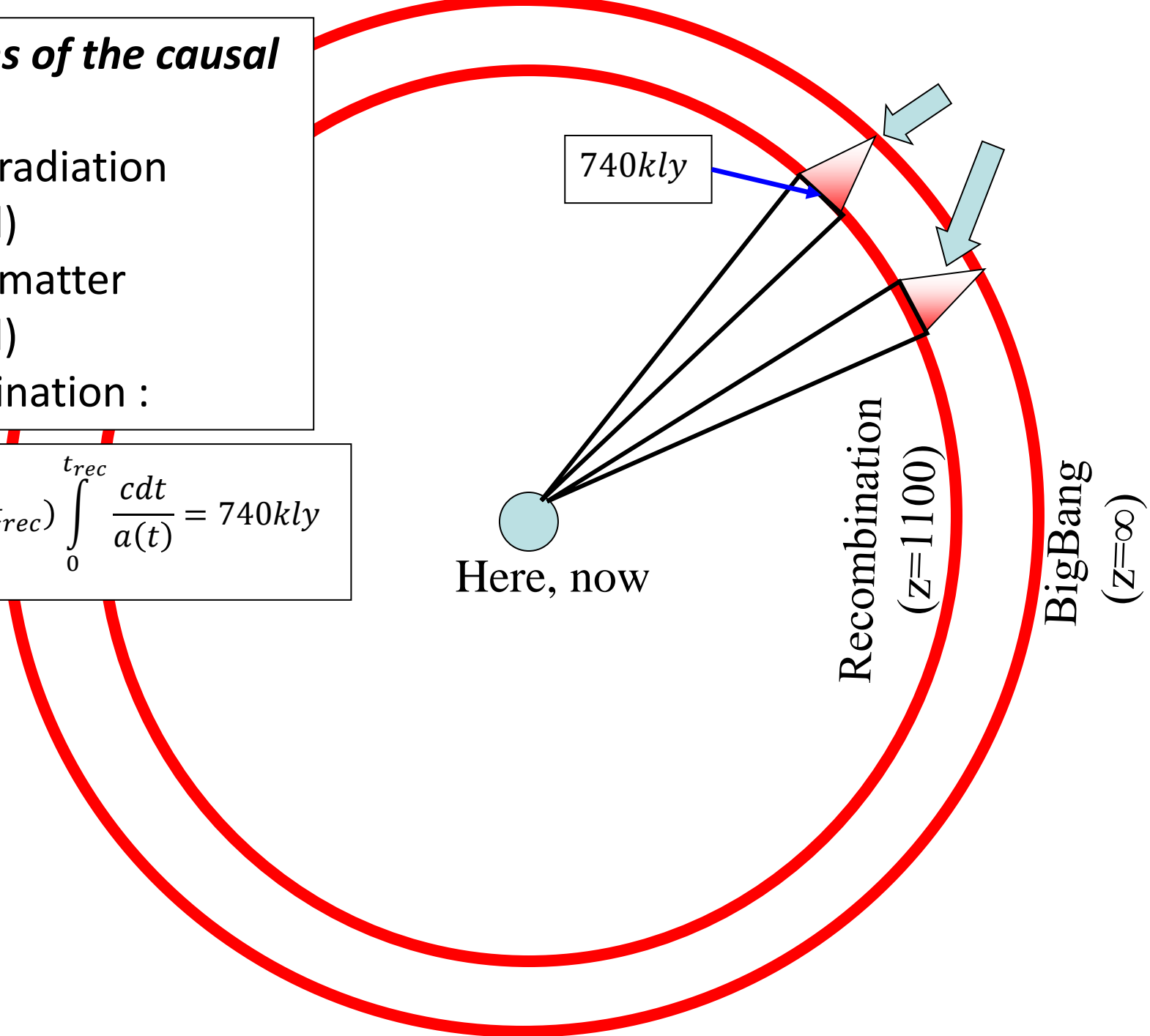
**Dimensions of the causal horizon:**

2ct (when radiation dominated)

3ct (when matter dominated)

At recombination :

$$d_h(t_{rec}) = a(t_{rec}) \int_0^{t_{rec}} \frac{cdt}{a(t)} = 740kly$$



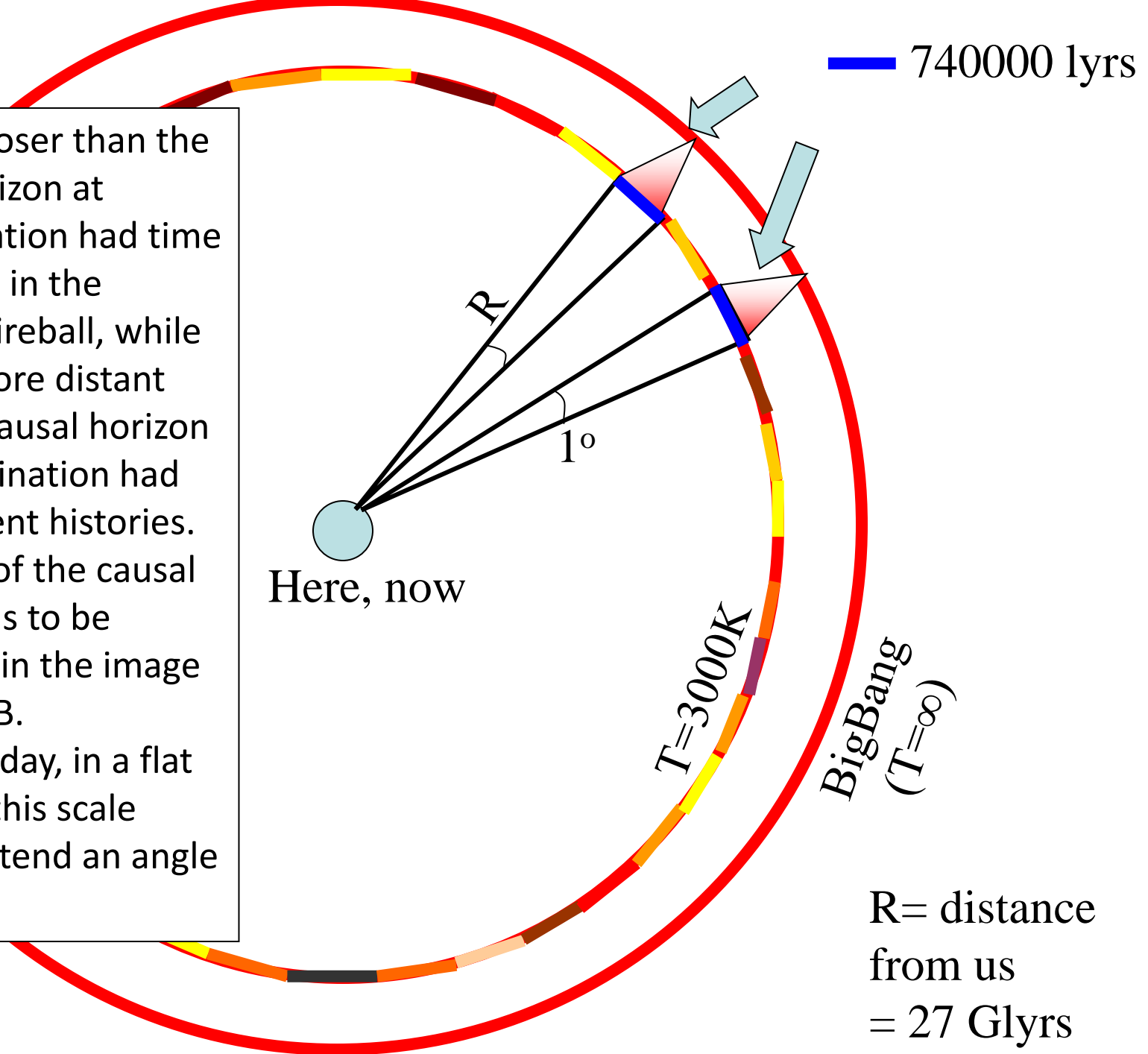
Here, now

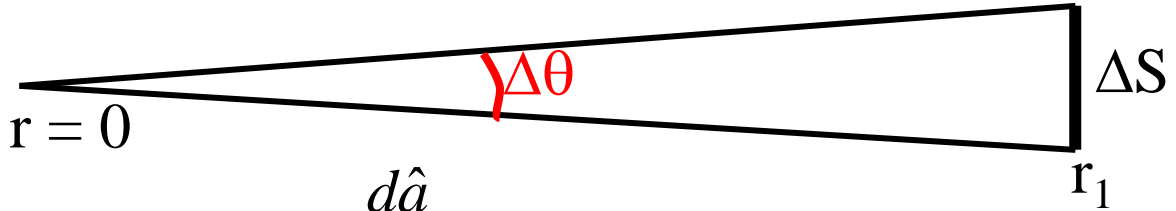
Recombination  
(z=1100)

BigBang  
(z=∞)



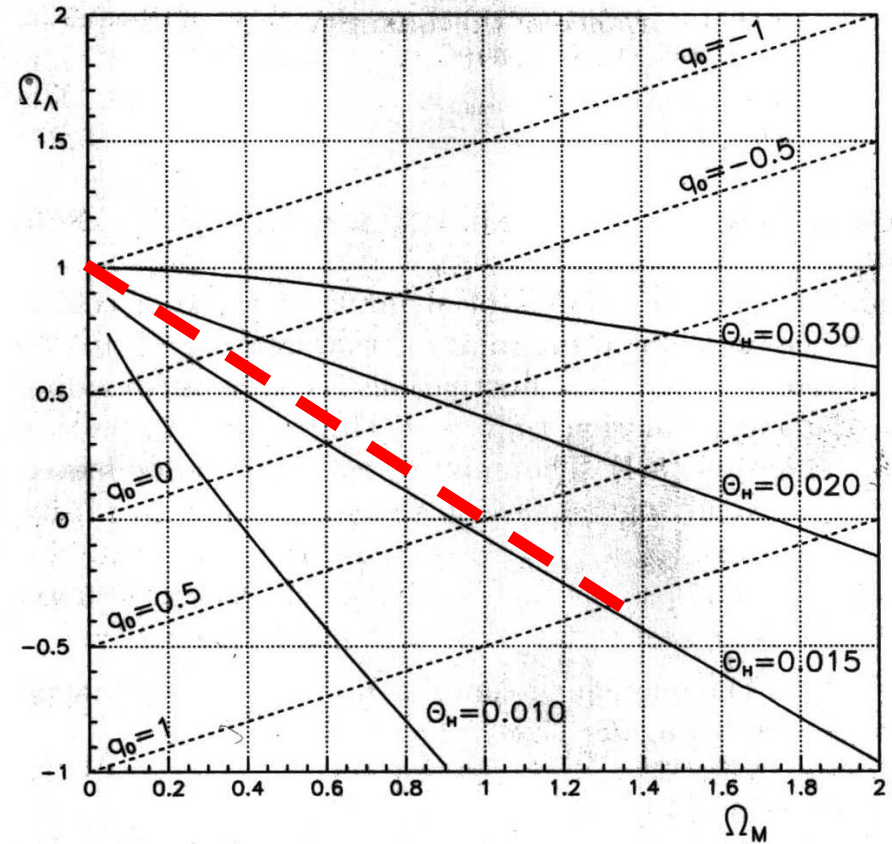
- Regions closer than the causal horizon at recombination had time to interact in the primeval fireball, while regions more distant than the causal horizon at recombination had independent histories.
- The scale of the causal horizon has to be imprinted in the image of the CMB.
- As seen today, in a flat universe, this scale would subtend an angle of  $1^\circ$ .



$$d_H(t_{rec}) = a(t_{rec}) \int_0^{t_{rec}} \frac{cdt}{a(t)}$$


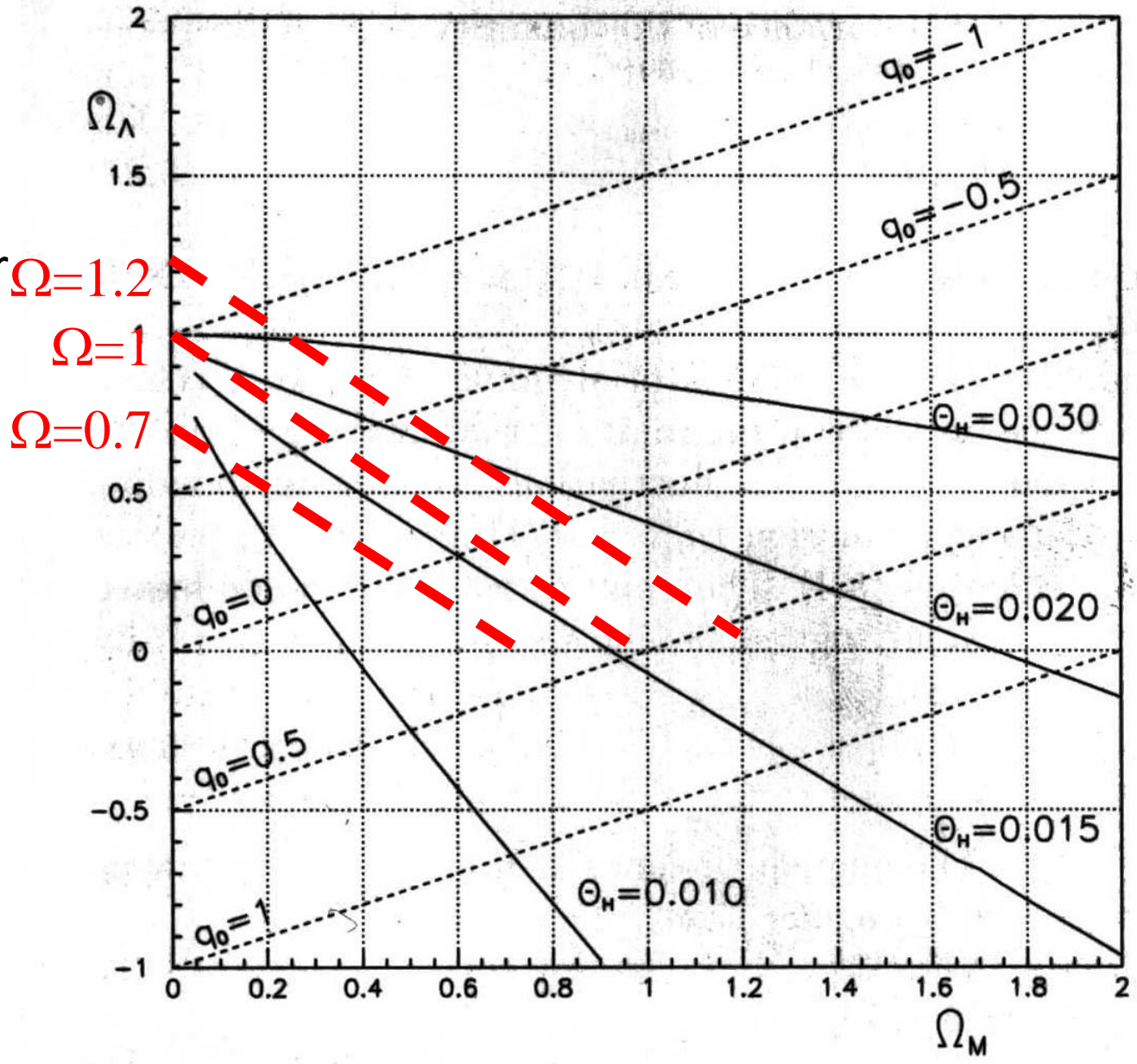
$$D_A = \frac{1}{(1+z_{rec})} \frac{c}{H_0} \int_0^1 \frac{d\hat{a}}{\hat{a}^2 [\Omega_{Mo} \hat{a}^{-3} + \Omega_{\Lambda} + (1 - \Omega_{Mo} - \Omega_{\Lambda}) \hat{a}^{-2}]^{1/2}}$$

- The physical dimension of the horizon at recombination is  $d_H(t_{rec})$ , and subtends an angle  $\theta_H$  which can be computed as  $\theta_H = d_H(t_{rec})/D_A$
- In general the  $\theta_H$  angle is a function of the two parameters  $\Omega_{Mo}$  and  $\Omega_{\Lambda}$ , but is always of the order of  $1^\circ$ .
- If  $\Omega = \Omega_{Mo} + \Omega_{\Lambda} = 1$  (red line),  $\theta_H$  does not depend on the values of  $\Omega_{Mo}$  and  $\Omega_{\Lambda}$  and is 0.015 radians ( $0.85^\circ$ ).



$$q_o = \frac{\Omega_{Mo}}{2} - \Omega_{\Lambda}$$

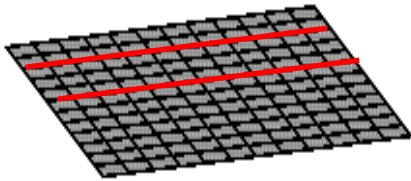
- The 0.015 radians angle is a sort of watershed: larger angles correspond to  $\Omega > 1$ ; smaller angles correspond to  $\Omega < 1$ .
- By measuring  $\Delta\theta$  we can infer the curvature and the average mass-energy density of the universe



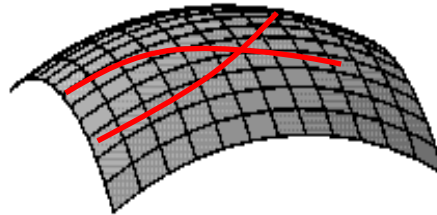
# Which is the geometry of our Universe ?

- According to General Relativity, the presence of mass and energy *curves* the space (see e.g. gravitational lensing effects). Also, the large scale geometry of the Universe is affected by the average mass and energy: their presence curves the background metric of the universe.

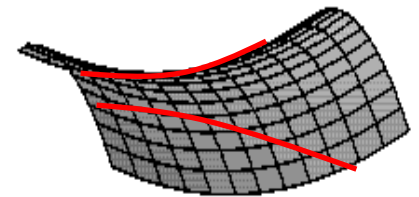
**Flat space in 2-D**



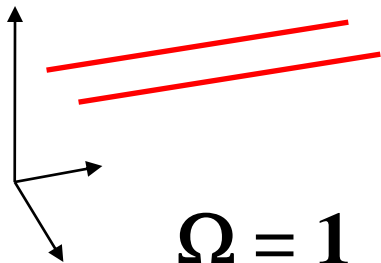
**Curved space in 2-D  
(positive curvature)**



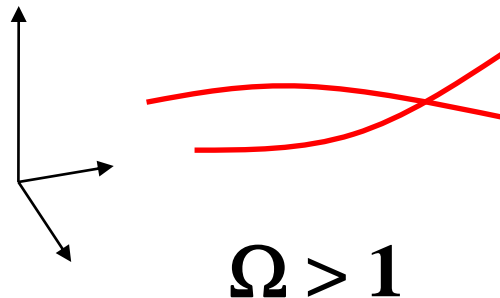
**Curved space in 2-D  
(negative curvature)**



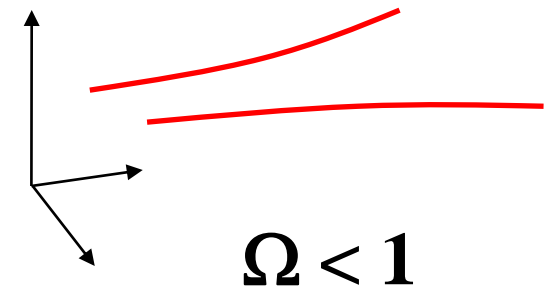
**Flat space in 3-D**

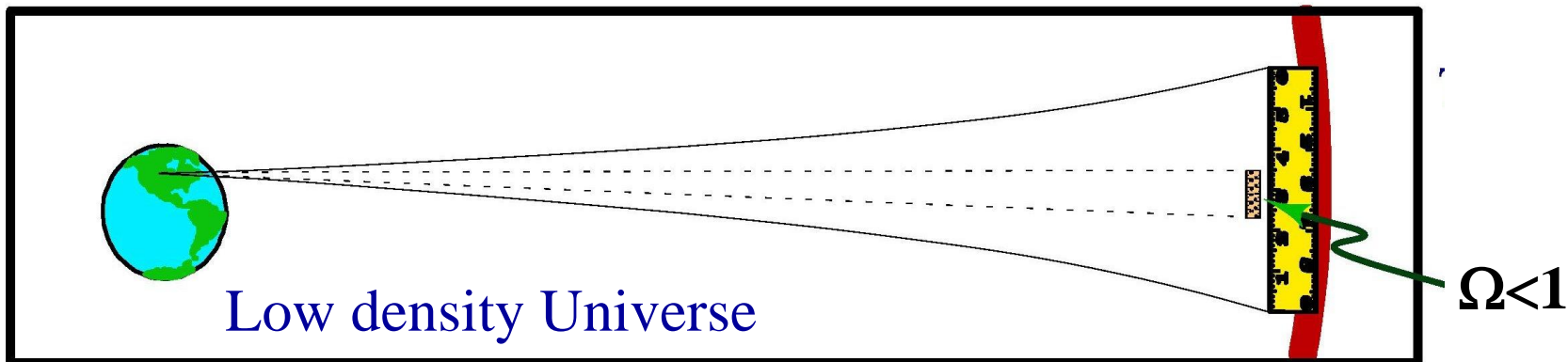
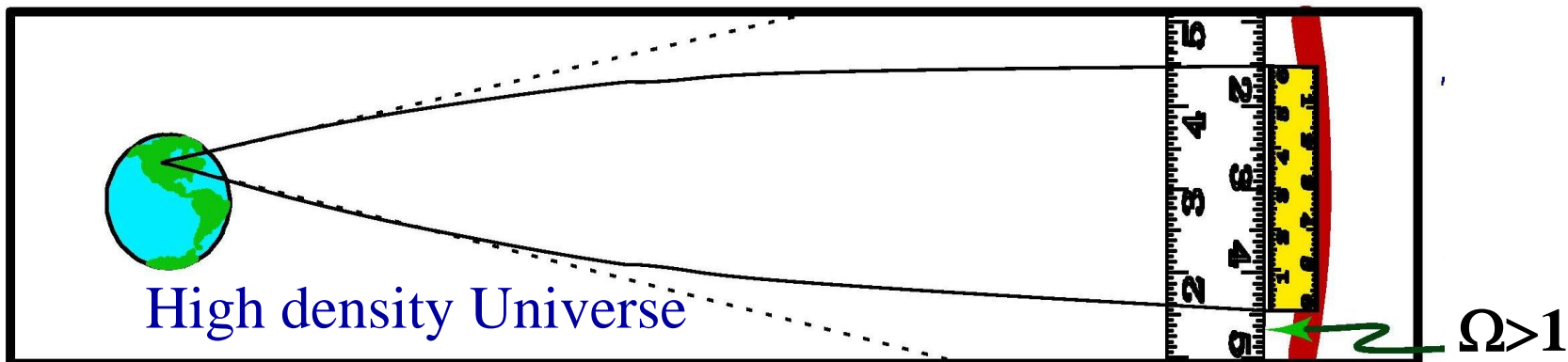
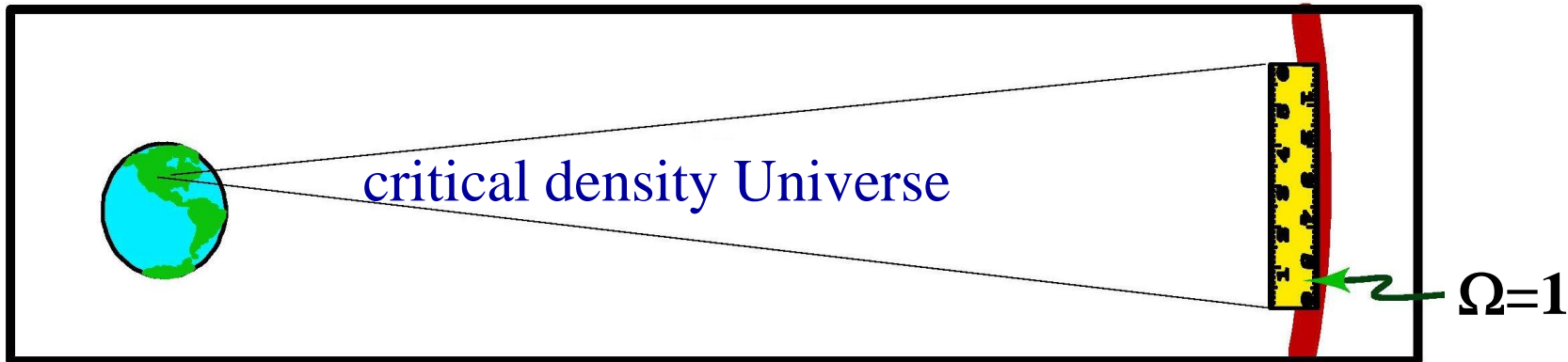


**Curved space in 3-D  
(positive curvature)**



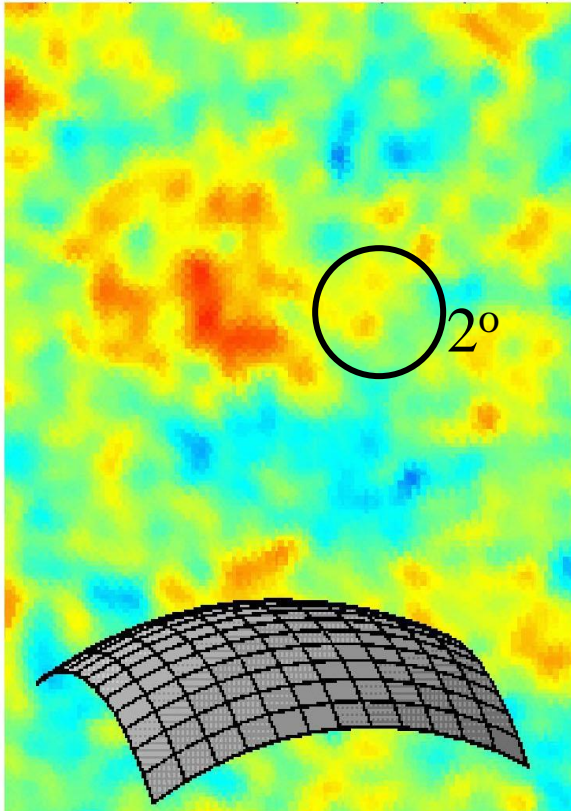
**Curved space in 3-D  
(negative curvature)**



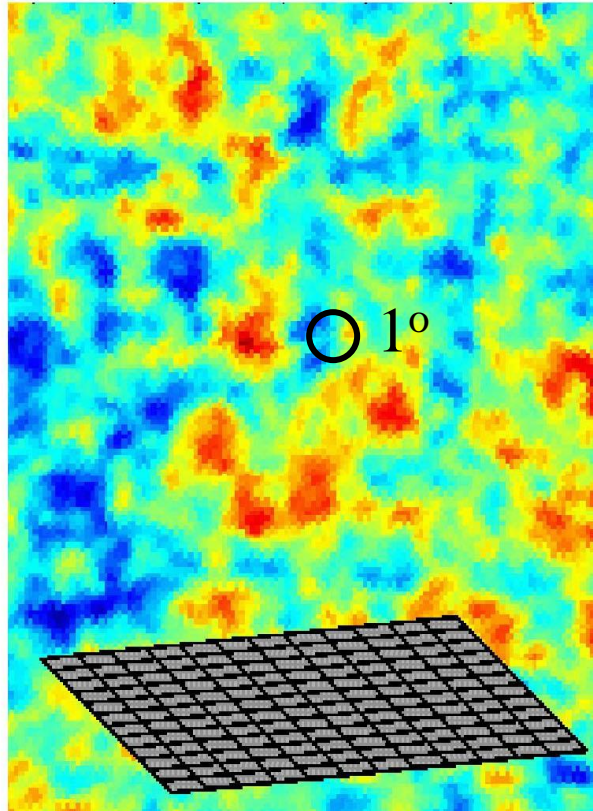


# $\Omega$ and the typical angular dimensions of the structures in the CMB

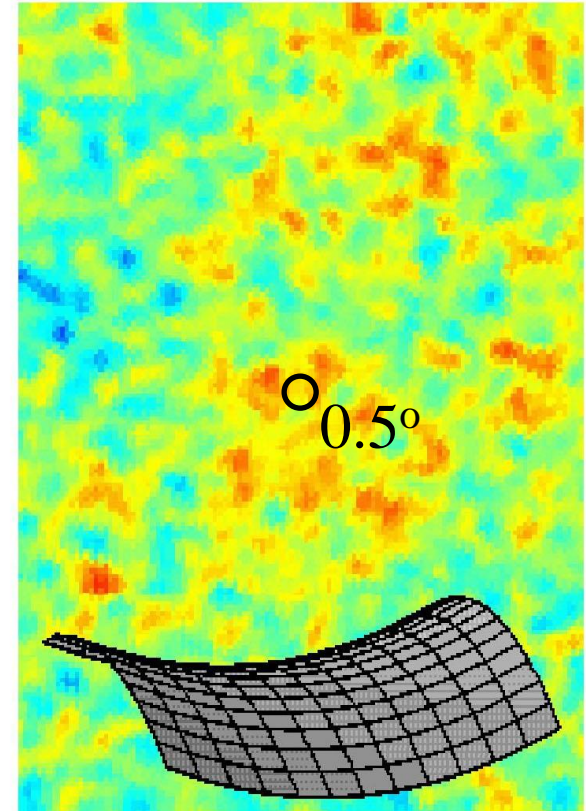
High density Universe  
 $\Omega > 1$



Critical density Universe  
 $\Omega = 1$



Low density Universe  
 $\Omega < 1$



# CMB anisotropy (intrinsic)

- Different physical effects, all related to the *small* density fluctuations  $\delta\rho / \rho$  present 380000 yrs after the big bang (recombination) produce CMB Temperature fluctuations:

$$\frac{\delta T}{T} = \frac{1}{3} \frac{\delta\varphi}{c^2} + \frac{1}{4} \frac{\delta\rho_\gamma}{\rho_\gamma} - \frac{\vec{v}}{c} \cdot \vec{n}$$

Sachs-Wolfe  
(gravitational  
redshift)

Photon  
density  
fluctuations

Doppler effect  
from velocity  
fields

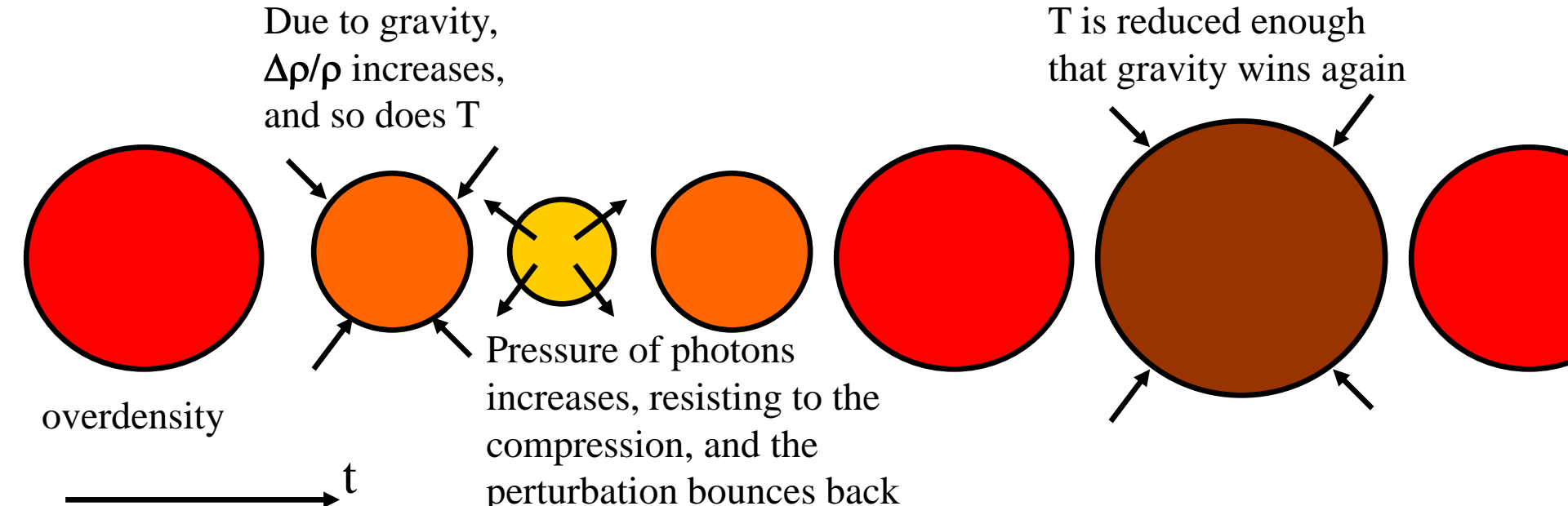
- Scales larger than the causal horizon are basically frozen in the pre-recombination era. The CMB anisotropy  $\delta T/T$  at large scales reflects the initial one.
- Scales smaller than the horizon undergo acoustic oscillations during the primeval fireball. Acoustic peaks in the power spectrum of  $\delta T/T$  at sub-degree scales.

# CMB anisotropy (intrinsic)

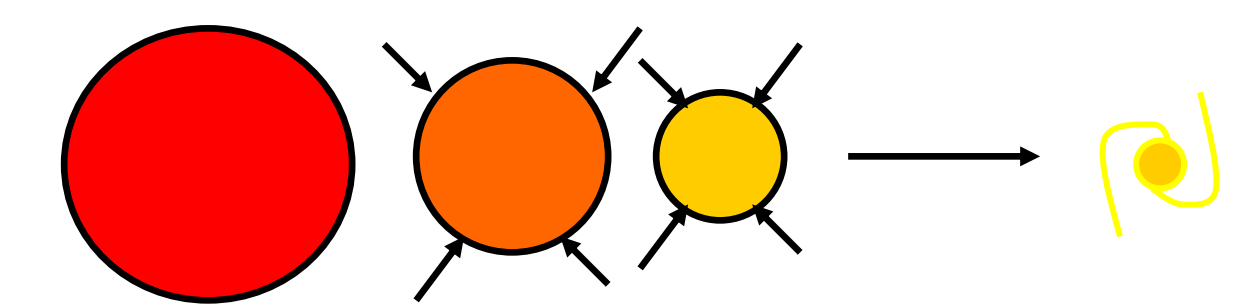
- The primeval plasma of photons and matter **oscillates** :
- self-gravity vs radiation pressure.
- We can measure the result of these oscillations as a weak anisotropy pattern in the **image** of the CMB.
- Statistical theory: all information encoded in the **angular power spectrum** of the image.



Density perturbations ( $\Delta\rho/\rho$ ) were **oscillating** in the primeval plasma (as a result of the opposite effects of gravity and photon pressure).

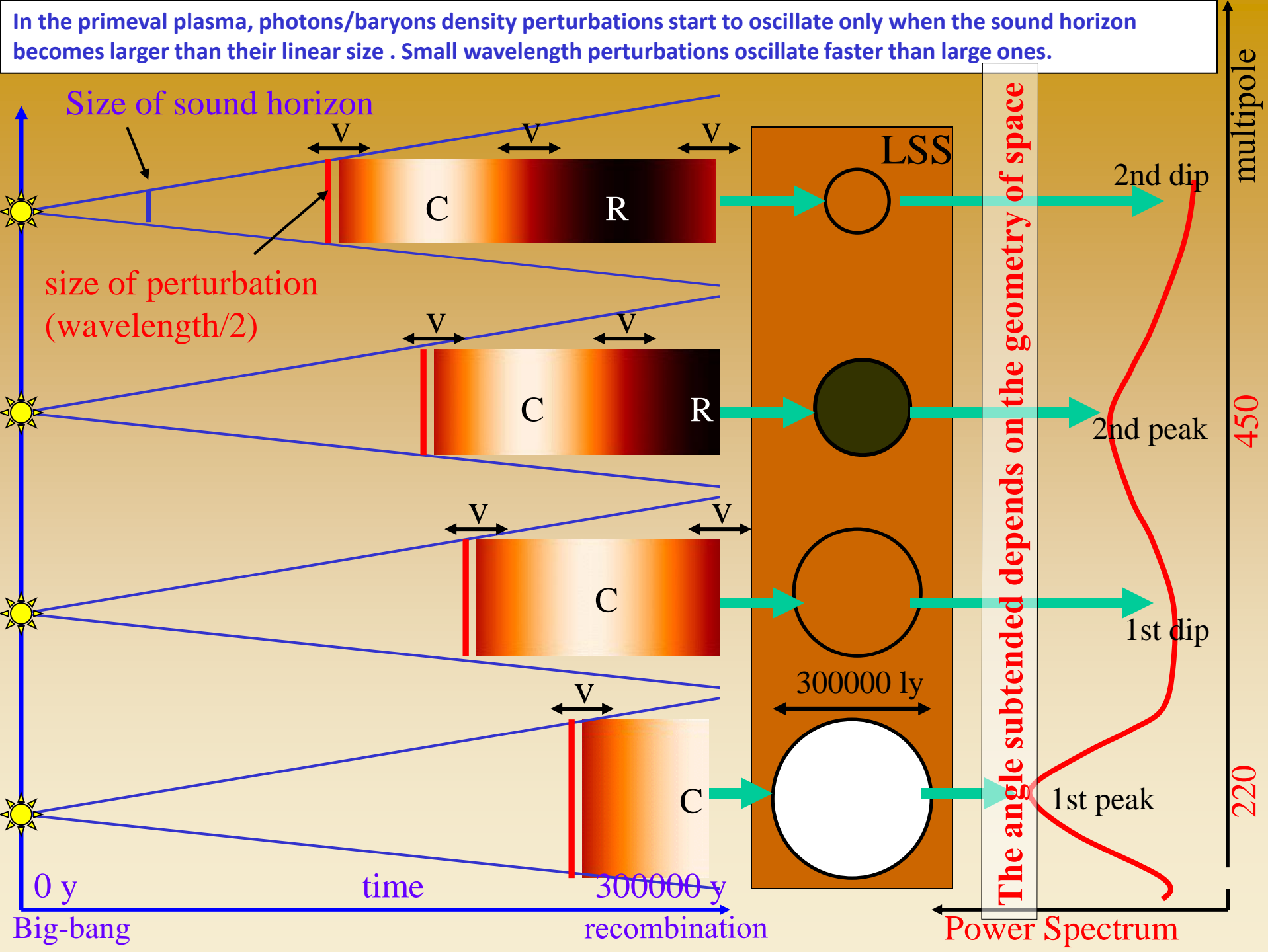


Before recombination  $T > 3000\text{ K}$



Here photons are not tightly coupled to matter, and their pressure is not effective. Perturbations can grow and form Galaxies.

After recombination, density perturbation can **grow** and create the hierarchy of structures we see in the nearby Universe.



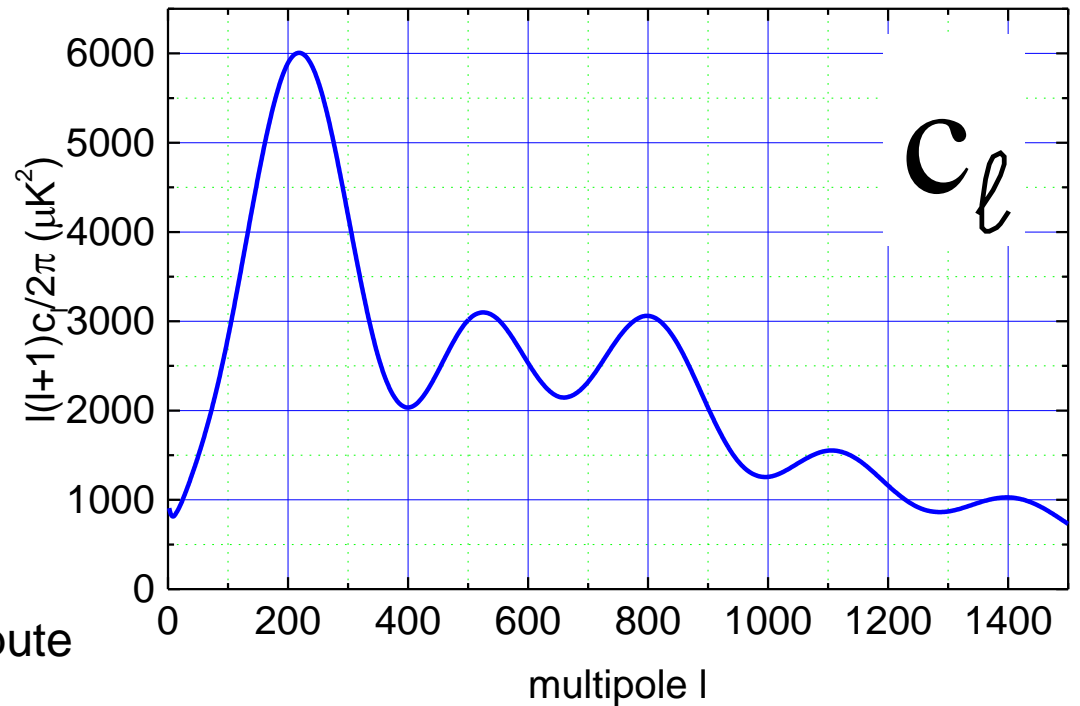
## Expected power spectrum:

$$\Delta T(\theta, \varphi) = \sum_{\ell, m} a_{\ell m} Y_{\ell}^m(\theta, \varphi)$$

$$c_{\ell} = \langle a_{\ell m}^2 \rangle$$

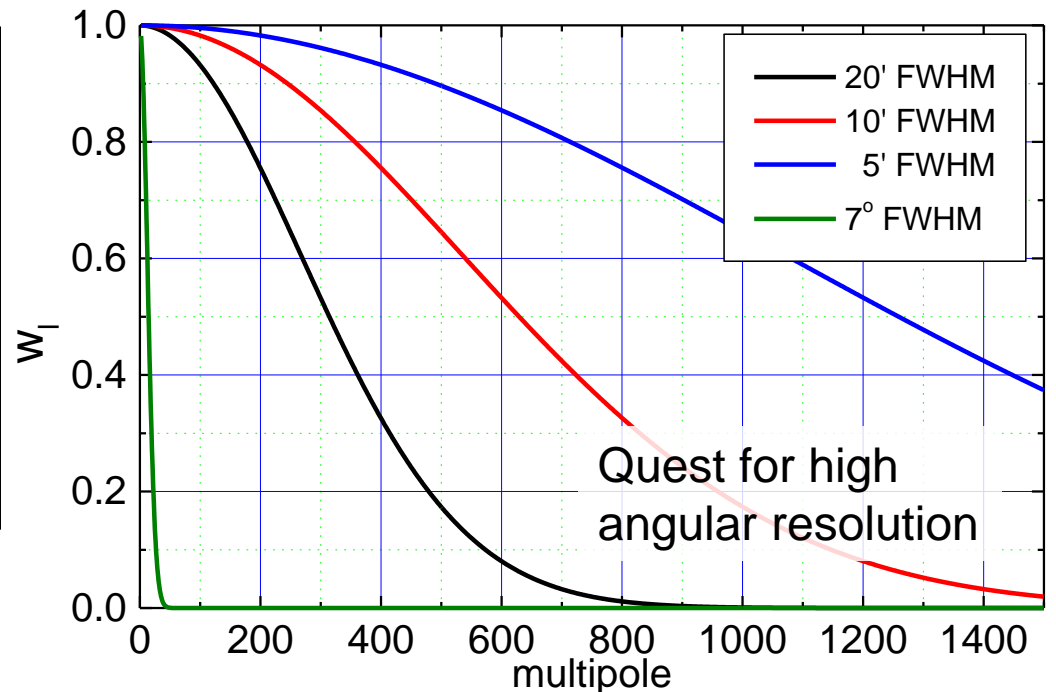
$$\langle \Delta T^2 \rangle = \frac{1}{4\pi} \sum_{\ell} (2\ell + 1) c_{\ell}$$

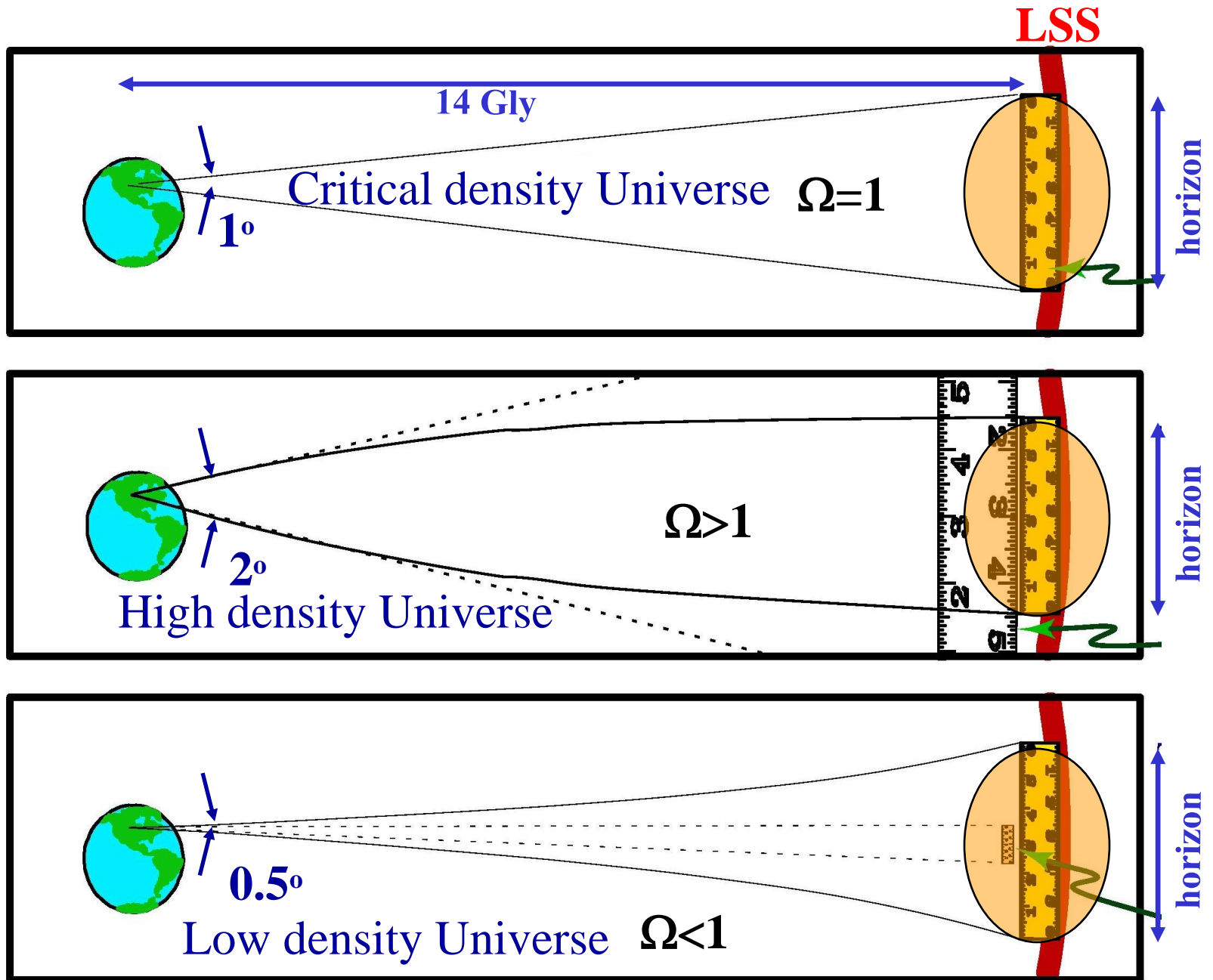
See e.g. <http://camb.info> to compute  $c_{\ell}$  for a given cosmological model



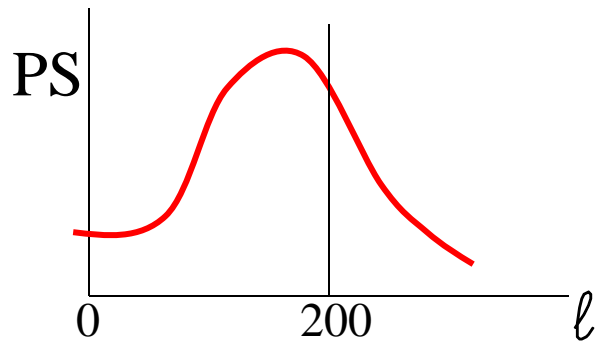
An instrument with finite angular resolution is not sensitive to the smallest scales (highest multipoles). For a gaussian beam with s.d.  $\sigma$ :

$$w_{\ell}^{LP} = e^{-\ell(\ell+1)\sigma^2}$$

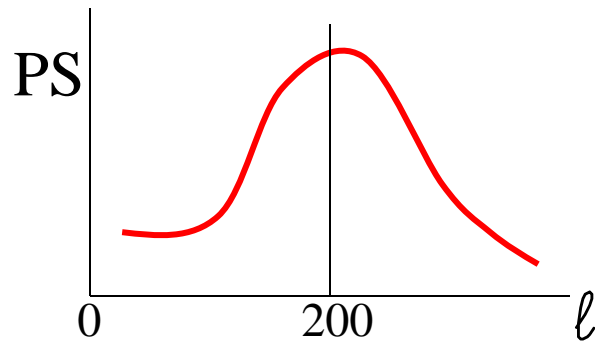




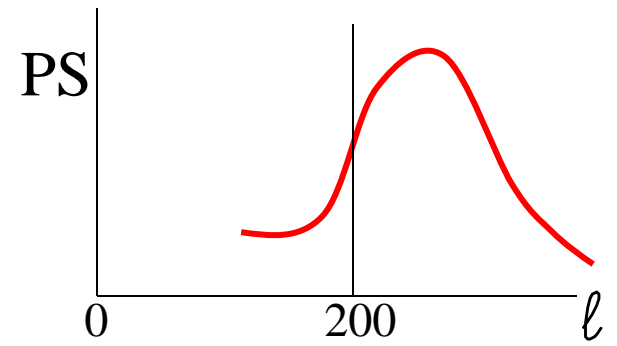
**The image and PS are modified by the geometry of the universe**



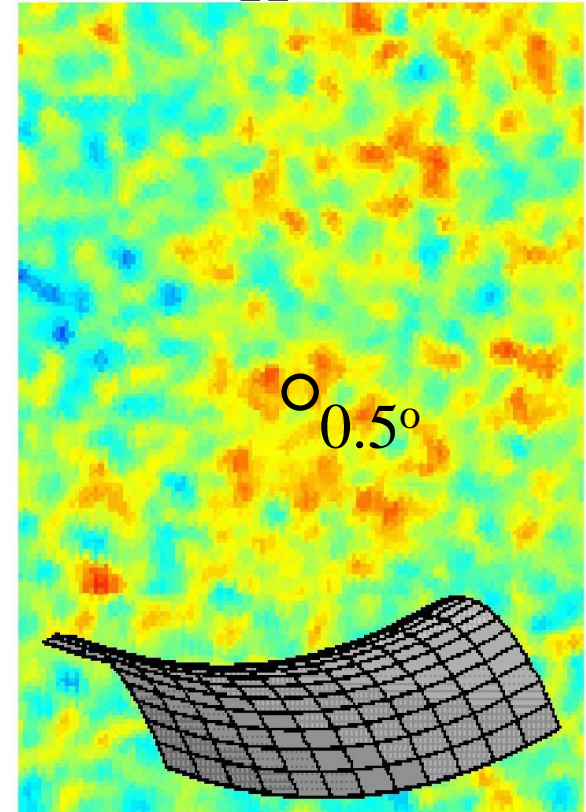
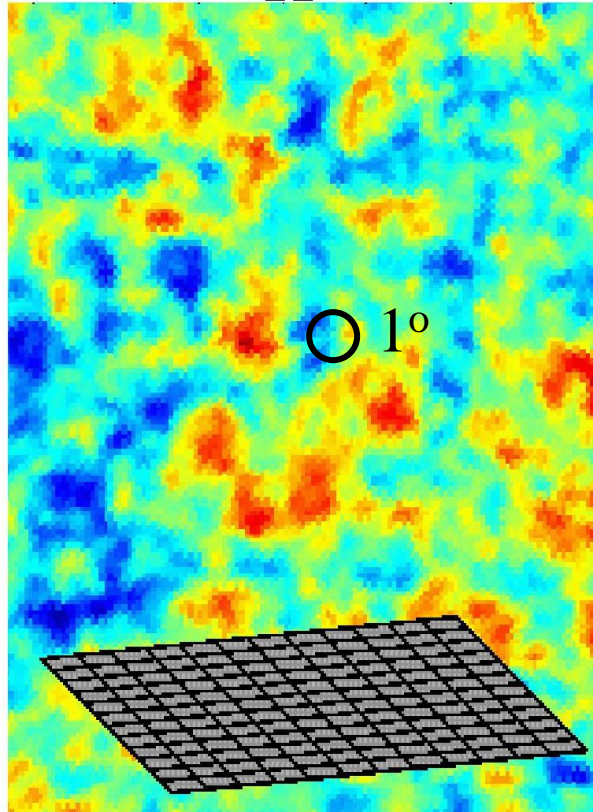
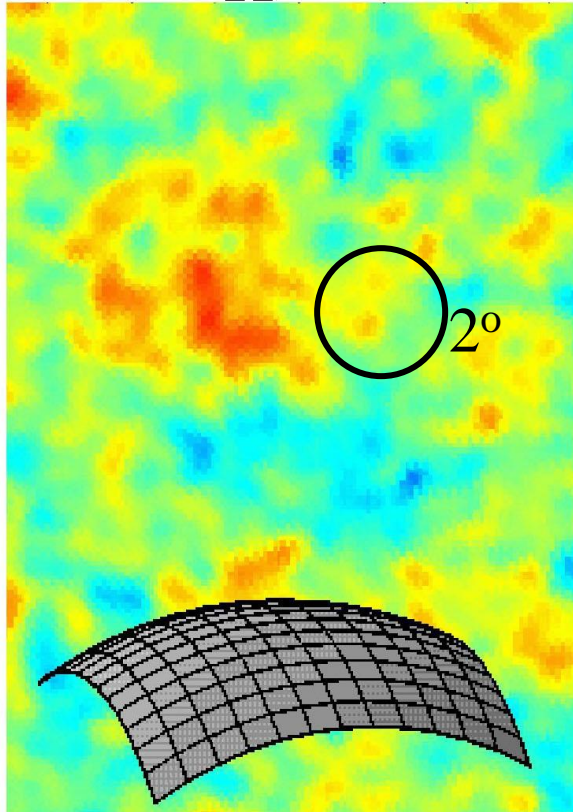
High density Universe  
 $\Omega > 1$



Critical density Universe  
 $\Omega = 1$



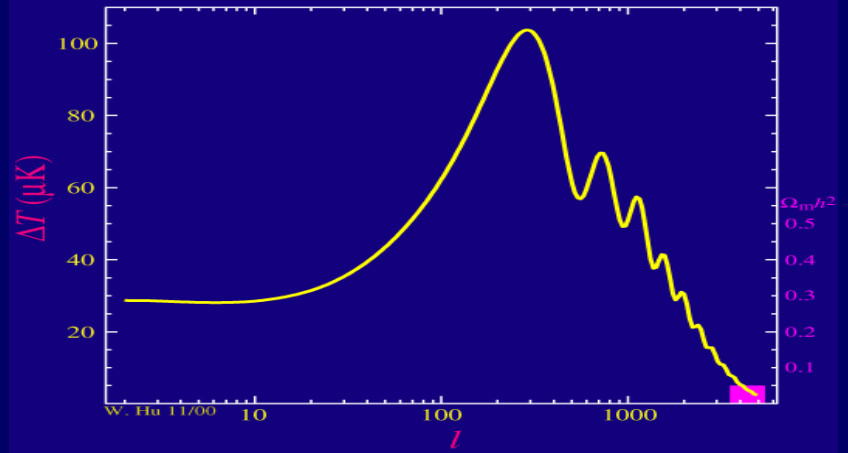
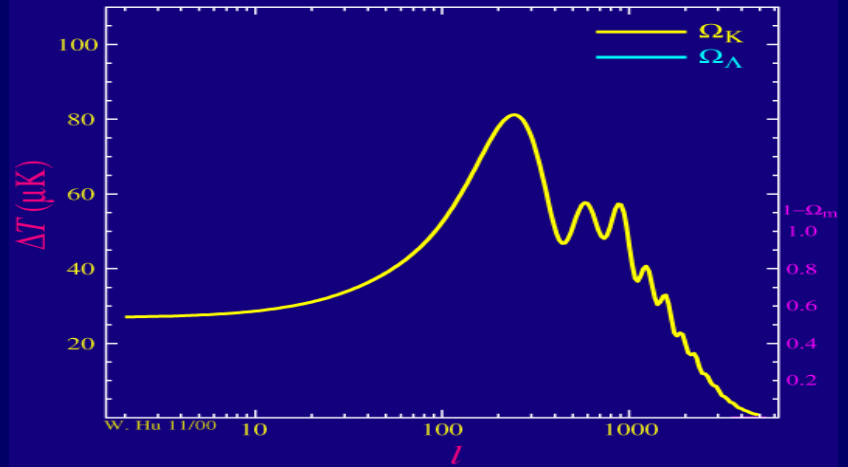
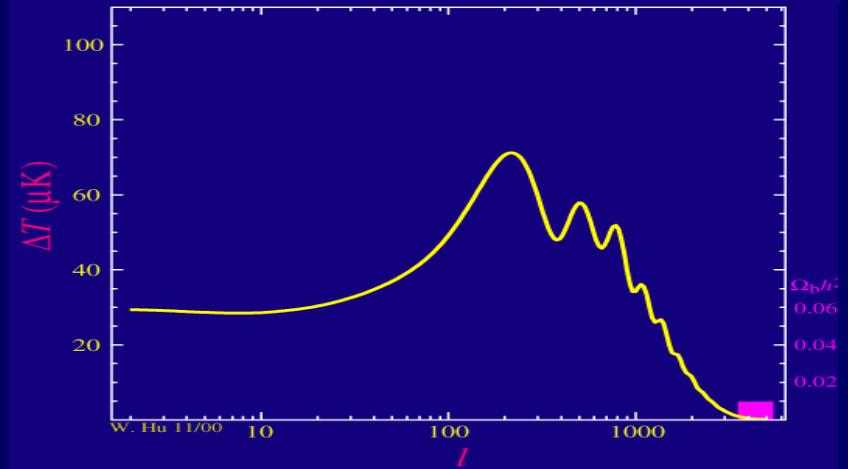
Low density Universe  
 $\Omega < 1$

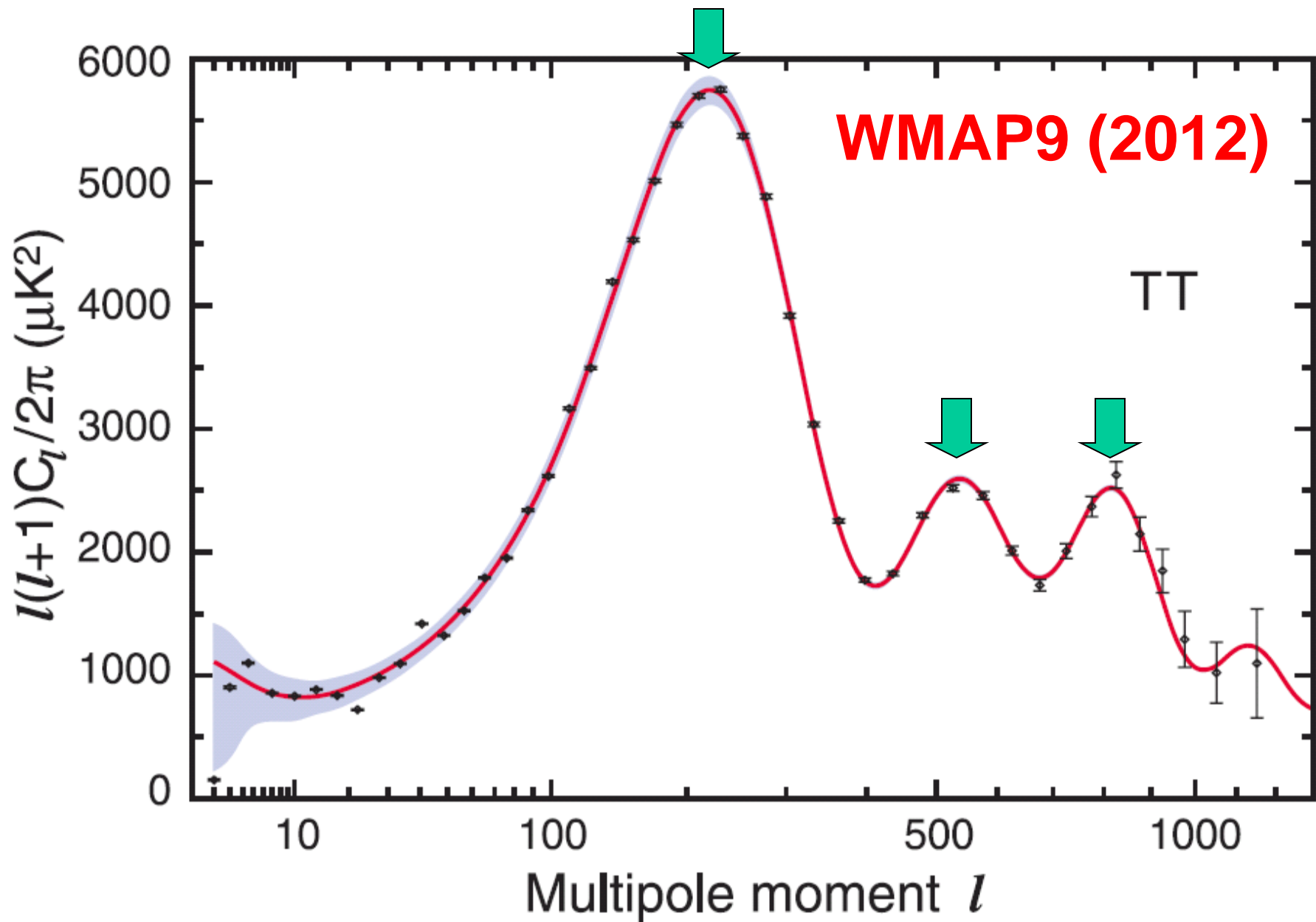


**The mass-energy density of the Universe can be measured in this way.**

# Composition

- The composition of the universe (baryons, dark matter, dark energy) affects the shape of the power spectrum.
- Accurate measurements of the power spectrum allow to constrain the energy densities of the different components of the universe.





Angular scale

90°

0.5°

0.2°

0.1°

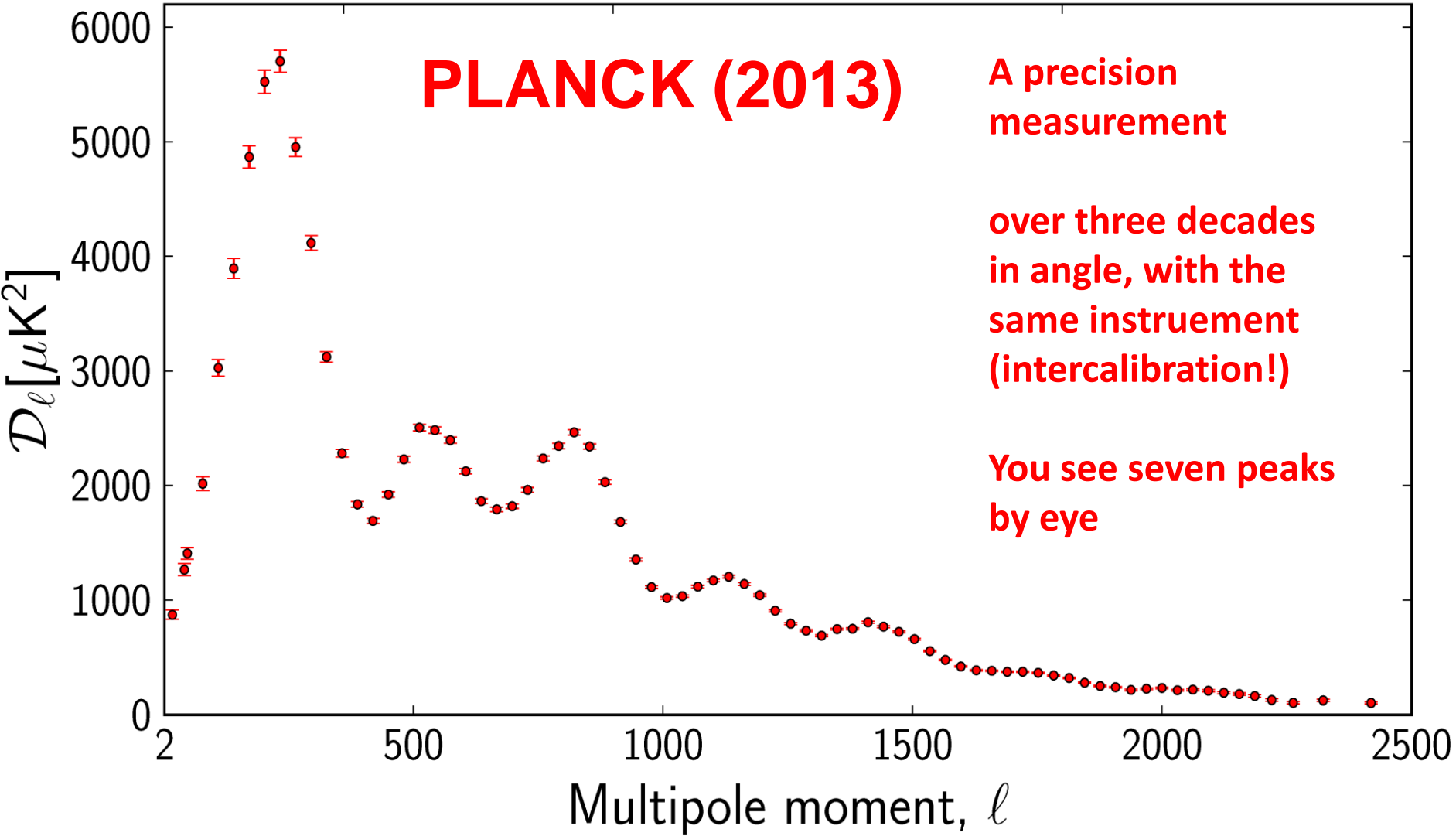
0.07°

**PLANCK (2013)**

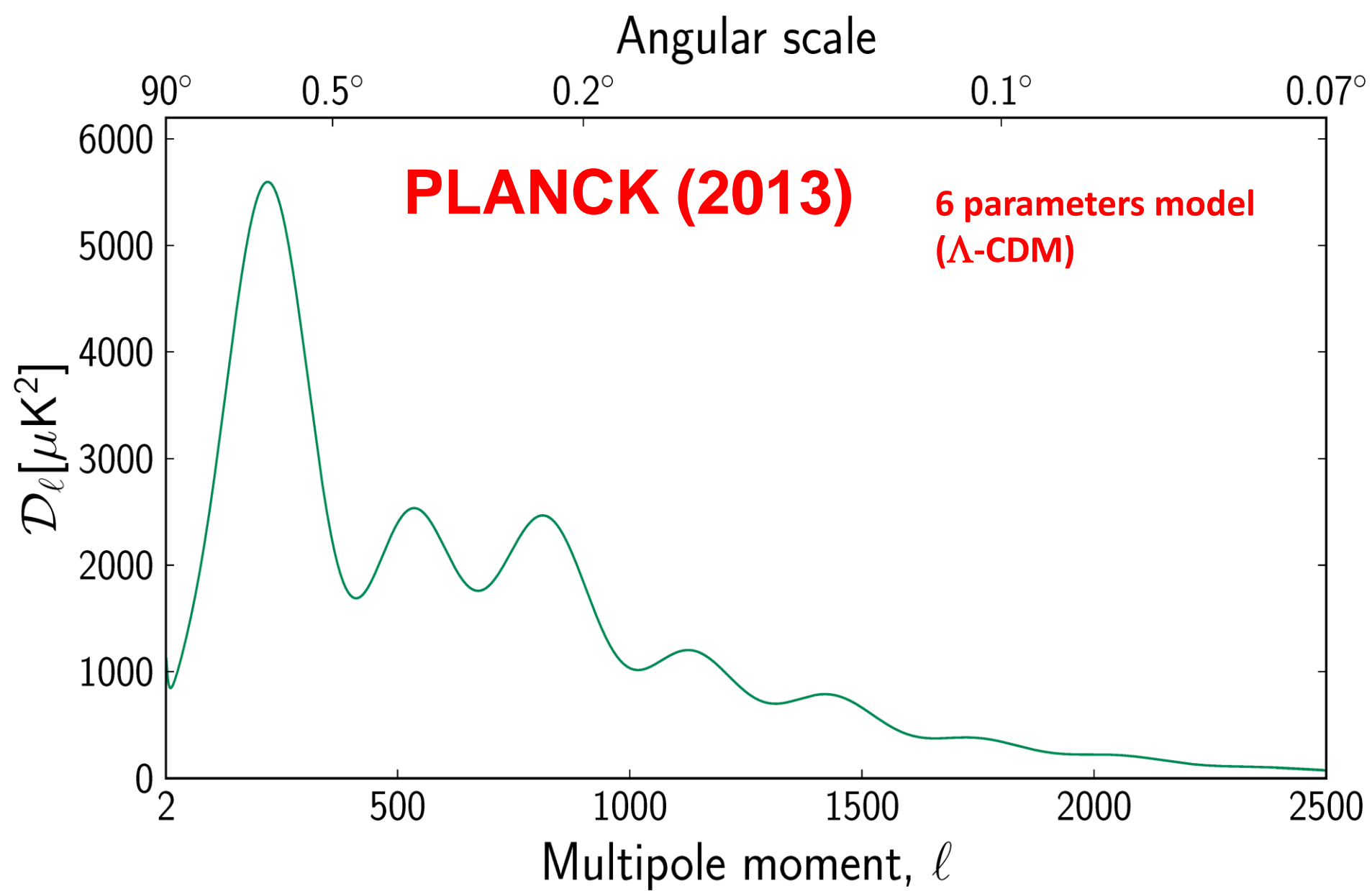
**A precision measurement**

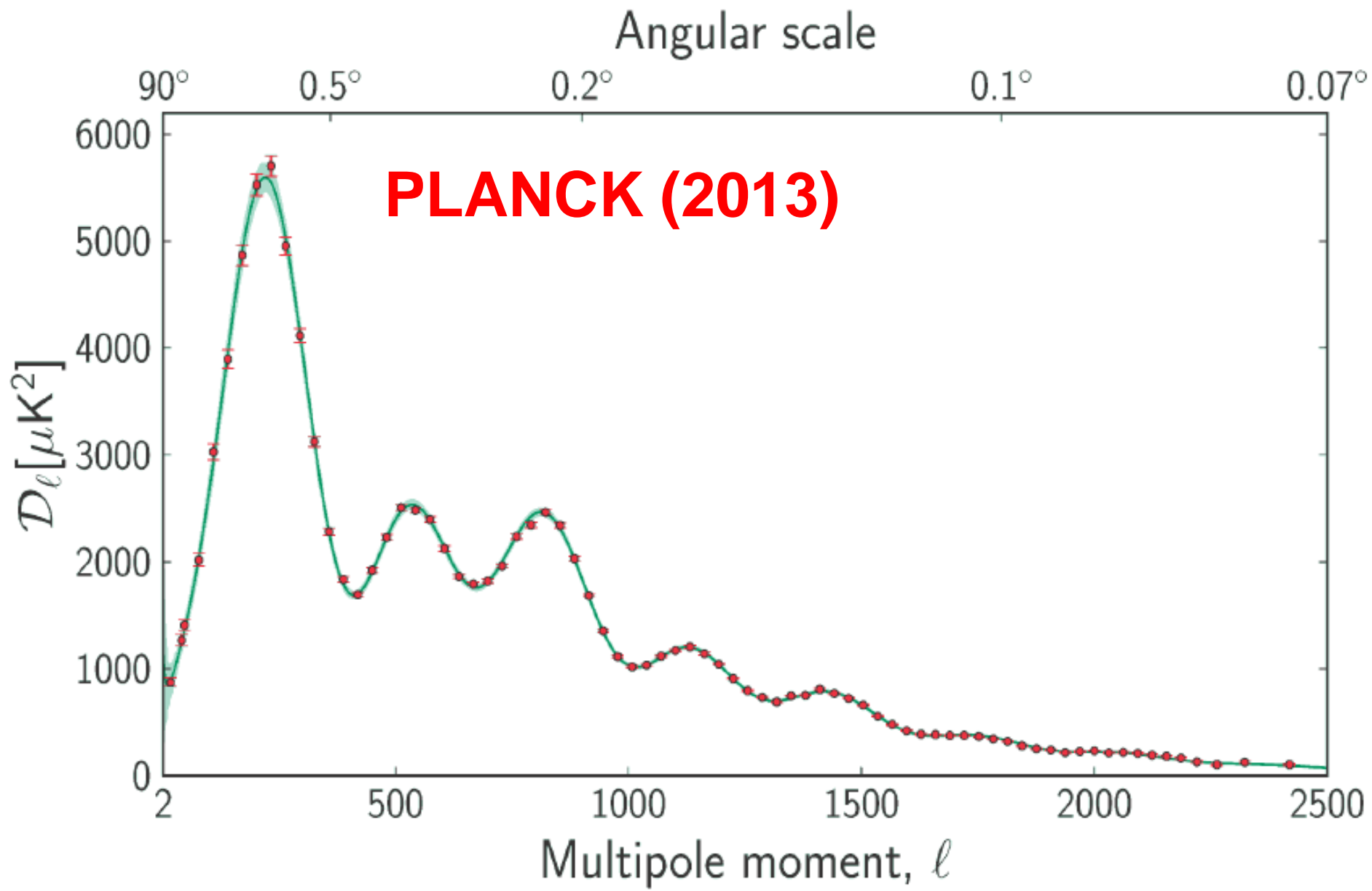
**over three decades in angle, with the same instrument (intercalibration!)**

**You see seven peaks by eye**

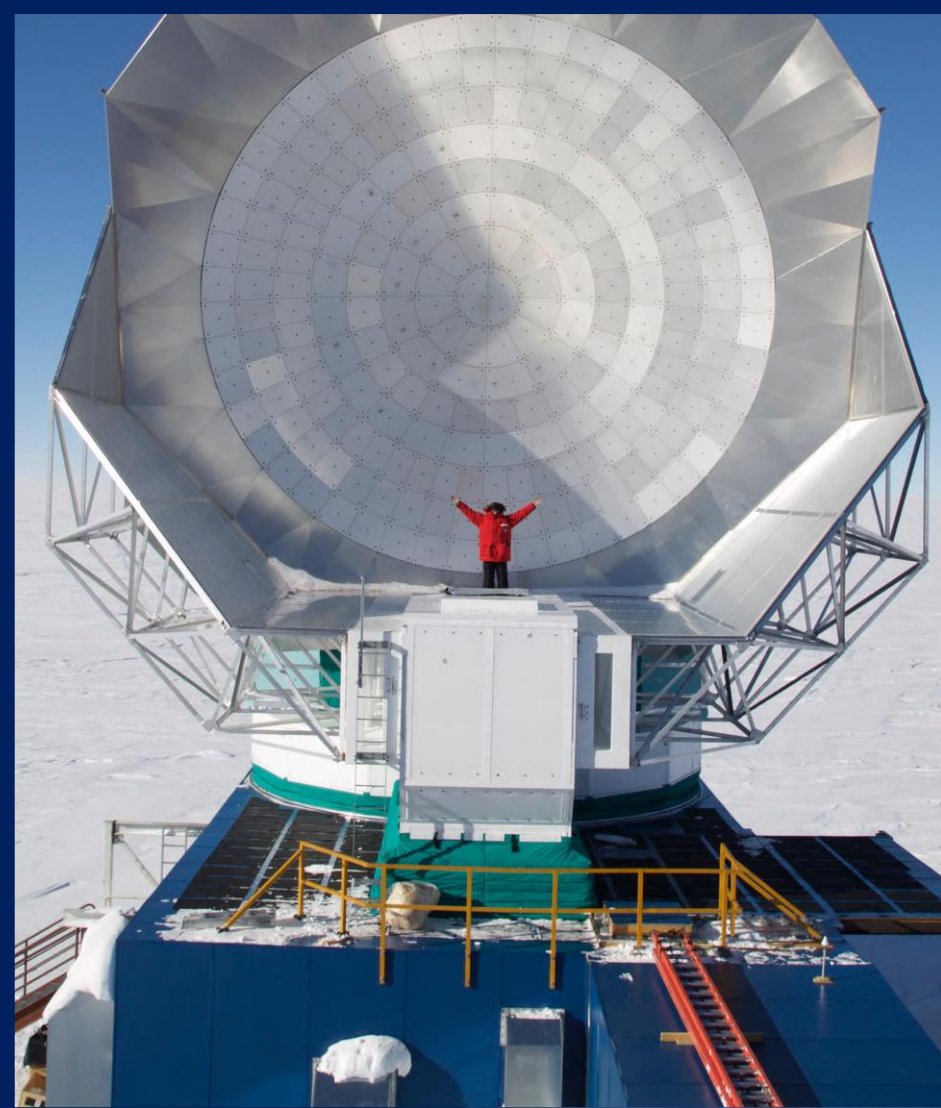


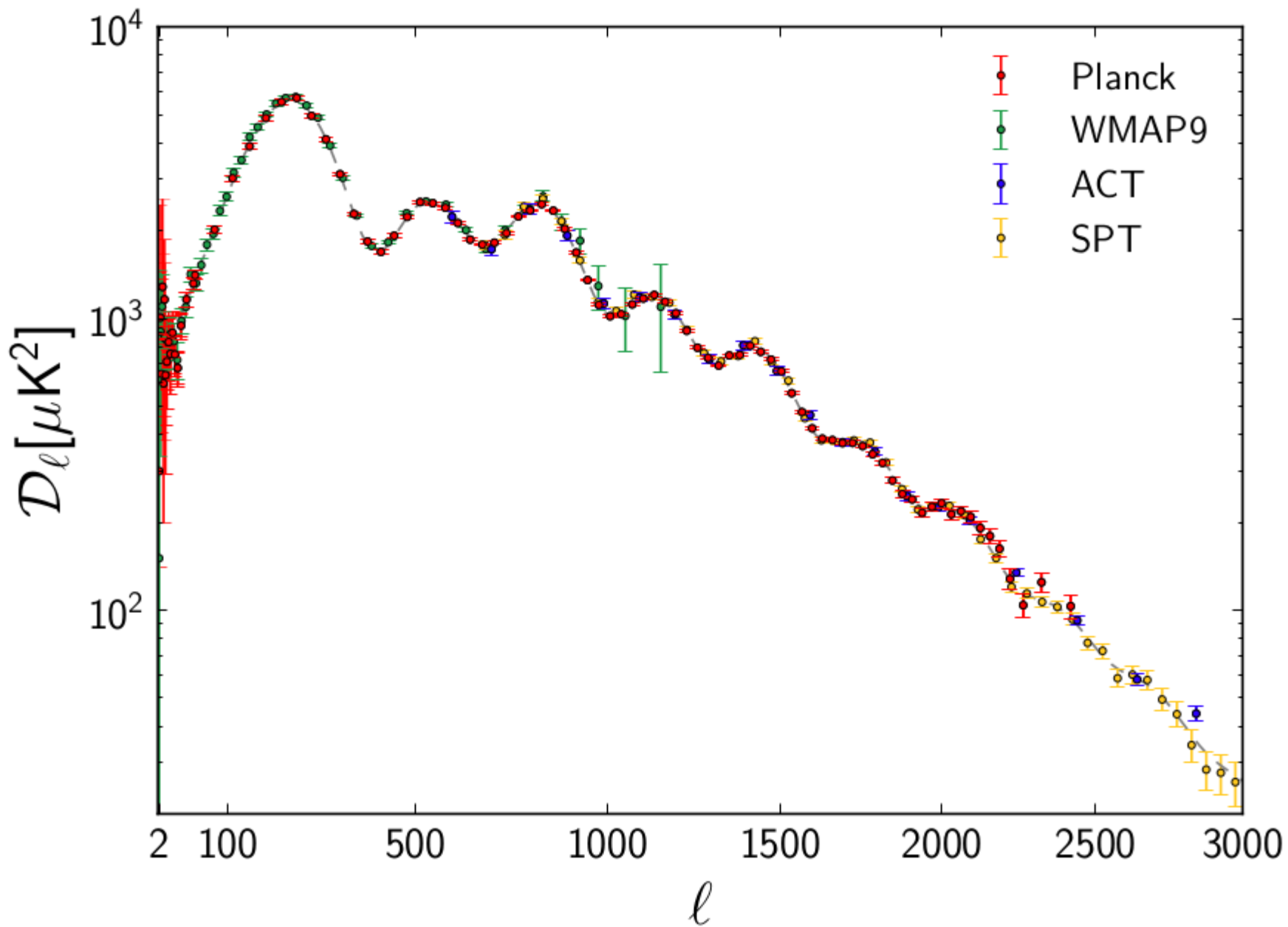


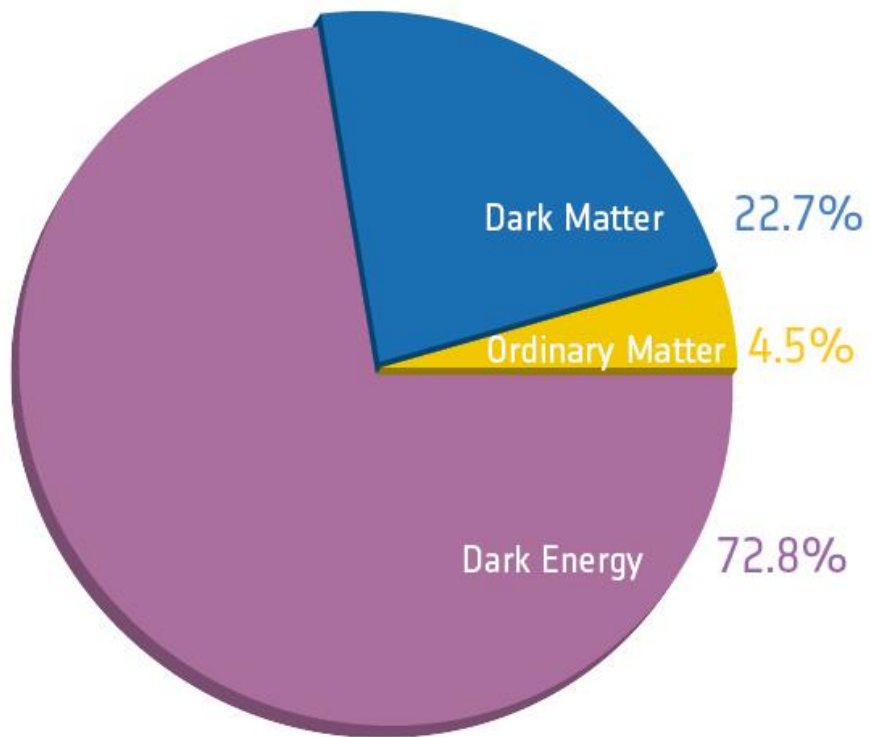




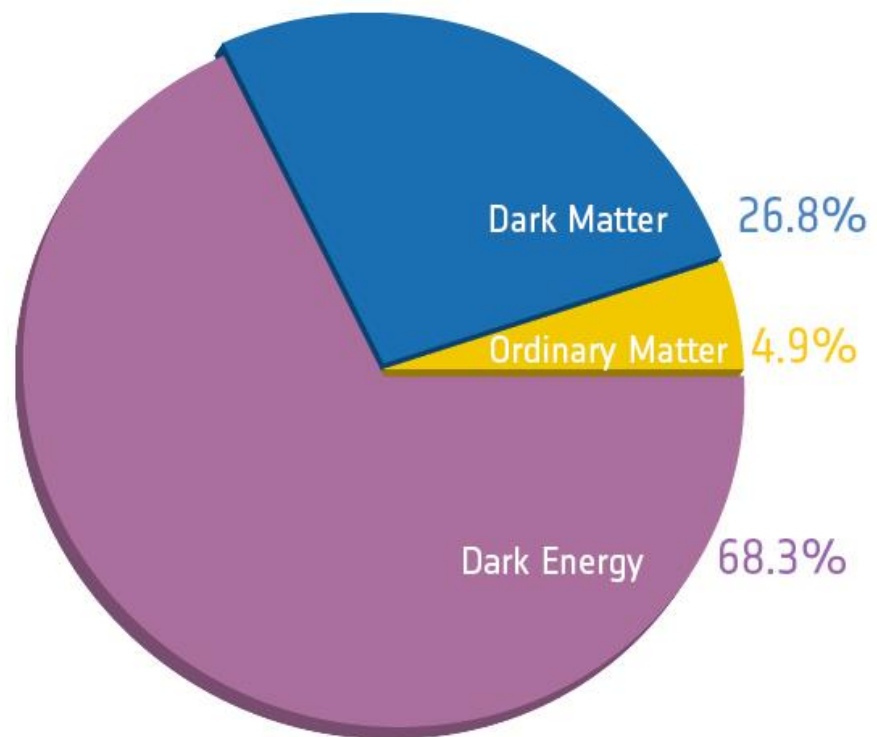
South Pole Telescope  
(10m diameter, 0.5' @150 GHz)







Before Planck



After Planck